
# VANADIUM AND TITANIUM EXTRACTION FROM TITANIFEROUS SLAG USING A ROAST-LEACH PROCESS

---

By

**Sanele Nkosi (NKSSAN003)**

A thesis submitted to the Faculty of Engineering and the Built Environment, University of Cape Town, in fulfilment of the requirements for the degree

**Master of Science in Engineering**

Department of Chemical Engineering

University of Cape Town

29 January 2025

| | |
|---|---|
| Supervisor | : Dr Thebe Mokone (UCT) |
| Co-supervisors | : Prof Jochen Petersen (UCT) |
| | : Dr Xolisa Goso (Mintek) |

# ABSTRACT

Vanadium (V) is typically extracted from the titaniferous magnetite (titanomagnetite) ore using either the V primary production and V and steel co-production process. The V primary production process is the roast-leach process which involves roasting, leaching, precipitation, and calcination of the titanomagnetite. The V and steel co-production process entails the smelting of titanomagnetite in the presence or absence of the fluxes. In the presence of flux i.e. the fluxed smelting approach, most of the V reports to the pig iron, whilst titania ($TiO_2$) reports the slag. This slag is discarded since the $TiO_2$ grade is considered too low for upgrading. Also, this titaniferous slag has a complex phase chemistry such that the spinel and pseudobrookite solid solution (ss) phase incorporate most of the V and Ti species. The objective of this project was to investigate a roast-leach process that would maximize the extraction of V from the titaniferous slag and remove high amounts of impurities from the water leach residue to maximize the $TiO_2$ grade in the product residue.

The slag produced by the now-defunct EVRAZ Highveld Steel and Vanadium Cooperation (EHSV) of South Africa (SA) was used as a case study. The EHSV titaniferous slag contains about 0.9% $V_2O_5$ and 35.6% $TiO_2$. The best roasting conditions were investigated through the variation of $Na_2CO_3$: NaOH ratios, stoichiometric Na additions, roasting temperatures, roasting times, particle size distribution (PSD), and Na reagents i.e. $Na_2CO_3$, NaOH, and $Na_2SO_4$ salts. The roasting stage is aimed at the conversion of $V_2O_5$ in the titaniferous slag to a water soluble sodium metavanadate ($NaVO_3$). The produced roast products were leached using water at standard conditions of 70°C, 120 minutes leaching time, s:l ratio of 1:4, and agitation speed of 350 rpm. The produced water leach residue was further subjected to acid leaching using HCl as a lixiviant with 20% acid concentration, at 110°C, 24 hours, s:l ratio of 1:4, and agitation speed of 350 rpm. The acid leaching stage was conducted in order to remove impurities such as Al, Ca, Mg, and Fe. The resulting acid leach residue was further upgraded through caustic leaching for Si impurity removal. The standard caustic leaching conditions that were used include 2.15 M NaOH solution as a lixiviant, leaching temperature of 100°C, leaching time of 3 hours, s:l ratio of 1:4, and agitation speed of 350 rpm.

The best roasting conditions were used to measure the best leaching conditions by variation of the leaching time from 1 to 24 hours and acid concentration from 15% to 25%. The residue from the best leaching conditions were subjected to standard caustic leaching conditions. The

high $TiO_2$ grade that resulted from the removal of impurities was washed to remove the Na present in the residue.

The best roasting conditions were 200% stoichiometric Na addition of $Na_2CO_3$: NaOH ratio of 100:0 and 0:100, 1000°C, 120 minutes, PSD of -850+105 µm. The best V extractions of 75.7% and 73.7% were attained when 200% stoichiometric $Na_2CO_3$ and NaOH were used respectively. $Na_2CO_3$ salt was the reagent that was used for downstream upgrading of the water-leach residue since it is cheap and used in industrial operations. The $TiO_2$ grade of 68.7% was attained in the caustic-leach residue when the best roasting conditions were used for roasting the titaniferous slag. The phase composition results showed that pseudobrookite ss and the spinel do decompose when excess Na was added. After this decomposition, the SEM showed that the $Na_3MgAlSi_2O_8$ phase forms after roasting. This phase also decomposed during water leaching to form the $Na_2MgTi_2O_6$ phase which contains high Ti and Si species and several impurities. Acid leaching results showed the possibility of minimising Mg, Ca, and Fe impurities. Al impurities in the acid-leach residue remained high in concentration. The phase composition results showed that Al species were present in all the phases that formed after acid-leaching. The caustic leaching process was a success since most of the Si impurities were removed. The phase composition results showed that the minor Si species present in the caustic-leach residue were in the rutile phase. The produced caustic-leach residue still contained several impurities.

The best leaching conditions were 24 hours leaching time and 25% HCl lixiviant concentration. Using these best conditions resulted in $TiO_2$ grades of 71% in the caustic leach residue. Washing of this caustic leach residue further increased the $TiO_2$ grade to 79.6%. The phase composition of the washed sample showed that the concentration of Na and Si impurities in the residue decreased. The rutile phase also contained a variety of Mg, Al, Cl, and Ca impurities.

The impurity extraction degrees showed an increase with increasing leaching time. The extraction degrees followed the order of Mg > Fe > Al > Ca when leaching times were varied. The $R^2$ values of Mg and Fe showed that the rate controlling mechanism is the surface chemical reaction whilst Al and Ca are controlled by diffusion across product layer and interface transfer.

The evaluation of V and impurity extraction from the titaniferous slag was possible at the attained best conditions. The impurities were not fully removed to their maximum, hence the high $TiO_2$ grade product was still contaminated with impurities. The produced $TiO_2$ grade did not meet the $TiO_2$ feedstock specifications as the MgO, CaO, $Al_2O_3$, and FeO impurities were still high in the final product, therefore further optimization work is required.

# DECLARATION

I, Sanele Belinda Nkosi, hereby declare that this thesis is my own work. It is being submitted for the degree of Master of Science in Engineering at the University of Cape Town. This thesis has not been submitted before for any degree or examination in any other university.

Signed by candidate

2025-01-29

Signature

Date

# ACKNOWLEDGEMENTS

I would like to express my sincere gratitude to my supervisor Dr Thebe Mokone for taking me under his wing and providing guidance, supervision, and advice at all times. This has been a learning curve, and it has helped me grow in many aspects of my life. Thank you for allowing me to do this research and for encouraging and even congratulating me before I even completed my research.

To my co-supervisors, Professor Jochen Petersen thank you for not refusing to give advice when it was required. I appreciate all the help, guidance, and advise you have given during my research. Dr Xolisa Goso, I would like to thank you for the encouragement and motivation I have received throughout the years of this research. The faith that you had in me is unmeasurable, and thank you for pushing me to complete this research even though at times I felt like it was not worth it. God bless you in everything that you do.

A huge appreciation to Mintek for granting the funds for the MSc at the University of Cape Town. This project was conducted and accomplished at Mintek under the science vote WasteRoast project.

Great thanks to analytical and mineralogy divisions of Mintek for helping the chemical analysis and phase characterisation of the products. A special thanks to Dr Yash Thakurdin from MNL division and Ms Thembakazi Ncedo from ACD who have always been able to assist with the characterisation.

A huge appreciation goes to Pyrometallurgy Division (PMD) especially the Technology Demonstration Group, they have all been amazing from the execution up to completion of this project. A special thank you particularly goes to Grace, Thabiso, Ncuthu, Simon, Vincent, Yonwaba, and Sibusiso. Without you guys, this project was not going to be successful.

Last but not least, to my family for the support I have received throughout this research has been marvellous, noticeable, appreciable, and amazing. I would like to thank all my family members from my parents (Themba and Thoko), my husband (Hactor), my sister (Samke), and my kids (Ambeswa, Oluthando, Lusanele, Hlelo, and Lelona).

# TABLE OF CONTENTS

# LIST OF FIGURES

# LIST OF TABLES

# CHAPTER 1

# INTRODUCTION

## 1.1 Background

Titaniferous magnetite (titanomagnetite/ TiMag) ore deposits are magmatic accumulations of magnetite ($Fe_3O_4$) and ilmenite ($FeTiO_3$) containing over 1% concentration of $TiO_2$. Some titanomagnetite deposits contain phases such as hematite ($Fe_2O_3$), rutile ($TiO_2$) and perovskite ($CaTiO_3$) (Fischer, 1975). These ore deposits are established sources of iron (Fe) and vanadium (V), and have the potential to be used as titania ($TiO_2$) sources (Sadykhov & Karyazin, 2007). Figure 1 shows the vanadium reserves throughout the world (Polyak, 2023).

Titanomagnetite is mainly processed in China, Russia, South Africa, and Brazil. China continues to be the largest producer of V throughout the world, followed by Russia. South Africa is the third V producer in the world and the fourth place is occupied by Brazil (Polyak, 2022). Australia has large reserves of V as shown in Figure 1, however, there is no current production. In South Africa, titanomagnetite deposits are mainly found in the Bushveld Complex (BC) (USAID, 2021).

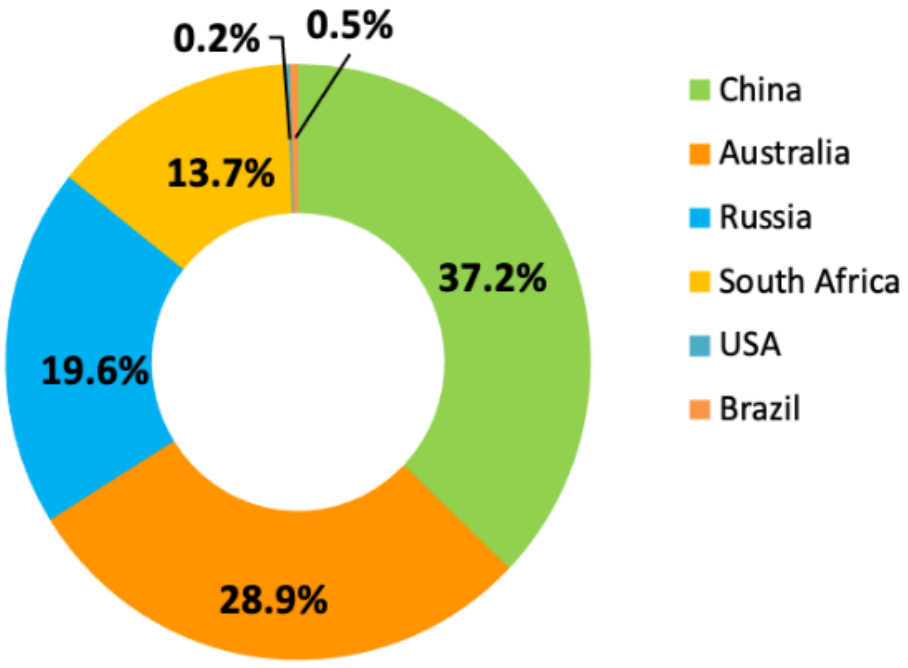


Figure 1: Vanadium reserves throughout the world (Vanitec, 2022; Polyak, 2022)

The major application of Fe is in the production of ferrous alloy products and steel. Fe can also be alloyed with other elements such as carbon (C), nickel (Ni), chromium (Cr), and tungsten (W) in the cast Fe and steel industries. The other applications of Fe as steel include the construction, manufacturing, and automotive industries. Vanadium is used mainly in the steel industry where it is added as ferrovanadium (FeV). Vanadium pentoxide ($V_2O_5$) is an important compound in catalysis industries as well as other chemical industries. Vanadium is gaining popularity in energy storage systems where it is used as an electrolyte for vanadium redox flow batteries (VRFBs) (Sutradhar, et al., 2020). Titanium is mainly used as titanium dioxide for the production of $TiO_2$ pigments used in many industries including paint, plastic, and paper (Wu, 2021).

Titanomagnetite is typically processed through two processes; namely, the vanadium primary production and vanadium and steel co-production processes. Vanadium primary production involves the roast-leach process, which includes roasting, leaching, precipitation, and calcination stages. The roasting stage is conducted at high temperatures in the presence of a sodium reagent or salt to convert the vanadium in the titanomagnetite to the water-soluble sodium metavanadate ($NaVO_3$). The sodium salts that can be used during the roasting stage include NaCl, NaOH, $Na_2CO_3$, and $Na_2SO_4$. These Na salts react with vanadium in the titanomagnetite according to equations [1] to [5] (Nasimifar & Mehrabani, 2022).

| | | |
|---|---|---|
| $2NaCl + V_2O_5 + 0.5O_2 \rightarrow 2NaVO_3 + Cl_2$ | chloride salt roasting in excess $O_2$ | [1] |
| $2NaCl + V_2O_5 + H_2O \rightarrow 2NaVO_3 + 2HCl$ | chloride salt roasting with water | [2] |
| $NaOH + V_2O_5 \rightarrow NaVO_3 + H_2O$ | caustic roasting | [3] |
| $Na_2CO_3 + V_2O_5 \rightarrow 2NaVO_3 + CO_2$ | soda ash roasting | [4] |
| $Na_2SO_4 + V_2O_5 \rightarrow 2NaVO_3 + SO_3$ | sulphate roasting | [5] |

The industrial vanadium and steel co-production process typically involves the smelting of the titanomagnetite in the presence of a carbonaceous solid reductant and flux, such as quartz and/or dolomite, using electric arc or blast furnaces (EAFs or BFs). The smelting process produces a V-bearing pig iron and a slag containing low grade of $TiO_2$. The $TiO_2$ content of the produced slag ranges between 20% - 40%. This titania-bearing slag is typically referred to as ‘titaniferous slag’ (McRae, et al., 1969; Lin & Guo, 2017). The V-bearing pig iron is typically subjected to a converting process for the production of V slag and high-purity pig iron for steelmaking.

Titaniferous slags are normally discarded in dedicated dumps. Table 1 shows typical chemical compositions of titaniferous slags produced around the world. As shown in the table, the $TiO_2$ contents in the titaniferous slags range between 20% and 40% $TiO_2$ (Hassell, et al., 2016; Steinberg, 2008; Sui, et al., 2004). In addition, the titaniferous slag produced by the now-defunct EVRAZ Highveld Steel and Vanadium Corporation (EHSV) in South Africa contains a relatively high content of vanadium (~ 0.9% $V_2O_5$) (Steinberg, et al., 2011). The total amount of titaniferous slag produced by EHSV during their years of operation remains in a huge dump located near the town of eMalahleni in South Africa. The slag dump is estimated to be about 45 million tonnes (Africa, Mining Review, 2017). The appreciable contents of $TiO_2$ and $V_2O_5$ in the titaniferous slag and that the slag is sitting above ground and requires no mining, have triggered interest towards investigating metallurgical processes for the valorisation of this slag for the extraction of vanadium and titanium products.

Table 1: Typical chemical composition (wt%) of some titaniferous slags that are produced worldwide

| Operation | Condition | **$TiO_2$** | **$V_2O_5$** | FeO | MgO | $Al_2O_3$ | $SiO_2$ | CaO |
|---|---|---|---|---|---|---|---|---|
| EHSV[+] (SA) | Fluxed | **35.6** | **0.90** | 1.00 | 14.1 | 18.0 | 16.2 | 14.1 |
| NMTK (Russia) and CHMP[#] (China) | Fluxed | **8-10** | **0.18-0.30** | 0.6-1.0 | 11-13 | 14-15 | 28-30 | 30-32 |
| NZS[#] (New Zealand) | Fluxed | **32.1** | **0.20** | 2.11 | 13.3 | 17.8 | 15.2 | 15.9 |
| Pangang[$] (China) | Fluxed | **22.0** | **-** | - | 7.00 | 14.0 | 22.0 | 27.0 |

([+] Steinberg, 2008, [#] Hassell, et al., 2016, [$] Sui, et al., 2004), -not reported

## 1.2 Problem Statement

Titaniferous slags, including those produced by EHSV in SA and Pangang and CHMP in China, make up huge waste dumps that are environmental nuisance. The land occupied by titaniferous slag dumps is a significant source of pollution of air, water and soil. This pollution can adversely affect human health, and the growth of plants. In addition, titaniferous slag dumps, which sit above ground and require no further mining, are a potential secondary resource for titanium and vanadium products, especially the EHSV titaniferous slag. However, the exploitation of these slag dumps using conventional processes is hampered by their complex phase and chemical compositions. V and Ti are typically distributed in at least three phases in the slag, including in pseudobrookite [(Mg, Ti, Fe, V)$_3O_5$, $M_3O_5$], perovskite ($CaTiO_3$) and the chemically inert spinel [(Mg, Fe)(Ti, Fe, Al, V)$_2O_4$, $M_3O_4$].

## 1.3 Focus of the study

This study focussed on the development of a technically viable integrated process flowsheet for the extraction of V from titaniferous slags using a modified conventional V primary production process, i.e. a roast-leach process, followed by beneficiation of the leach solids or residue through a modified Upgraded Slag (UGS) process involving sequential acid and caustic leach stages for the removal of impurities. The products of the integrated process flowsheet are a V-pregnant leach solution that can be processed further using conventional processes to produce many V products including $V_2O_5$, FeV, and V electrolyte, and a marketable titania ($TiO_2$) feedstock.

The study of V extraction from titaniferous slag, using the EHSV as a case study, involved investigating the best combination of roasting conditions for the decomposition of the V-bearing phases and liberation of V for water leaching. The current study differed from the conventional roast-leach in that the current study used excessive Na reagent additions to stoichiometric requirements, during the roasting stage. Thus, the extraction of V was conducted by roasting the slag in excess Na additions for the destabilisation of V-bearing phases and the formation of a water-soluble $NaVO_3$. V was extracted through the water leaching process into the solution. V extraction efficiencies were measured.

The produced residues were subjected to an acid leaching process with the aim of removing impurities such as Al, Ca, Mg, and Fe. Acid leaching dissolved impurities into a solution, leaving an upgraded residue with higher $TiO_2$ concentrations. Since the raw titaniferous slag contained significant concentration of $SiO_2$, it was crucial to remove these impurities through the caustic leaching process. The residue produced after caustic leaching contained high $TiO_2$ concentrations.

To study the extraction of V and the removal of impurities aimed at upgrading the concentration of $TiO_2$ in the residue, the following objectives were formulated.

- Determination of the best combination roasting conditions by variation of $Na_2CO_3$: NaOH mass ratio, type of Na reagent between $Na_2CO_3$, NaOH and $Na_2SO_4$, stoichiometric Na addition, temperature, time, and particle size distribution (PSD) of slag. The addition of Na reagents requires to be higher than 100% stoichiometric

addition since these additions resulted in lower V extractions and $TiO_2$ grades, in previous studies (Lekobotja, et al., 2017; Goso, et al., 2016).

- Study the phase chemistry of the roasted material and residues water, acid, and caustic leach residues to determine the phases that incorporate V, if any, and Ti and the phases that contain impurities such as Al, Ca, Mg, and Fe. Phase chemical analysis was very important to understand the phase chemical composition before and after each leaching stage, for identifying the phases that might be containing the targeted species by leaching.
- Optimize the leaching conditions by varying the leaching time and acid concentration. Study the phase chemistry of the upgraded $TiO_2$ products and determine the phases that incorporated most of the impurities. Determine the kinetics of leaching the impurities present in the water leach residue and measure the impurity extraction efficiencies and rate-controlling mechanisms.

# CHAPTER 2

# LITERATURE REVIEW

The literature study involving the different deposits and extractions of V and $TiO_2$ of titanomagnetite is explained in the following sections.

## 2.1 Titaniferous magnetite deposit

Titaniferous magnetite also known as titanomagnetite, is explained as a magmatic accumulation of ilmenite ($FeTiO_3$) and magnetite ($Fe_3O_4$) ( Hosseinzadeh, et al., 2017; Yang, et al., 2020). Some titanomagnetite contain hematite ($Fe_2O_3$), rutile ($TiO_2$) and perovskite ($CaTiO_3$). Discrete vanadium minerals have not been reported to be occurring in titanomagnetite deposits, except that some of the vanadium is found in ilmenite and other titanium minerals, but it is mostly found in the magnetite structure and also associated with iron oxide in the form of coulsonite ($FeV_2O_4$) (Nasimifar & Mehrabani, 2022). The concentrations of $V_2O_5$ in the titanomagnetite ranges from 0.2% to 1% and the higher grade deposits have shown to have $V_2O_5$ content of above 2% (Boni, et al., 2023), whilst the $TiO_2$ concentrations are more than 1% . Titanomagnetite is the principal source of vanadium (Fischer, 1975; Boni, et al., 2023). The titanomagnetite deposits provides an opportunity to extract iron, titanium, and vanadium from a single resource (Lv & Bai, 2019).

The titaniferous magnetite deposits are found throughout the world in countries (Fischer, 1975; Technology, 2022; Polyak, 2023)such as:

- China – Lanjiahuoshan deposit, Panzhihua layered intrusion
- Australia – Jameson range, Barrambie, Buddadoo, Coates, Gabanintha, and Balla Balla
- Russia – Mount Kachkanar
- South Africa – Bushveld Complex
- Brazil – Rio Jacaré intrusion
- United States – Laramie range, Shanton, Taylor and different deposits located in southeast Wyoming

Table 2 The titanomagnetite reserves in the world (Polyak, 2023; Gambogi, 2022).

| Country | Reserves (thousand metric tonnes) |
|---|---|
| China | 9 500 |
| Australia | 7 400 |
| Russia | 5 000 |
| South Africa | 3 500 |
| Brazil | 140 |
| United States | 45 |

## 2.2 South African Bushveld Complex

Bushveld Complex (BC) is one of the largest deposit of titanomagnetite in the world, with layered intrusions estimated to be around of 66 000 $km^2$. The titanomagnetite thickness in the BC is approximately 9 km. The Rustenburg layered suite, which contains most minerals, is divided into four zones namely; lower, critical, main and upper zone as shown in Figure 2 (Boni, et al., 2023; Cawthorn, 2015; Kinnaird, 2005). These zones are distributed in three major mineral areas that are situated in the BC. These zones are known as the northern, eastern, and western limbs. The minerals found in the lower, main, and upper zones are distributed in all the limbs, whilst those in the critical zone only spread in the eastern and western limbs. The upper zone host the V-bearing titanomagnetite deposits. The highest V-bearing titanomagnetite deposit is situated in the eastern limb, in a layer known as the Main Magnetite Layer (MML)
The minerals present in the different zones (Kinnaird, 2005; Barnes, et al., 2004) are:-

- Lower zone – magnesium (Mg), chromium (Cr), nickel (Ni), precious metals (Ir, Rh, Pt, Pd, Au)
- Critical zone – platinum group metals (PGMs), chromite
- Main zone – PGMs, chromite
- Upper zone – Fe, Ti, V, phosphorus bearing layers

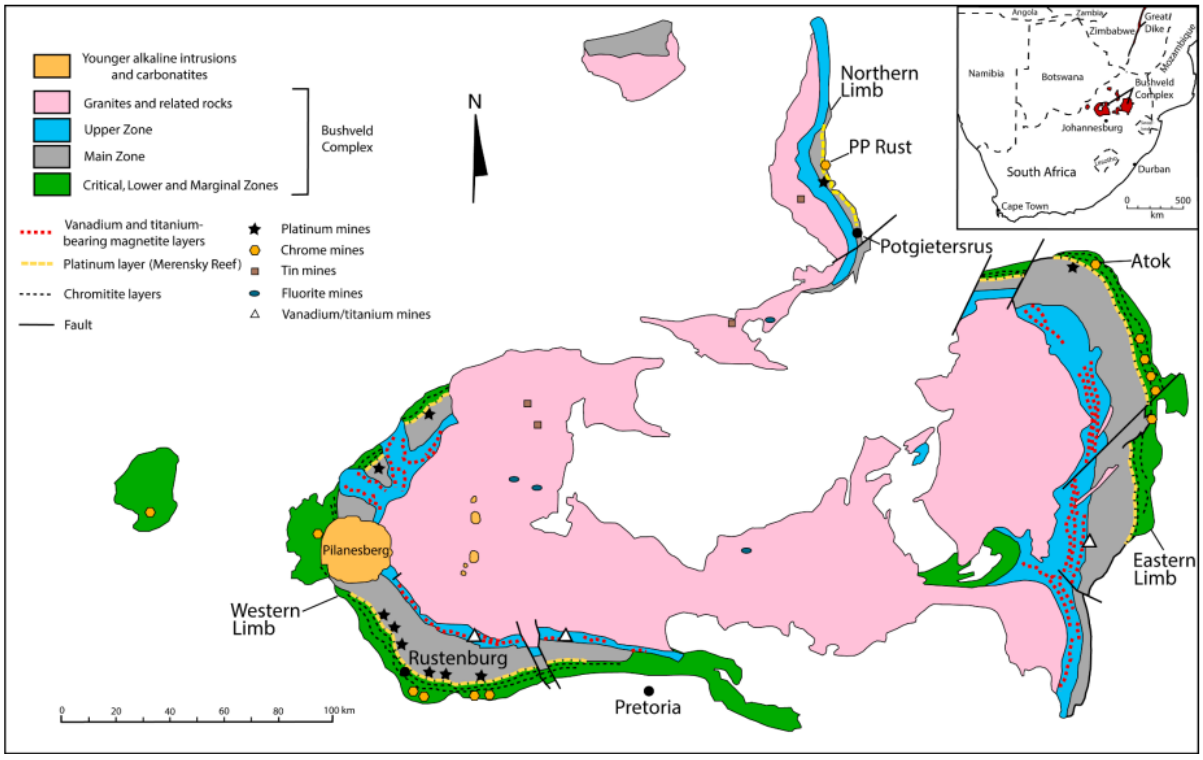


Figure 2 Geographical layout of the Bushveld Complex (Cawthorn, 2015; Kinnaird, 2005)

The Bushveld Complex has two types of titaniferous magnetite grades namely; MML and P-Q magnetite zone. The MML has relatively high vanadium of approximately 1.48%$V_2O_5$ when compared with the P-Q with 0.21% $V_2O_5$ as shown in Table 3. (Bushveld Minerals, 2014)

Table 3: Typical chemical composition of the MML and P-Q deposits (mass %) (Bushveld Minerals, 2014)

| Deposit | Fe | $TiO_2$ | $V_2O_5$ | $SiO_2$ | $Al_2O_3$ | $P_2O_5$ | S |
|---|---|---|---|---|---|---|---|
| MML | 44.7 | 9.70 | 1.48 | 11.2 | 8.30 | 0.01 | 0.01 |
| P-Q zone | 33.3 | 10.8 | 0.21 | 22.6 | 9.73 | 0.04 | 0.39 |

## 2.3 Metallurgical processing of titanomagnetite

Titanomagnetite is an important source of vanadium throughout the world. It accounts for approximately 85% of the world's $V_2O_5$ production. Titanomagnetite is mostly mined in China, South Africa, and Russia (Vanitec, 2022).

The different metallurgical methods for extracting vanadium and iron from titanomagnetite are V primary production process and V and steel coproduction process. The V primary production process is basically a roast-leach process in which the titanomagnetite is roasted in the presence

of a sodium reagent to produce a water-soluble sodium metavanadate. The produced sodium metavanadate is leached out into the solution using either water or acid. The solution is further treated by impurity rejection, precipitation, and calcination processes for the production of high purity $V_2O_5$. The V and steel coproduction process involves the smelting of titanomagnetite in the presence of a carbonaceous reductant and fluxes to produce a V bearing pig iron which is processed further for V and steel production; and low Ti slag which is discarded as waste material (Steinberg, et al., 2011). Recently, the Ti-containing slag is further processed for the beneficiation of V and $TiO_2$ (Vanitec, 2022).

### 2.3.1 V primary production process

There are three industrial companies that produce V through the V primary production process. These companies include Largo Inc from Russia, Bushveld Minerals, and Glencore Plc both from South Africa. The V primary production process accounts for about 17% of the world's V supply (Blue Project, 2022). V primary production process is essentially a roast-leach process which involves roasting the titanomagnetite ore or concentrate in the presence of sodium salt for the production of a water-soluble sodium vanadate. The V is then recovered from the pregnant leach solution (PLS) by precipitation (Vanitec, 2022). This process results in the extraction of V only from the titanomagnetite resource, both Ti and Fe form part of by-product stream (Steinberg, et al., 2011).

The different stages involved in the conventional V primary production process (Vanitec, 2022) include:

- Roasting
- Leaching
- Impurity rejection and precipitation
- Calcination

#### *2.3.1.1 Roasting*

The aim of roasting is to react the $V_2O_5$ present in the titanomagnetite with the Na reagent for the production of a water-soluble sodium metavanadate ($NaVO_3$). The different sodium reagents that can be used during this stage include NaCl, NaOH, $Na_2CO_3$, and $Na_2SO_4$. The chemical reactions of vanadium from titaniferous magnetite with these salts can be represented

according to the following reaction equations (Nkosi, et al., 2017, Nasimifar & Mehrabani, 2022):

| | | |
|---|---|---|
| $2NaCl + V2O5 + 0.5O2 \rightarrow 2NaVO3 + Cl2$ | chloride salt roasting in excess O2 | [1] |
| $2NaCl + V2O5 + H2O \rightarrow 2NaVO3 + 2HCl$ | chloride salt roasting with water | [2] |
| $NaOH + V2O5 \rightarrow NaVO3 + H2O$ | caustic roasting | [3] |
| $Na2CO3 + V2O5 \rightarrow 2NaVO3 + CO2$ | soda ash roasting | [4] |
| $Na2SO4 + V2O5 \rightarrow 2NaVO3 + SO3$ | sulphate roasting | [5] |

The use of the different Na reagents for the extraction of V from titanomagnetite resources has advantages and disadvantages associated with them. The use of NaCl is cost-effective since NaCl is readily available and require low operating temperatures. The disadvantage of using NaCl in the roasting process is the production of toxic by-products namely $HCl_{(g)}$ and $Cl_{2(g)}$. Also, the use of NaCl in the roasting process produces low V extractions since NaCl selectively reacts with V (Nkosi, et al., 2017; Mefos, 2006).

The $Na_2SO_4$ salt is highly "selective" but it produces toxic $SO_3$ gases which are not friendly to the environment. Nkosi et al (2017) confirmed that this salt requires relatively high operating temperatures of 1200°C to achieve the typical V extraction efficiencies of >85%. (Nkosi, et al., 2017). The widely used salt, $Na_2CO_3$, is non-selective (such that the reaction of $Na_2CO_3$ and V is favoured and may result in high V extractions) and requires moderate operating temperatures of up to 1150°C. The environmental impact of using $Na_2CO_3$ instead of the others salts is preferred as it does not produce toxic gases when compared with the other Na reagents. Also, the $Na_2CO_3$ cost is generally lower as compared to the other Na reagents.

The use of NaOH reagent is thermodynamically and environmentally favoured as the conversion produces $H_2O$ as a by-product when compared to the other sodium reagents which produces toxic by-products. The only challenge with using this Na reagent is the low melting temperature of NaOH (Gilligan & Nikoloski, 2020).

The V primary production process highly depends on the efficiency of the roasting stage, i.e. conversion of $V_2O_5$ to $NaVO_3$ according to equation [1] to [5] above. The challenges that were found during the roasting process include the availability of free CaO and $SiO_2$. Regarding free CaO, there is high possibility of formation of insoluble vanadates ($CaO*V_2O_5$) which can be

minimised by limiting the CaO concentration to <1% (Mefos, 2006). The challenge with free $SiO_2$ is the possibility of forming low melting ($Na_2O*Fe_2O_3*4SiO_2$) phase (Mefos, 2006). To avoid the formation of this low melting phase, the free $SiO_2$ must be limited to <3%. Since the roasting stage requires an oxidative environment, the available free oxygen must be >4% to ensure maximum oxidation of vanadium (Mefos, 2006).

#### *2.3.1.2 Leaching*

The leaching process is conducted in order to dissolve the $NaVO_3$ formed during the roasting process into a solution using a lixiviant. The different lixiviants that can be used for leaching out $NaVO_3$ is either water ($H_2O$) or an acid such as $H_2SO_4$ (Yang & Yang, 2023, Nasimifar & Mehrabani, 2022). Depending on whether water or acid is used as a lixiviant, the leaching process can proceed according to the reaction equation [6] or [7].

| | | |
|---|---|---|
| $NaVO_3 + H_2O \rightarrow H_2VO_4^- + Na^+$ | $H_2O$ leaching | [6] |
| $NaVO_3 + H^+ \rightarrow VO_2^+ + Na^+ + H_2O$ | acid leaching | [7] |

The acid/ $H_2SO_4$ lixiviant is non-selective but effective. The use of $H_2SO_4$ lixiviant can dissolve all vanadates that formed during the roasting process and can results in precipitation of many impurities such as Ca and Mg as shown in equations [8] and [9].

| | | |
|---|---|---|
| $Mg_2V_2O_7 + 3H_2SO_4 \rightarrow (VO_2)_2SO_4 + 2MgSO_4 + 3H_2O$ | magnesium vanadate | [8] |
| $Ca_3V_2O_8 + 4H_2SO_4 \rightarrow (VO_2)_2SO_4 + 3CaSO_4 + 4H_2O$ | calcium vanadate | [9] |

The most commonly used lixiviant is $H_2O$ due to its selectivity and $NaVO_3$ dissolution efficiency, it also costs less and is freely available (Nasimifar & Mehrabani, 2022; Mefos, 2006).

#### *2.3.1.3 Impurity rejection and precipitation*

The aim of the impurity rejection stage is to remove silicon (Si) and aluminium (Al) impurities through the addition of aluminum sulfate ($Al_2SO_4$) as shown by the chemical reaction in equation [10]. The Si and Al impurities precipitate as $Al_2SiO_5$ and the $NaVO_3$ concentrate in the solution with the removal of impurities. This process occurs at pH between 7 and 8.

$$Al_2(SO_4)_{3(s)} + Na_2SiO_3 + 2H_2O \rightarrow Al_2SiO_{5(s)} + Na_2SO_{4\,(aq)} + 2H_2SO_{4(aq)} \quad [10]$$

The precipitation stage involves the introduction of ammonium sulfate $(NH_4)_2SO_4$ for the production of ammonium metavanadate as shown in equation [11]. Ammonium metavanadate (AMV) ($NH_4VO_3$) is commonly precipitated from the purified PLS at pH 8.2 and above (Goso, et al., 2016). Using AMV is problematic since it produces ammonia and this is an environmental challenge (Nasimifar & Mehrabani, 2022).

$$(NH_4)_2SO_{4(s)} + 2NaVO_{3(aq)} \rightarrow 2NH_4VO_{3(s)} + Na_2SO_{4(aq)} \quad [11]$$

#### *2.3.1.4 Calcination*

The aim of the calcination stage is the removal of $H_2O$ and ammonia- ($NH_4$) for the production of high purity $V_2O_5$. The calcination stage involves the introduction of heat to the produced $NH_4VO_3$ for the production of $V_2O_5$ through equation [12] (Gilligan & Nikoloski, 2020).

$$NH_4VO_3(s) + heat \rightarrow V_2O_5(s) + H_2O(g) + NH_3(g) \quad [12]$$

### 2.3.2 V and steel coproduction process

V and steel coproduction process supports about 70% of the global V production from the processing of titanomagnetite. The co-production process mainly occurs in China and Russia. China is the largest producer of V via the coproduction process. The industrial companies involved in the coproduction process include; Pangang Group, HBIS Chengsteel, Chengde Jianlong, SichuanTranvic, and Sichuan Deshang as the key players in V production. Russia is the second largest producer of V through the coproduction process at EVRAZ. The 3$^{rd}$ producer of V in the world is South Africa which has declined in production since EHSV is no longer in operation. The major players in South Africa that produce V are Glencore and Bushveld Minerals The 4$^{th}$ V production company, Largo Inc, is situated in Brazil (Blue Project, 2022).

The V and Fe coproduction process, also known as the smelting process, involves smelting the titanomagnetite concentrate in a blast or electric arc furnace (BF or EAF) for the production of vanadium-bearing pig iron and titanium-bearing slag (commonly known as the titaniferous slag). The pig iron produced in the furnace oxidized to produce a V-rich slag and high purity iron, which is used in steelmaking, by blowing air through it. The produced V-rich slag is then subjected to the roast-leach process for the production of $V_2O_5$. The smelting of titanomagnetite can be conducted either in the presence (fluxed) or absence (fluxless) of fluxes.

#### *2.3.2.1 Fluxed smelting of titanomagnetite*

The smelting of titanomagnetite has been conducted in blast furnace (BF) and electric-arc furnaces (EAF) by mixing the ore with the reductant and fluxes such as dolomite or quartz to lower operational temperatures. Addition of fluxes, enables the $TiO_2$ to be fluxed out into the slag and also minimize the crystallization of the spinel phase. The use of the BF requires excessive reductant addition that will aid in the reduction of FeO to its metallic state. The use of blast furnace requires good management of the feed composition when the feed has high concentrations of $TiO_2$ (Taylor, et al., 2006; Steinberg, et al., 2011).

Fluxed smelting of the titanomagnetite, requires high reducing condition for the reduction of $Fe_3O_4$ and $V_2O_5$ as per equations [13] and [14] (Maphutha, et al., 2017; Sitefane, et al., 2017). The demands of high reducing conditions can cause challenges in the furnace as high melting titanium compounds form. These compounds may result in an increased viscosity of the slag. The other challenges that were reported with high reducing conditions include poor burden permeability, a decrease in productivity and foaming of the slag. These encounters can be resolved by diluting the feed material with high grade iron ore, or fluxing, or through physical separation process aiming at lowering the $TiO_2$ content. These solutions also have an adverse influence on the recovery of elements of interest (Steinberg, 2008).

The produced titanium bearing slag is discarded as the $TiO_2$ concentrates are relatively low at ~35%.

$$Fe_3O_4 + 3C \rightarrow 3Fe + 4CO \quad [13]$$

$$V_2O_5 + 5C \rightarrow 2V + 5CO \quad [14]$$

Figure 3 shows the flowsheet used by the now-defunct EHSV (Steinberg, et al., 2011). From the flowsheet it can be seen that the first stage involve the mixing of the titanomagnetite, with a carbonaceous reductant, and fluxes. The fluxes that used include dolomite and quartz. These are subjected to a pre-reduction stage using the kiln. Pre-reduction is conducted at temperatures of 1140°C. The pre-reduced material is then introduced into a hot furnace for smelting at 1350°C. The smelting process produces a Ti-bearing slag which, is discarded, and V-bearing pig iron. The pig iron is then transferred into the shaking ladle furnace and the oxygen ($O_2$) is blown in order to remove the V. The ladle furnace is kept at temperatures above 1400°C, and this is done to maximize the V oxidation. The iron is then transferred into the basic oxygen

furnace (BOF) for further processing and production of steel products. The V-rich slag produced from the ladle furnace is further processed through the roast-leach process for the extraction of V (Taylor, et al., 2006, Steinberg, et al., 2011).

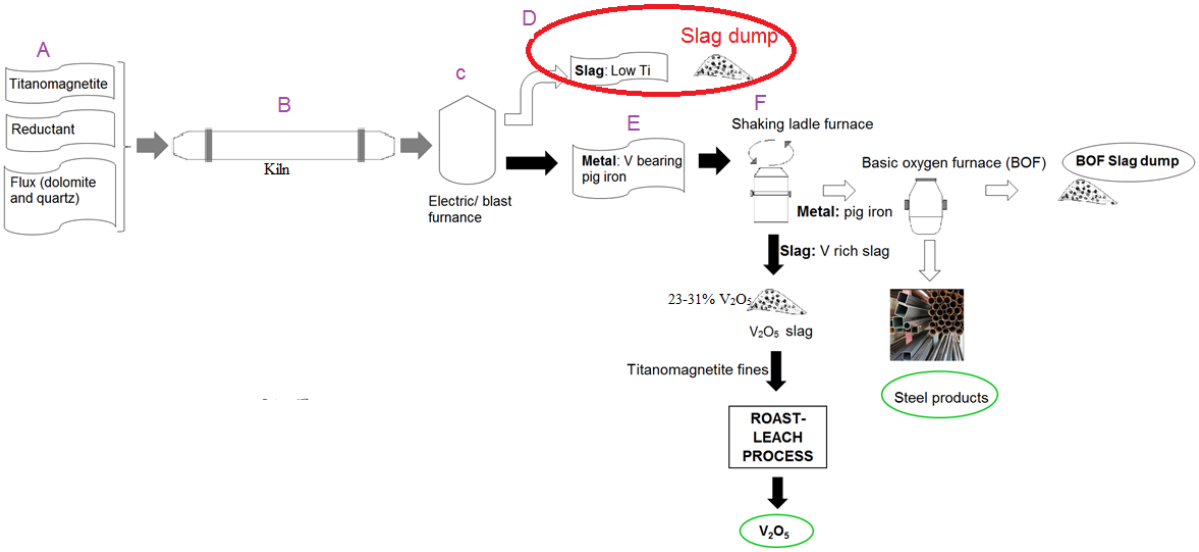


Figure 3 Typical flowsheet of the fluxed smelting technology from EHSV (Steinberg, et al., 2011)

### *2.3.2.2 Fluxless smelting of titanomagnetite*

The fluxless smelting approach of the titanomagnetite is basically aimed at Fe extraction in the absence of fluxes. The iron oxide is reduced by a carbonaceous solid reductant into its metallic Fe. The fluxless smelting normally takes place at temperatures of 1650°C (Boyd, et al., 1993). Fluxless smelting results in high Fe in the slag. The residual FeO in the fluxless smelting act as a self-fluxing agent. This process produce a $TiO_2$-bearing slag and metallic Fe. Majority of the V reports to the slag since the process is less reducing. The produced V-rich slag is further processed for V recovery. The possibility of producing Ti-bearing slag with a higher $TiO_2$ content (i.e. $TiO_2$ grade above 48%) through the fluxless smelting approach is possible if the impurities are minimised.

Figure 4 shows a typical flowsheet of the fluxless smelting technology. From the figure, it can be seen that the titanomagnetite is reacted with a reductant in an arc furnace. The resulting products include the Ti-bearing slag which is further processed for the production of sponge Ti. The produced metallic Fe is further processed for the production of pig iron.

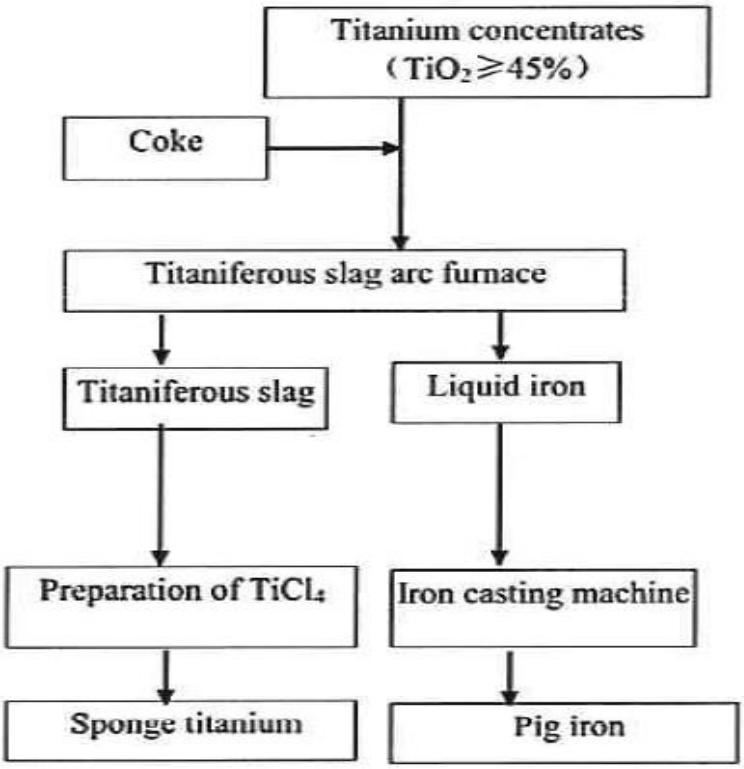


Figure 4 Typical flowsheet of the fluxless smelting technology

## 2.4 Beneficiation of titaniferous slags

A number of investigations have been conducted for the valorization of titaniferous slags for the extraction of V and $TiO_2$ present (Goso, et al., 2021; Goso, et al., 2016; Hassell, et al., 2016; Van Vuuren & Tshilombo, 2011; Pistorius, 2011; Xiao-hua, et al., 2008; Zhang, et al., 2007; Fouad, 2005; Becker & Dutton, 2002). The different approaches/techniques proposed by some of these studies are discussed in the following sections.

V extraction from titaniferous slags has been investigated using the V primary production process. The major modifications have been conducted in the roasting and leaching stages. In the most recent study, Yao, et al. (2023) investigated the direct roasting approach to determine the effect of temperature and time on the phase transformation of the spinel and fayalite phases from the V-Cr slag. The direct roasting process involved roasting their V-Cr slag in the furnace without the addition of salts. The study showed that at high temperatures of 900°C and 1.5 hours, the spinel that was present in the investigated slag was completely destroyed. The V extraction of 97% was achieved after leaching using $H_2SO_4$ as a lixiviant. Lee, et al. (2021) explained the aim of direct roasting process as breaking of the iron phases that surround the

spinel phase in order to enable the Ca and Mg to form vanadates that are leachable in acid. This approach is commonly used for slags with high CaO/ MgO ratio. These results agree with those of Li & Xie, (2012) who investigated direct roasting on a high calcium vanadium slag. Their results showed the complete decomposition of the spinel phase at 800°C. Also, the highest V leaching rate of 90.6% was obtained when the slag was roasted at 850°C for 60 minutes (Li & Xie, 2012).

The decomposition of the spinel phase of the titaniferous slag has been proved to be possible by using the conventional salt roast leach process. The aim of using sodium salt is to form the soluble vanadates that can be leached out. Lee, et al. (2021) reported Gibbs free energies for using different salt. The results showed that the formation of sodium vanadates were favourable provided the roasting temperature is sufficient to form these sodium vanadates (Lee, et al., 2021). Lekobotja, et al. (2017) also investigated the effect of Na salt addition on V extractions of the titaniferous slag. Their results showed an increase in V extractions with increasing Na salt additions. The highest V extractions of 27% were attained at 100% stoichiometric Na addition, also the decomposition of the spinel phase was achieved. The chemically inert phase was replaced by the formation of the nepheline phase (Lekobotja, et al., 2017).

The lime roasting approach has been specifically aimed at high Cr containing slags. The main aim of lime roasting is to acquire leachable calcium vanadates. These reactions have been proven to be spontaneous as the Gibbs free energies were favorable at temperatures between 400°C to 1000°C (Lee, et al., 2021).

Tawane, et al. (2021) showed that the extraction of V using sulfation roasting was also possible on the titaniferous slag. The V extraction efficiencies attained by Tawane, et al. (2021) were generally low at 12%.

Goso, et al., (2021) demonstrated the possibility of upgrading the titaniferous slag to a synthetic rutile with $TiO_2$ grade >90%. The titanifeorus slag was upgraded using a modified UGS process aimed at removing the Al and Mg impurities that were present (Goso, et al., 2021). The UGS process is aimed at removing alkaline impurities through five stages namely; sizing, oxidation, reduction, leaching, and washing and calcination. The modified UGS process involved the use of the leaching stage for the removal of alkaline impurities.

Van Vuuren & Tshilombo, (2011) proposed the beneficiation of the titaniferous slag by nitriding the slag at high temperatures of 1300°C and an excessively reducing environment. The produced titanium nitride was further subjected to the chlorination process for the production of titanium tetrachloride. The produced titanium tetrachloride is an important intermediate product for production of $TiO_2$ pigment or Ti metal (Van Vuuren & Tshilombo, 2011). Zhang, et al., (2007) aerated the molten Pangang titaniferous slag with compressed air in order to oxidize Ti and Fe. The dispersed Ti was enriched in the perovskite phase, which was further upgraded for the production of $TiO_2$-rich material (Zhang, et al., 2007). The upgrading of $TiO_2$ from the perovskite phase was proved possible through alkaline roasting followed by leaching conducted to remove impurities (Wang, et al., 2010).

## 2.5 Titanium mineral concentrates

$TiO_2$ is the main source of Ti and about 90% of the world's consumption of $TiO_2$ originates from ilmenite resources. The most common minerals where Ti-bearing ores generally occurs include the primary ilmenite ($FeTiO_3$), rutile ($TiO_2$), and leucoxene (weathered ilmenite), and some substitutes that compete as $TiO_2$ feedstock. The concentration of $TiO_2$ in ilmenite ranges from 40% to 65%, whilst in rutile it is restricted to roughly 95% in nature and leucoxene $TiO_2$ content remains above 95% (Subasinghe & Ratnayake, 2022; Gambogi, 2022; Moitse, 2008; Ngugen & Lee, 2019).

The major Ti reserves in the world are situated in China, Australia, India, Brazil, Norway, Canada, SA, Mozambique, and Madagascar as shown in Table 4. In SA, Ti mineral resources are mainly found along the coasts in beach placer sands. Figure 5 shows the mine production of $TiO_2$ per country. China has the highest reserves and is also the world first producer of $TiO_2$ and consumer Ti mineral concentrate with 36% reported in 2021. The second world best Ti mineral consumer is Mozambique at 12%. SA is placed third country for Ti mineral consumption ranking at 10% (Statista , 2023; Gambogi, 2022).

Table 4 Titanium mineral reserves in the world (Gambogi, 2022)

| Country | Reserves (thousand metric tonnes) |
|---|---|
| China | 230 000 |
| Australia | 160 000 |
| India | 85 000 |
| Brazil | 43 000 |
| Norway | 37 000 |
| Canada | 31 000 |
| South Africa | 30 000 |
| Mozambique | 26 000 |
| Madagascar | 22 000 |

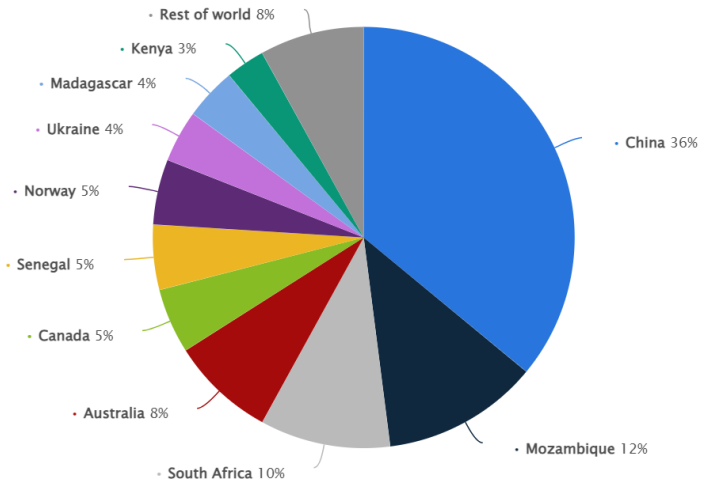


Figure 5 Mine production of $TiO_2$ by country (Statista , 2023)

## 2.6 Processing of ilmenite

Ilmenite has low $TiO_2$ grade and therefore requires upgrading in order to be a suitable feedstock for $TiO_2$ pigment production. This upgrading of the ilmenite ore generally occurs through the smelting process (Maphango, 2013). Ilmenite ore normally contains $TiO_2$ and FeO with impurities such as Mg, Ca, Si, Cr, V etc. to name a few. Ilmenite smelting involves a carbothermic reaction of C with FeO and $TiO_2$, as per equations [15] and [16], for the production of a primary $TiO_2$-rich slag and pig iron as a by-product at temperatures between 1650°C - 1700°C (Murty, et al., 2007). Since all the impurities reports to the slag, the produced $TiO_2$-rich slag can either contain high or low impurities depending the ore grade and type of reductant used during smelting. The amount of CaO and MgO present in the $TiO_2$-rich slag determine the downstream hydrometallurgical process for $TiO_2$ pigment production. The

hydrometallurgical processes involved in $TiO_2$ pigment production include the sulfate and chloride processes and these are shown by the flowsheets in Figure 6 and Figure 7 respectively.

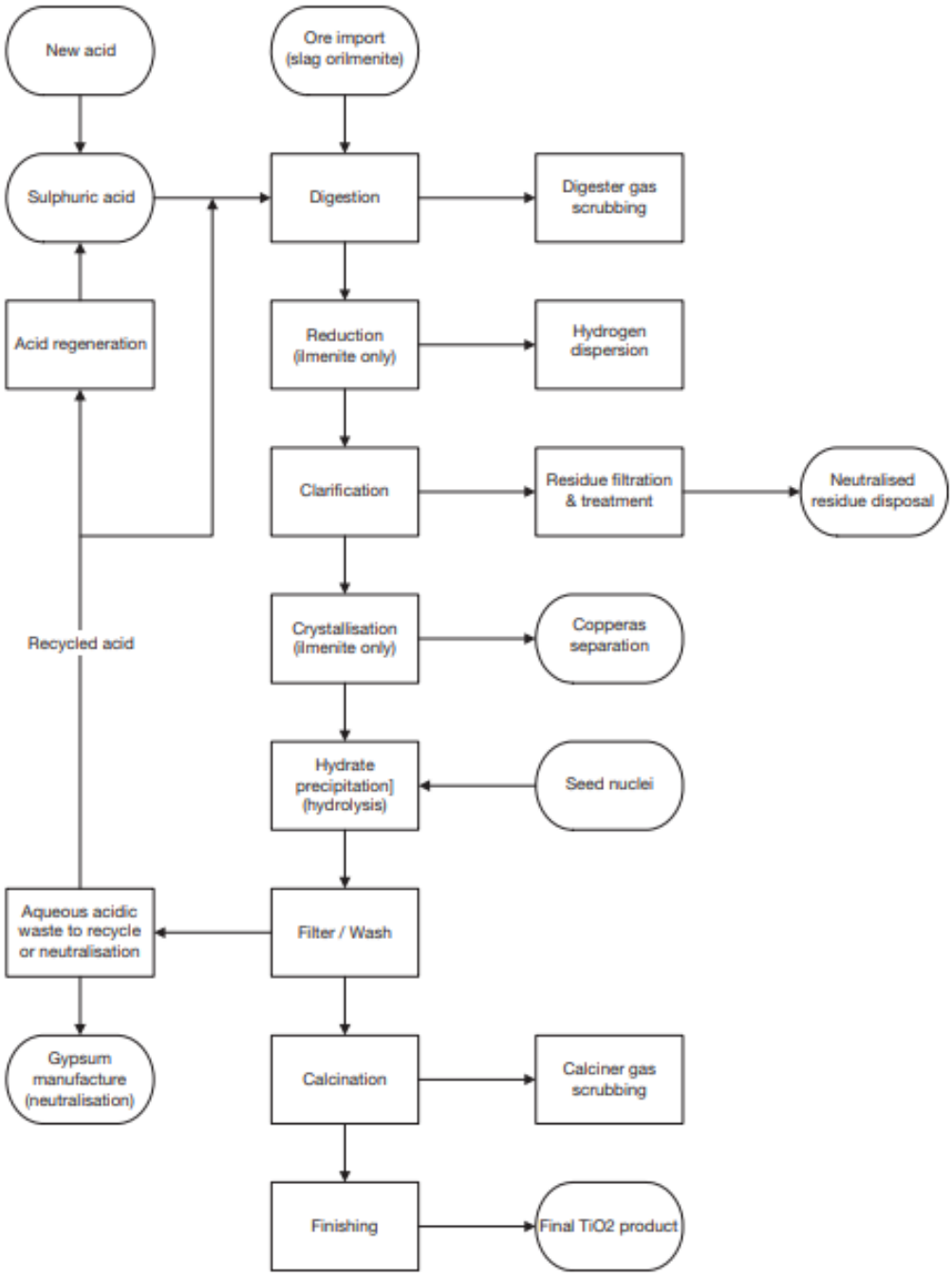


Figure 6 Typical flowsheet of $TiO_2$ pigment production using sulfate process

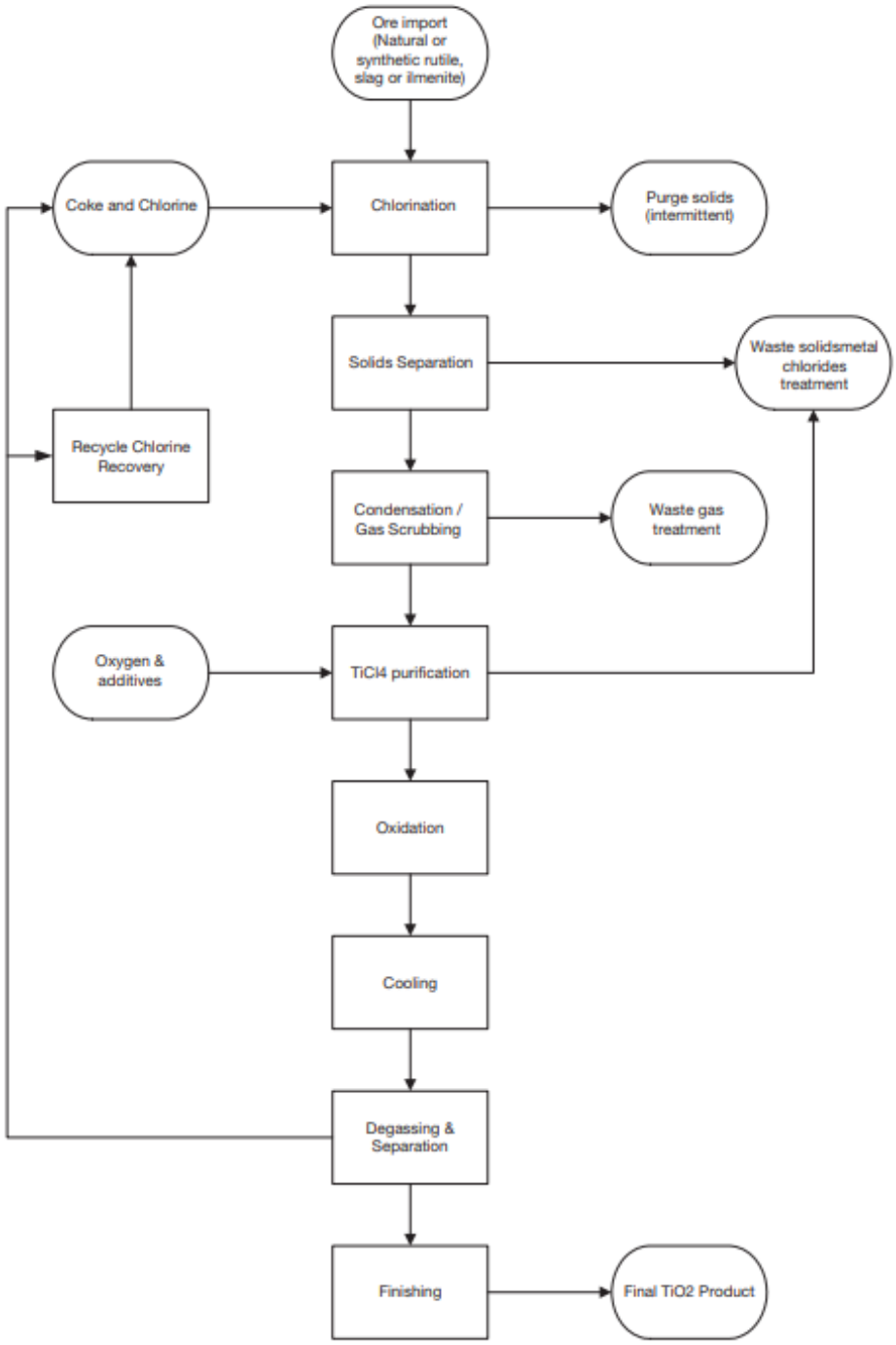


Figure 7 Typical flowsheet of $TiO_2$ pigment production using chloride process

The chloride process, which is the preferred $TiO_2$ pigment production, is sensitive to impurities present in the slag. The slag with high CaO and MgO impurities normally contains about 80% $TiO_2$ and require further upgrading through the sulfate process. Low CaO and MgO impurity containing slags generally have a $TiO_2$ content of >85% and can follow the chloride process for $TiO_2$ pigment production (Murty, et al., 2007; Pistorius, 2008; Gázquez, et al., 2014). Over the years, the chloride process has been the preferred process for slag upgrading.

$$FeO + C \rightarrow Fe + CO \quad [15]$$

$$TiO_2 + C \rightarrow Ti_2O_3 + CO \quad [16]$$

### 2.6.1 Competitive $TiO_2$ feedstock requirements

According to Stanaway, 1994, the $TiO_2$ feedstock requires to have the properties shown in Table 5 for the concentrate to be accepted as a competitive feedstock. Chloride process is conducted in the fluidized bed reactor and it involves the reaction of $TiO_2$ feedstock with a carbonaceous material and in the presence of chlorine gas. This reaction is conducted at 900°C and follows equations [17] and [18] for the production of titanium tetrachloride ($TiCl_4$), carbon dioxide ($CO_2$), and other metal chloride impurities. The next step involves condensation and purification of $TiCl_4$ by cooling down the gas stream such that other metal chlorides precipitates and separated as impurities. The final stage involves oxidation of $TiCl_4$ for the production of $TiO_2$ and $Cl_2$ as per equation [19]. (Kitsara, et al., 2023; Stanaway, 1994).

$$2C + O_2 \rightarrow 2CO \quad [17]$$

$$TiO_2 + 2Cl_2 + 2CO \rightarrow TiCl_4 + 2CO_2 \quad [18]$$

$$TiCl_4 + O_2 \rightarrow TiO_2 + 2Cl_2 \quad [19]$$

The required specification in the chloride process include the:-

- Grain size and bulk density of the $TiO_2$ feedstock. The grain size and bulk density are important since the chloride process is conducted in a fluidized bed reactor. These will minimise the blow-over of the material in the reactor.
- Low MgO and CaO impurities in the feedstock. At the reaction temperature, the alkalines form liquid chlorides that normally prevent fluidization of the material.
- Low FeO concentrations in the feedstock. Chlorine reacts with Fe to produce iron chloride and this minimize the amount of the ‘required’ reagent which is chlorine.

- Low $SiO_2$ as it has the possibility of coating the mineral grain and preventing their reaction with chlorine.
- Minimum radioactive elements as they accumulate in the waste and product streams.

The basic requirement in sulfide process is for all impurities present in the $TiO_2$ feedstock to dissolve in concentrated sulfuric acid ($H_2SO_4$) (Borowiec, et al., 1998). The sulfate process involves dissolution of $TiO_2$ in concentrated $H_2SO_4$ to produce titanyl sulfate ($TiOSO_4$), iron sulfate ($FeSO_4$), and $H_2O$ as shown in equation [20]. The solution is then precipitated and hydrolized to produce hydrated $TiO_2$ as illustrated in equation [21]. The hydrated $TiO_2$ is separated through filtration before removal of water and acid through calcination as shown by chemical reaction [22] (Kitsara, et al., 2023; Stanaway, 1994).

$$FeTiO_3 + 2H_2SO_4 \rightarrow TiOSO_4 + FeSO_4 + H_2O \quad [20]$$

$$TiOSO_4 + H_2O \rightarrow TiO_2nH_2O + H_2SO_4 \quad [21]$$

$$TiO_2nH_2O \rightarrow TiO_2 + nH_2O \quad [22]$$

For the success of the sulfate process, the required specifications include:-

- Fine grains as they favour the reactivity of $TiO_2$ feedstock with $H_2SO_4$.
- Low Fe content in the $TiO_2$ feedstock. Fe forms $FeSO_4$ in the dissolution stage and must discarded as waste. The lower the Fe content, the minimal the waste that must be disposed.
- Low Cr, V, and Nb content as high amounts change the $TiO_2$ pigment color.
- Minimum Ca and P because they prevent the crystal development above a certain level.
- Low radioactive materials since they become concentrated in the waste and product streams.

Table 5 Competitive $TiO_2$ feedstock specifications (Stanaway, 1994)

| Characteristic | Value |
|---|---|
| $TiO_2$ | >90% |
| $SiO_2$ | <1.5% |
| $Al_2O_3$ | <1.0% |
| $MnO_2$ | <1.0% |
| $Cr_2O_3$ | <0.1% |
| $P_2O_5$ | <0.05% (required by sulfate process) |
| $Nb_2O_5$ | <0.1% |
| CaO | <0.2% (required by chloride process) |
| MgO | <1.0% (required by chloride process) |
| U + Th | <100 ppm (prefer <50) |
| Size: 100 mμ | +50% (required for chloride process) |
| 40 mμ | +95% (required for chloride process) |
| Bulk density | +2 kg/L (required for chloride process) |

### 2.6.2 Upgraded titania slag (UGS) process

In 1998, Borowiec, et al., developed a method for the $TiO_2$-rich slags and naturally occuring ilmenite that contain high alkaline oxides. This method is aimed at the removal of alkaline impurities for the products to be used in the preferred chloride process as opposed to be restricted to the sulfate process. This process comprises of five steps, namely;-

i. Sizing of the $TiO_2$ source

   Since this process uses the fluidized bed reactor, the particle size of the $TiO_2$ material is crucial to prevent the blockage. The particle size of the $TiO_2$ source was maintained between 75 – 850 microns.

ii. Oxidation stage

   This step is conducted at temperatures between 950°C and 1025°C, and not exceeding 1100°C, in an oxidized atmosphere. The oxidation stage is aimed at oxidation of $Ti^{3+}$ to $Ti^{4+}$ and $Fe^{2+}$ to $Fe^{3+}$ as shown in the chemical reaction [23]. The main products of the oxidation stage are rutile and pseudobrookite

$$(FeTi_2O_5)_{0.32}(MgTi_2O_5)_{0.33}(Ti_3O_5)_{0.35} + 0.255O_2 \rightarrow (Fe_2TiO_5)_{0.16}(MgTi_2O_5)_{0.33} + 1.53TiO_2 \quad [23]$$

iii. Reduction stage

   Reduction step is also conducted in a fluidized bed reactor at temperatures between 800°C - 850°C, and not exceeding 900°C, in a reductive environment. The reducing agent can either be natural gases such as CO, $H_2$ or solid carbon such as coke or coal

fines. This stage involves selective reduction of $Fe^{3+}$ to $Fe^{2+}$ or metallic Fe without reducing the $Ti^{4+}$ previously oxidized. This reduction reaction is presented by chemical reactions presented by equations [24] and [25].

$$Fe_2O_{3(s)} + 3C_{(s)} \rightarrow 2FeO_{(s)} + 3CO_{(g)} \quad [24]$$

$$FeO_{(s)} + C_{(s)} \rightarrow Fe_{(s)} + CO_{(g)} \quad [25]$$

iv. Removal of impurities through leaching

Removal of impurities can be conducted through acid (HCl) and/or caustic leaching. The treated $TiO_2$ is mixed with HCl at elevated temperatures to leach the impurities and upgrade the product. Most of the impurities are removed in HCl leaching, except for Si which is leached out in caustic leaching through the chemical reaction shown in equation [26].

$$SiO_{2(s)} + 2NaOH_{(aq)} \rightarrow Na_2SiO_3(aq) + H_2O(l) \quad [26]$$

v. Washing and calcination

The upgraded residue is then washed and calcined at high temperatures to remove water and residual adsorbed species.

# CHAPTER 3

# EXPERIMENTAL PROCEDURES

This chapter describes the materials and equipment used to achieve the project's objectives. It also includes the experimental flowsheet showing step-by-step procedures undertaken to complete the investigation.

## 3.1 Materials

The materials used for these experiments include titaniferous slag, Na reagents, hydrochloric acid (HCl), and deionized water. Titaniferous slag was obtained from the EHVS waste slag dump. The Na reagents used are $Na_2CO_3$, $Na_2SO_4$ and NaOH which were purchased from ACE (Associated Chemical Enterprises), with purities of 99.5%, 99.0% and 98.0% respectively. Hydrochloric acid that was used for leaching tests was purchased from Sigma-Aldrich, and it has a concentration of 37.0%. The deionized water used during the leaching testwork was from a Millipore water purification system designed to supply laboratories with few litres of deionized water per day.

## 3.2 Equipment

Different equipment used for the laboratory scale roasting and leaching testwork are explained in the following sections.

### 3.2.1 Sample preparation equipment

Large chunks of titaniferous slag were randomly selected from EHSV slag dump at ten different locations. A representative sample was prepared by crushing the large chunks of the slag into a single batch using the crushing machine called Jaw Crusher. The crushed titaniferous slag was splitted using a rotary splitter and screened using a Sieve Shaker in order to measure the particle size distribution (PSD) range of -850 + 106 µm. The sieve sizes used for sample collection were 1000, 850, 600, 425, 300, 212, 150, 106, and 75 µm. For drying, a Gallenkamp hotbox oven set at the required drying temperature was used.

### 3.2.2 Roasting equipment

Roasting tests were conducted in a chamber furnace. The chamber furnace is equipped with a thermocouple that is used to measure the temperature inside the furnace. The temperature is measured by a controller which programs the operation temperature, heat rate and the residence time. Figure 8 shows the photographic image of the chamber furnace used to conduct the roasting experiments. The dimensions for the inside chamber of the furnace are 46 x 20 x 18 cm. Commercially available silicon carbide (SiC) trays were used for roasting. The trays were procured from GeeKay Industrial Ceramics Pty (Ltd) and the dimensions are 234 x 135 x 40 mm.


Figure 8: Photographic image of the chamber furnace

### 3.2.3 Leaching equipment

Leaching tests were conducted in a 500 mL round bottom flask with double necks and fitted with a condenser. The condenser's water inlet tube was connected to the tap whilst the outlet pipe was placed on the draining channel. The reactor was placed in an oil bath placed on top of the magnetic hotplate, make and model Heidolph MR Hei-Tec from Labotec, to maintain the required leaching temperature. The temperature inside the reactor was measured with a thermometer.

### 3.2.4 Analytical instrumentation

Raw materials, roasting, and leaching base metal products were analysed by Induction Coupled Plasma Optical Emission Spectroscopy (ICP-OES) using Thermo iCAP 7600, Agilent 5900 with detection limits that vary by elements and method. The sodium present in the raw material and products were analysed using the Atomic Absorption Spectroscopy (AAS) from the Perkin Elmer PinAccle instrument. The phase chemistry was conducted by scanning electron microscopy (SEM) with model Zeiss MA15 EVO® equipped with a Bruker energy-dispersive spectrometer (EDS). The X-ray diffractometer (XRD) was measured using a Bruker D8 instrument.

## 3.3 Experimental

A summary of the experimental flowsheet is shown in Figure 9. The flowsheet gives the different stages that were used for vanadium and titanium extraction. Vanadium extraction follows the stages in the order of roasting, water leaching, precipitation and calcination for the production of $V_2O_5$. Extraction of titanium uses the residue from the water leaching stage to undergo acid and caustic leaching steps for the concentration of $TiO_2$ in the produced residues.

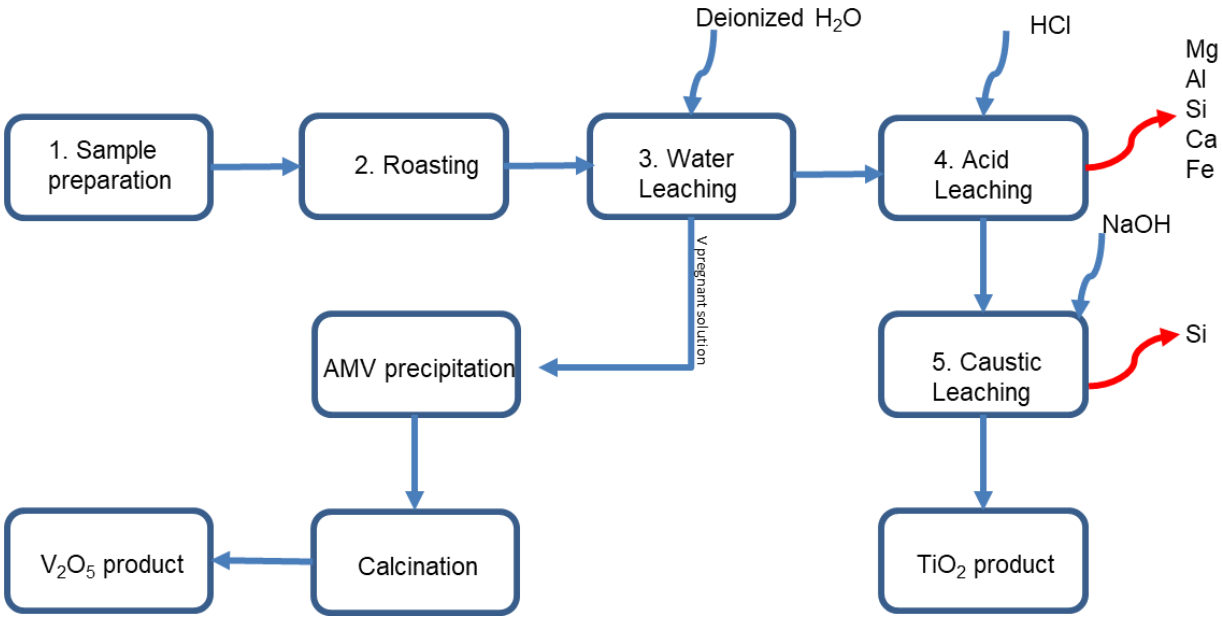


Figure 9 Flowsheet of the experimental procedures conducted

### 3.3.1 Sample preparation

Large chunks of titaniferous slag from EHVS were crushed to -2 mm particle sizes. The crushed material was subjected to screening using different screen sizes. The particle size ranges used in the current study are -850 to +106 µm and -300 µm + 106 µm. A 200 g of the screened material was mixed with a prepared sodium salt reagents (i.e. $Na_2CO_3$, NaOH and $Na_2SO_4$) at either 115% or 200% calculated stoichiometric addition. The selection of the Na addition was a build-up from Lekobotja, et al., 2017 who demonstrated the decomposition of the spinel phase at 100% stoichiometric Na addition.

Preparation of Na salt reagent involved weighing the accurate amount of salt into a glass beaker and dissolving it using deionized water. This solution was mixed with 200 g titaniferous slag to make a slurry. The prepared slurry was dried in an oven, set at a temperature of 110°C, for a period of 12 hours. After 12 hours, the slurry was removed from the oven and allowed to cool down. Since the dried mixtures had the particles compacted together, the mixtures were rolled up using a cylindrical alumina tube to separate the particles and release the particles to the PSD of the titaniferous slag initially used. Table 4 and 5 below shows the test matrix that was used for roasting and leaching experiments, respectively.

Table 6: Test matrix for different roasting parameters at constant leaching conditions

| Test | Temperature °C | Time (hours) | $Na_2CO_3$:NaOH | Stoichiometric Na addition | PSD (µm) |
|---|---|---|---|---|---|
| 1 | 1000 | 2 | 100:0 | 115% | +106 to -850 |
| 2 | | | 85:15 | | |
| 3 | | | 50:50 | | |
| 4 | | | 15:85 | | |
| 5 | | | 0:100 | | |
| 6 | 1000 | 2 | 100:0 | 200% | |
| 7 | | | 50:50 | | |
| 8 | | | 0:100 | | |
| 9 | 800 | 2 | Best ratio | Best stoichiometric addition | |
| 10 | 900 | | | | |
| 11 | Best temperature | 1 | Best ratio | Best stoichiometric addition | |
| 12 | | 3 | | | |
| 13 | Best temperature | Best time | Best ratio | Best stoichiometric addition | +106 to -300 |
| 14 | Best temperature | Best time | $Na_2CO_3$:$Na_2SO_4$ | Best stoichiometric addition | Best PSD |

Table 7 Test matrix for best roasting conditions at different HCl leaching parameters

| Test | Roasting conditions | $H_2O$ leaching conditions | HCl leaching time (hours) | HCl concentration | NaOH leaching condition |
|---|---|---|---|---|---|
| 15 | 1000°C, 2 hours, 100:0 $Na_2CO_3$:NaOH ratio, 200% stoichiometric Na | 70°C, 2 hours, s:l of 1:4, 350 rpm | 1 | 20% | 100°C, 3 hours, s:l of 1:4, 350 rpm, 2.15M NaOH solution |
| 16 | | | 4 | | |
| 17 | | | 8 | | |
| 18 | | | 16 | | |
| 19 | | | 24 | | |
| 20 | | | 24 | 15% | |
| 21 | | | | 25% | |

### 3.3.2 Roasting

The prepared mixtures of roasting salt and slag were placed in SiC trays and masses were recorded. The trays were placed in preheated muffle furnace where the temperatures of investigation will be maintained at 800°C, 900°C, and 1000°C. During the introduction of the SiC trays into the muffle furnace, the furnace temperature decreases due to the opening of the furnace. Once opened, the SiC tray is placed inside the furnace and the furnace door is closed. The furnace temperature then increases to the set temperature. Upon reaching the set temperature, the measurement of the test duration begins. The test duration at temperature varied from 1, 2, and 3 hours. After the roasting period, the tray was removed from the furnace and allowed to cool down. The mass after roasting was recorded to calculate the mass loss/ gain after the roasting test.

### 3.3.3 Water leaching

The leaching setup is shown in Figure 10. Water leaching experiments involved boiling deionized water in a beaker using the magnetic hotplate. Boiled water was then measured and poured into the reactor before adding 50 g of roasted titaniferous slag to achieve a pulp density with a solid to liquid (s:l) ratio of 1:4. The magnetic stirrer was placed inside the reactor before immersing the reactor into an oil bath placed on top of the magnetic hotplate. The temperature of the magnetic hotplate was raised and set in order to attain a leaching temperature of 70°C. The leaching temperature was measured with a thermometer positioned inside the reactor to measure the temperature of the leaching solution at 15 minutes intervals. The hot-place temperature was either increased or decreased when the leaching solution was lower or higher that the reaction temperature. The slurry was constantly agitated at a speed of 350 rpm for a period of 2 hours. After 2 hours the agitation was stopped and the leach reaction slurry was filtered, whilst hot, through Whatman 542 hardened ashless filter paper using a Buchner funnel. The leach liquor was collected and stored separately. The reactor with the remaining residue was filled with 200 mL of deionized water to remove all the remaining leach residue and the filter cake was washed three times with 200 mL of deionised water. The produced filter cake was dried overnight at 105°C. The filter cake and solution were subjected to bulk chemical and mineralogical analysis.

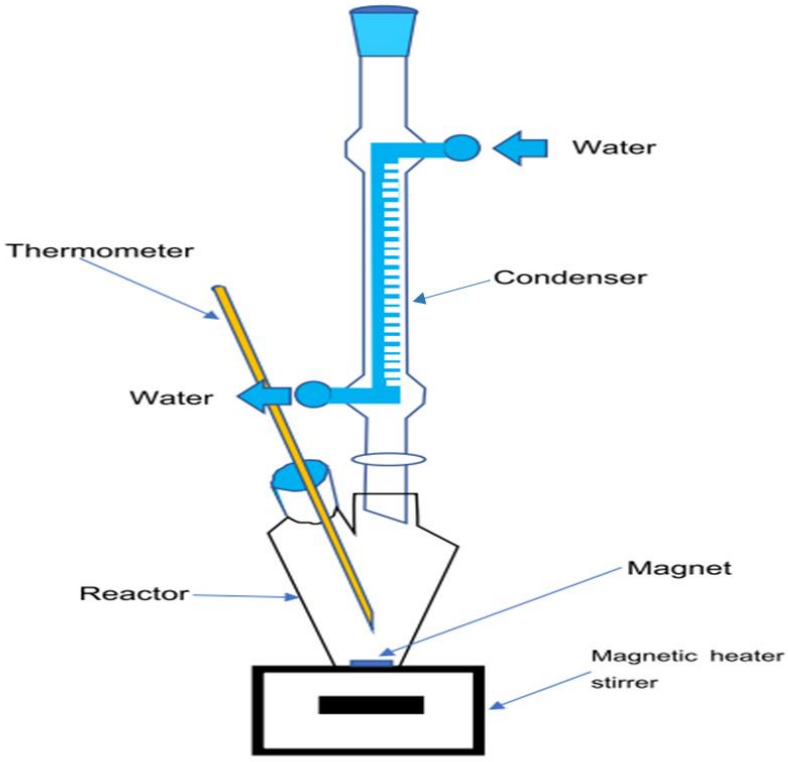


Figure 10 Schematic image of leaching setup

The vanadium extractions were calculated based on the chemical analysis of the leach residues using equation [27].

$$\%V \text{ extraction} = [1 - (\text{Mass } V_{\text{leach solids}}/\text{Mass } V_{\text{roast products}})] \text{ X } 100 \quad [27]$$

### 3.3.4 Acid leaching

Acid leaching was firstly conducted using 20% HCl solution prepared by diluting 37% concentrated HCl with deionized water for the test matrix in Table 6. The 20% HCl solution was measured and poured into the reactor before adding the water leach residue to maintain the s:l ratio of 1:4. Magnetic stirrer was then added into the mixture before placing the reactor in an oil bath. The magnetic hotplate was then heated up to a temperature that maintained the slurry at 110°C. The slurry was kept at temperature for different leaching times of 1, 4, 8, 16, and 24 hours while the agitation speed was maintained at 350 rpm before filtration. The filtration process was similar to that of water leaching where the slurry was poured onto the filter paper and the solution was collected in the Buchner funnel. The produced solution was collected before washing the remaining residue and filter cake with deionized water. The filter

cake was dried overnight at 50°C overnight. The produced filter cake and solution were analysed for bulk chemical analysis and mineralogical characterization.

The best leaching time was used to measure the leaching efficiency at different HCl solutions of 15% and 25%. The other parameters which include the temperature, stirring speed, solid to liquid ratio were kept constant during the leaching process.

### 3.3.5 Caustic leaching

Caustic leaching was conducted using NaOH prepared to a concentration of 2.15 M. The prepared NaOH solution was measured and transferred to the reactor before mixing with acid leach residue to achieve a s:l ratio of 1:4. The reactor was immersed in an oil bath while maintaining the agitation speed at 350 rpm using the magnetic stirrer. The magnetic hotplate was heated to maintain the reaction temperature at 100°C for a period of 3 hours before filtration. The filtration process was conducted in the presence of a filter paper that held the filter cake whilst the leach solution was collected in a Buchner funnel. The filtered solution was collected before rinsing the remaining residue from the reactor with deionized water and washing the filter cake. The produced filter cake was dried in an oven at 110°C overnight. The resulting filter cake and leach solutions were further examined for chemical and mineralogical analysis.

The $TiO_2$ recoveries based on the residues were calculated using equation [28]:

$$\%\ TiO_2\ \ recovery\ to\ residue = \frac{\%TiO_{2\ residue}\ x\ Mass_{residue}}{\%TiO_{2\ feed}\ x\ Mass_{feed}}\ \ x\ 100 \qquad [28]$$

where $\%TiO_{2\ residue/feed}$ is the concentration of $TiO_2$ in the residue or feed and
$mass_{\ residue/\ feed}$ is the mass of the residue or feed

### 3.3.6 Sample characterization

XRD analysis involved pulverization of each sample before characterization. Each sample was analysed with a Bruker D8 diffractometer, using a step size of 0.02º 2 theta (Ɵ) and a counting time of 3 seconds per step, applied over a range of 5 to 80º 2Ɵ (3 hours). The XRD method uses the net intensity of the main peaks of the mineral, and identification is based on the crystal structure of the mineral/ phase. Only crystalline minerals in amounts sufficient to diffract,

usually not less than 5 mass percent, are detectable. Amorphous phases cannot be detected with this technique. For qualitative XRD, phases are subdivided into predominant (>50 mass %), major (30-50 %), intermediate (15-30 %), minor (5-15 %), and trace (<5 %) abundances.

Characterisation of the sample with SEM involved mounting of each sample within the epoxy resin and polishing with paraffin to prevent the sample dissolution. The sample was subjected to SEM analysis using a Zeiss EVO® MA15 SEM equipped with a Bruker energy dispersive X-ray analyser (EDX/EDS). Standard operating conditions include an accelerating voltage of 20kV and a beam current of 200 pA. Note that EDS numerical data are normalised compositions (normalised weight percent).

## 3.4 Experimental difficulties

The difficulties that were encountered while conducting the experiments are discussed below. The ways in which these problems were minimized are also discussed in the following sections.

### 3.4.1 Roasting

The decreasing furnace temperature during insertion of the SiC tray was the first challenge that was encountered. This challenge could not be avoided since it was required for the furnace to be opened before inserting the material inside the furnace for a reaction to occur. The drop in furnace temperature was minimised by having 2 personnel to be involved during this stage. One person would open the furnace whilst the other would insert the SiC tray instead of one person opening and inserting the material before closing the furnace. The decrease in the furnace temperature was minimized to less than 50°C as compared to more than 100°C when one person was involved.

Another challenge that was faced during the roasting process was the sintering of material at high temperatures. Reaction temperatures above 1000°C proved to produce a sintered roast material. Sintering hinders further treatment of the roasted material as the leaching process was demonstrated to be impossible. The decrease in roasting temperature was successful as the roasted material did not require crushing or milling before the leaching process.

### 3.4.2 Leaching

Acid leaching was the only process that showed some difficulties in terms of the process and the products that were produced. The first challenge with acid leaching was seen during the stirring stage. It was seen that the addition of the residue to the reactor before adding the HCl solution did not agitate the material. The magnetic stirrer became stuck at the bottom of the reactor irrespective of the speed used. The agitation of the material was successful when the HCl solution was added first prior to the residue addition.

The next challenge encountered was during the drying stage of the leach residue. High-temperature drying of the acid leach residue at 110°C resulted in a mushy sample that was difficult to pulverize for chemical analysis. It was found that lowering the drying temperature to 50°C resulted in a dry material that was able to pulverize.

# CHAPTER 4

# ROASTING RESULTS

Experimental results for all the $V_2O_5$ extraction experiments conducted to optimize the roasting conditions are presented in this chapter. This chapter presents the chemical composition results of the raw/ feed, roasted, and leach solid/ residue materials. It also presents and discusses the effects of Na reagent composition, temperature, time, PSD, and different Na reagents on V extractions. Also, the phase chemistry of the material that produced the best results is presented and discussed in this chapter.

## 4.1 Characterisation of materials

### 4.1.1 Chemical composition of raw materials

The bulk chemical composition of the raw/ feed titaniferous slag is presented in Table 8. The results confirm that the slag contained 0.95% $V_2O_5$ and 35.6% $TiO_2$ as reported by Steinberg, et al., (2011). The chemical composition results also show that the slag contained high concentrations of impurities namely; $Al_2O_3$, CaO, FeO, MgO, and $SiO_2$. All these impurities were generally at concentrations higher than 7%. $Cr_2O_3$, MnO, and S were generally low at <1% concentrations.

Table 8 Chemical composition of the titaniferous slag (mass %)

| $Al_2O_3$ | CaO | $Cr_2O_3$ | *FeO | MgO | MnO | $SiO_2$ | $V_2O_5$ | $TiO_2$ | S |
|---|---|---|---|---|---|---|---|---|---|
| 7.90 | 14.3 | 0.38 | 7.18 | 9.45 | 0.64 | 19.2 | 0.95 | 35.6 | 0.34 |

*Total Fe expressed as FeO

### 4.1.2 Phase chemistry of raw materials

Figure 11 and Table 9 present the backscattered electron (BSE) image, EDS and XRD analysis results for the raw titaniferous slag used to complete these experiments. The different phases that were present in the titaniferous slag include spinel, pseudobrokite, titanaugite, and the Fe-rich alloy. V was mainly present in the spinel, pseudobrookite cc, and alloy phases, whilst Ti was present in all the phases but dominant in pseudobrookite cc and perovskite phases. As confirmed by Borowiec, et al.(1998) and Wang, et al (2018), the Ti in their titaniferous slag is mostly present in the pseudobrookite cc phase. The impurities, which include Mg, Ca, Al, Fe, and Si were present in the different phases of the raw titaniferous slag. Mg and Al impurities

were present in the spinel, pseudobrookite ss, and titanaugite while Ca was found in titanaugite and perovskite phases. Si and Fe impurities were found in titanaugite and alloy phases respectively.

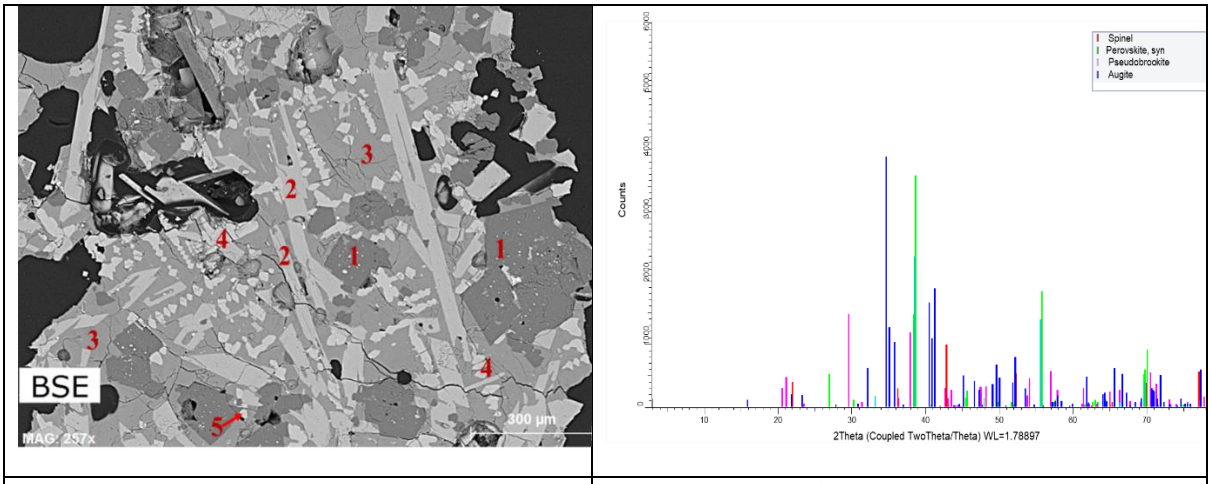


*a) BSE image* | *b) XRD spectra*

Figure 11 a) Backscattered electron image of the raw titaniferous slag, b) XRD spectra of the raw titaniferous slag

Table 9 EDS analysis results of the BSE phases and XRD phase composition of the raw titaniferous slag (mass %)

| **Spot** | **O** | **Mg** | **Al** | **Si** | **Ca** | **Ti** | **V** | **Fe** | **XRD results** |
|---|---|---|---|---|---|---|---|---|---|
| 1 | 44.3 | 18.2 | 32.8 | | | 4.1 | 0.5 | | Spinel |
| 2 | 40.4 | 6.7 | 2.7 | | | 49.7 | 0.5 | | Pseudobrookite ss |
| 3 | 42.3 | 7.7 | 8.2 | 14.7 | 18.1 | 8.9 | | | Titanaugite |
| 4 | 34.9 | | | | 32.0 | 33.1 | | | Perovskite |
| 5 | | | | | | 1.0 | 1.5 | 97.5 | Fe-Ti-V alloy |

## 4.2 Roasting of titaniferous slag

Roasting of titaniferous slag in high stoichiometric Na additions was conducted to destabilise the V-bearing phase for maximum V extractions. The reaction that occurs during the roasting of $Na_2CO_3$ and NaOH salts with the titaniferous slag spinel [(Mg, Fe)(Al, Ti, V)$_2O_4$] can be described by equations [29] to [36] (Lv, et al., 2022; Lee, et al., 2021; Parirenyatwa, et al., 2016). The main endmembers of the spinel were assumed to be $MgAl_2O_4$, $MgV_2O_4$, $FeAl_2O_4$, and $FeV_2O_4$ (Nkosi, et al., 2024). The Ti-containing endmembers such as $MgTi_2O_4$ and $FeTi_2O_4$ were not included since the solubility of $TiO_2$ in the solid solution of the spinel is limited (Goso, et al., 2024).

$$MgAl_2O_4 + Na_2CO_3 \rightarrow 2NaAlO_2 + MgO + CO_2 \quad [29]$$

$$MgV_2O_4 + Na_2CO_3 + O_2 \rightarrow 2NaVO_3 + MgO + CO_2 \quad [30]$$

$$FeAl_2O_4 + Na_2CO_3 + 0.25O_2 \rightarrow 2NaAlO_2 + 0.5Fe_2O_3 + CO_2 \quad [31]$$

$$FeV_2O_4 + Na_2CO_3 + 1.25O_2 \rightarrow 2NaVO_3 + 0.5Fe_2O_3 + CO_2 \quad [32]$$

$$MgAl_2O_4 + 2NaOH \rightarrow 2NaAlO_2 + MgO + H_2O \quad [33]$$

$$MgV_2O_4 + 2NaOH + O_2 \rightarrow 2NaVO_3 + MgO + H_2O \quad [34]$$

$$FeAl_2O_4 + 2NaOH + 0.25O_2 \rightarrow 2NaAlO_2 + 0.5Fe_2O_3 + H_2O \quad [35]$$

$$FeV_2O_4 + 2NaOH + 1.25O_2 \rightarrow 2NaVO_3 + 0.5Fe_2O_3 + H_2O \quad [36]$$

## 4.3 Effect of Na reagent composition and addition

The chemical composition of the roasted slags, leach residues, calculated V extractions, and resulting $TiO_2$ grades and $TiO_2$ recoveries to the residues are reported in the following sections. These results were reported for different stoichiometric Na additions and $Na_2CO_3$:NaOH ratios, at constant roasting temperature of 1000°C and a reaction period of 2 hours.

### 4.3.1 Chemical composition of the roasted slags and leached residues

The chemical composition of the titaniferous slags roasted in the presence of 115% and 200% stoichiometric Na addition and at different $Na_2CO_3$:NaOH ratios are presented in Table 10 and Table 11, respectively. The chemical composition results of the roast material showed dilution in the chemical compositions since excess Na additions were used. The concentrations of $TiO_2$ ranged from 22.5% to 26.4% and $V_2O_5$ varied between 0.60 – 0.68%% at different

$Na_2CO_3$:NaOH ratios. The concentrations that were significanlty diluted include $Cr_2O_3$, FeO, $SiO_2$, $V_2O_5$, and $TiO_2$. The concentrations of CaO, MgO, and MnO were generally the same whilst a substantial increase in $Al_2O_3$ concentrations was observed. The increase in $Al_2O_3$ concentrations might be attributed to the formation of a new stable phase after roasting. The chemical reactions [29], [31], [33], and [35] showed that the decomposition of the spinel phase in the presence of $Al_2O_3$ forms $NaAlO_2$ which might be the stable phase that caused high $Al_2O_3$ concentrations after roasting.

Table 10 Chemical composition (mass %) of the titaniferous slags roasted in the presence of 115% stoichiometric Na addition

| Test | $Na_2CO_3$:NaOH | $Na_2O$ | $Al_2O_3$ | CaO | $Cr_2O_3$ | FeO | MgO | MnO | $SiO_2$ | $TiO_2$ | $V_2O_5$ |
|---|---|---|---|---|---|---|---|---|---|---|---|
| 1 | 100:0 | 16.4 | 14.5 | 14.5 | 0.14 | 4.00 | 10.1 | 0.56 | 12.4 | 25.8 | 0.67 |
| 2 | 85:15 | 16.3 | 14.7 | 14.3 | 0.13 | 3.82 | 10.2 | 0.55 | 12.0 | 25.3 | 0.66 |
| 3 | 50:50 | 16.3 | 14.6 | 14.5 | 0.13 | 4.15 | 10.1 | 0.56 | 12.5 | 25.8 | 0.68 |
| 4 | 15:85 | 18.5 | 14.3 | 14.6 | 0.14 | 4.24 | 10.1 | 0.57 | 12.3 | 25.8 | 0.68 |
| 5 | 0:100 | 19.7 | 13.4 | 14.2 | 0.10 | 3.80 | 9.93 | 0.58 | 11.9 | 26.4 | 0.60 |

Table 11 Chemical composition (mass %) of the titaniferous slags roasted in the presence of 200% stoichiometric Na addition

| Test | $Na_2CO_3$:NaOH | $Na_2O$ | $Al_2O_3$ | CaO | $Cr_2O_3$ | FeO | MgO | MnO | $SiO_2$ | $TiO_2$ | $V_2O_5$ |
|---|---|---|---|---|---|---|---|---|---|---|---|
| 6 | 100:0 | 15.1 | 11.5 | 10.4 | 0.15 | 5.57 | 9.58 | 0.52 | 13.4 | 22.8 | 0.64 |
| 7 | 50:50 | 14.2 | 11.7 | 10.3 | 0.15 | 5.78 | 9.83 | 0.52 | 13.5 | 23.2 | 0.66 |
| 8 | 0:100 | 14.7 | 11.8 | 9.86 | 0.13 | 5.39 | 9.20 | 0.50 | 13.1 | 22.5 | 0.64 |

Table 12 and Table 13 present the chemical compositions of the water leached residues after roasting the titaniferous slags in the presence of 115% and 200% stoichiometric Na additions respectively. The concentrations of $V_2O_5$ in the residues decreased for both titaniferous slag roasted at different stoichiometric Na additions with the 200% stoichiometric Na additions being the lowest. Low $V_2O_5$ concentrations in the water leach residue suggest that most of the V was leached out into the solution as anticipated. The 200% stoichiometric Na additions decreased to approximately 0.15% $V_2O_5$ whilst 115% stoichiometric additions decreased to about 0.36% $V_2O_5$ in the water-leach residue. These results suggest that the leaching of V was achieved in both stoichiometric Na additions investigated but more effective at 200% stoichiometric Na additions.

Table 12 Chemical composition (mass %) of the water leached residues from the titaniferous slag roasted with the presence of 115% Na addition

| Test | $Na_2CO_3$:NaOH | $Na_2O$ | $Al_2O_3$ | CaO | $Cr_2O_3$ | FeO | MgO | MnO | $SiO_2$ | $TiO_2$ | $V_2O_5$ |
|---|---|---|---|---|---|---|---|---|---|---|---|
| 1 | 100:0 | 17.3 | 14.3 | 12.6 | 0.15 | 2.83 | 11.6 | 0.56 | 15.1 | 24.8 | 0.36 |
| 2 | 85:15 | 15.8 | 13.9 | 12.0 | 0.23 | 4.10 | 11.2 | 0.53 | 15.5 | 26.0 | 0.39 |
| 3 | 50:50 | 17.7 | 14.0 | 12.5 | 0.17 | 3.95 | 11.4 | 0.56 | 14.8 | 24.2 | 0.36 |
| 4 | 15:85 | 15.9 | 13.7 | 12.2 | 0.15 | 4.00 | 11.1 | 0.54 | 15.5 | 25.5 | 0.38 |
| 5 | 0:100 | 14.1 | 13.8 | 12.9 | 0.09 | 3.31 | 11.7 | 0.60 | 15.9 | 26.6 | 0.40 |

Table 13 Chemical composition (mass %) of the water leached residues from the titaniferous slag roasted with the presence of 200% Na addition

| Test | $Na_2CO_3$:NaOH | $Na_2O$ | $Al_2O_3$ | CaO | $Cr_2O_3$ | FeO | MgO | MnO | $SiO_2$ | $TiO_2$ | $V_2O_5$ |
|---|---|---|---|---|---|---|---|---|---|---|---|
| 6 | 100:0 | 14.1 | 10.4 | 12.4 | <0.05 | 5.50 | 10.4 | 0.63 | 14.8 | 24.1 | 0.17 |
| 7 | 50:50 | 14.2 | 10.1 | 12.3 | <0.05 | 5.60 | 10.4 | 0.62 | 14.9 | 24.0 | 0.16 |
| 8 | 0:100 | 14.7 | 10.2 | 12.4 | <0.05 | 6.13 | 10.5 | 0.63 | 15.0 | 24.2 | 0.15 |

The chemical composition of the acid-leached residues produced by the titaniferous slags roasted at 115% and 200% stoichiometric Na reagents are summarised in Table 14 and Table 15. As explained in the literature review, the aim of acid leaching was to remove detrimental species such as Mg, Al, Ca, and Fe. This concept proved to be successful for CaO, FeO, and MgO which showed a significant reduction in concentrations after acid leaching. The $Al_2O_3$ and $V_2O_5$ contents remained the same after acid leaching. A slight increase in $SiO_2$ and $TiO_2$ concentrations was visible in the acid leach residue. Borowiec, et al., (1998) reported that the removal of impurities such as V, Al, and Si is not fully effective during the upgrading of titaniferous materials through HCl acid leaching. These results are comparable with those found by Borowiec, et al., (1998) as the $Al_2O_3$ content remained the same after acid leaching whilst $SiO_2$ increased in concentration after acid leaching. This was also true for $V_2O_5$ concentrations in the residue produced from roasting the slag at 115% stoichiometric Na additions. The concentration of $V_2O_5$ in the residue that was produced after roasting the slag at 200% stoichiometric Na additions remained the same. The success of the acid leaching stage could be measured by the resulting concentrations of impurities and the $TiO_2$ in the residue. The $TiO_2$ concentrations have increased to >40% when comparing the water-leach and acid-leach residues for both stoichiometric Na additions investigated.

Table 14 Chemical composition (mass %) of the acid-leached residues produced after leaching water leach residues produced from 115% stoichiometric Na reagent additions to the titaniferous slag

| Test | $Na_2CO_3$:NaOH | $Na_2O$ | $Al_2O_3$ | CaO | $Cr_2O_3$ | FeO | MgO | MnO | $SiO_2$ | $TiO_2$ | $V_2O_5$ |
|---|---|---|---|---|---|---|---|---|---|---|---|
| 1 | 100:0 | 11.5 | 10.6 | 2.27 | 0.14 | 1.14 | 5.31 | 0.13 | 23.6 | 44.3 | 0.56 |
| 2 | 85:15 | 9.01 | 10.8 | 1.65 | 0.19 | 1.31 | 5.55 | 0.11 | 27.1 | 43.3 | 0.59 |
| 3 | 50:50 | 12.6 | 8.63 | 2.94 | 0.10 | 0.71 | 4.77 | 0.11 | 24.8 | 44.3 | 0.58 |
| 4 | 15:85 | 13.6 | 9.50 | 2.75 | 0.08 | 0.69 | 4.01 | 0.11 | 23.1 | 44.5 | 0.60 |
| 5 | 0:100 | 13.1 | 10.6 | 2.45 | 0.08 | 0.53 | 5.60 | 0.12 | 24.4 | 41.2 | 0.58 |

Table 15 Chemical composition (mass %) of the acid-leached residues produced after leaching water leach residue produced from 200% stoichiometric Na reagent additions to the titaniferous slag

| Test | $Na_2CO_3$:NaOH | $Na_2O$ | $Al_2O_3$ | CaO | $Cr_2O_3$ | FeO | MgO | MnO | $SiO_2$ | $TiO_2$ | $V_2O_5$ |
|---|---|---|---|---|---|---|---|---|---|---|---|
| 6 | 100:0 | 12.1 | 11.0 | 4.28 | <0.05 | 1.59 | 3.57 | 0.19 | 23.9 | 40.3 | 0.14 |
| 7 | 50:50 | 13.3 | 10.2 | 4.38 | <0.05 | 1.65 | 3.69 | 0.21 | 22.1 | 40.1 | 0.15 |
| 8 | 0:100 | 13.5 | 10.3 | 4.50 | <0.05 | 1.78 | 3.73 | 0.26 | 21.5 | 40.4 | 0.13 |

The chemical composition of the caustic leached residues are reported in Table 16 and Table 17. The caustic leaching was aimed at the removal of Si impurities and further upgrading the TiO2 concentrations in the residue. This process was a success for all the residues produced at different stoichiometric Na additions. The $SiO_2$ concentration were minimised from approximately 23% to 4%. $Al_2O_3$ concentrations in the residue remained high at >15.5%. With the removal of Si during caustic leaching, the other impurities concentrated in the final residue. The removal of $SiO_2$ during caustic leaching, upgraded the $TiO_2$ further to <64% in concentration.

Table 16 Chemical composition (mass %) of the caustic leached residues at 115% Na addition

| Test | $Na_2CO_3$:NaOH | $Na_2O$ | $Al_2O_3$ | CaO | $Cr_2O_3$ | FeO | MgO | MnO | $SiO_2$ | $TiO_2$ | $V_2O_5$ |
|---|---|---|---|---|---|---|---|---|---|---|---|
| 1 | 100:0 | 2.93 | 14.9 | 2.54 | 0.14 | 1.11 | 7.59 | 0.16 | 3.51 | 65.7 | 0.80 |
| 2 | 85:15 | 3.35 | 15.4 | 2.49 | 0.14 | 0.81 | 7.79 | 0.15 | 2.84 | 64.4 | 0.85 |
| 3 | 50:50 | 3.96 | 14.1 | 4.27 | 0.13 | 0.94 | 7.41 | 0.17 | 3.29 | 64.0 | 0.84 |
| 4 | 15:85 | 4.88 | 14.7 | 6.43 | 0.14 | 1.57 | 7.90 | 0.25 | 5.61 | 57.6 | 0.74 |
| 5 | 0:100 | 3.96 | 12.9 | 4.18 | 0.14 | 0.90 | 6.74 | 0.16 | 3.14 | 66.0 | 0.87 |

Table 17 Chemical composition (mass %) of the caustic leached residues at 200% Na addition

| Test | $Na_2CO_3$:NaOH | $Na_2O$ | $Al_2O_3$ | CaO | $Cr_2O_3$ | FeO | MgO | MnO | $SiO_2$ | $TiO_2$ | $V_2O_5$ |
|---|---|---|---|---|---|---|---|---|---|---|---|
| 6 | 100:0 | 3.04 | 13.0 | 4.19 | <0.05 | 1.54 | 5.05 | 0.28 | 2.95 | 68.7 | 0.51 |
| 7 | 50:50 | 3.29 | 13.6 | 4.33 | 0.10 | 1.57 | 6.16 | 0.36 | 4.21 | 64.8 | 0.53 |
| 8 | 0:100 | 2.93 | 13.1 | 4.56 | 0.37 | 1.81 | 6.31 | 0.31 | 4.86 | 66.8 | 0.53 |

### 4.3.2 Extraction efficiencies of V at different Na reagent composition and addition

Figure 12 shows the V extraction efficiencies calculated using equation [27] for the slags roasted at 115% and 200% stoichiometric Na additions. The results show that the highest V extractions were attained when the slag was roasted at 200% stoichiometric Na additions as compared to the 115% stoichiometric Na additions. The 115% stoichiometric Na additions show a decrease in vanadium extraction with an increase in the amount of NaOH added to the $Na_2CO_3$. The highest V extraction of 66% was attained at Na2CO3:NaOH mass ratio of 0:100 of the 115% stoichiometric Na additions followed by 65.7% at Na2CO3:NaOH mass ratio of 100:0. The mixed salt resulted in lower V extractions for both 115% and 200% stoichiometric Na additions. The 200% stoichiometric Na additions resulted in high V extractions when the salts were not mixed. Duplicate V extraction results of Na2CO3:NaOH mass ratio of 100:0 were 76.7% and 74.7% whereas $Na_2CO_3$:NaOH of 0:100 ratio resulted in duplicate V extraction efficiencies of 76.0% and 71.3%. For $Na_2CO_3$, the average V extractions of 75.7% with a standard deviation of 1.4% were attained whilst NaOH tests resulted in an average of 73.7% V extractions and a standard deviation of 3.3%. The standard deviation lower than 5% suggests that the experimental process and results were reproducible. These results show that there is a limitation in V recoveries when a combination of the salts was used. The 115% and 200% stoichiometric Na addition results suggest that the individual addition of salts results in higher V extractions as compared to the combination of the salts.

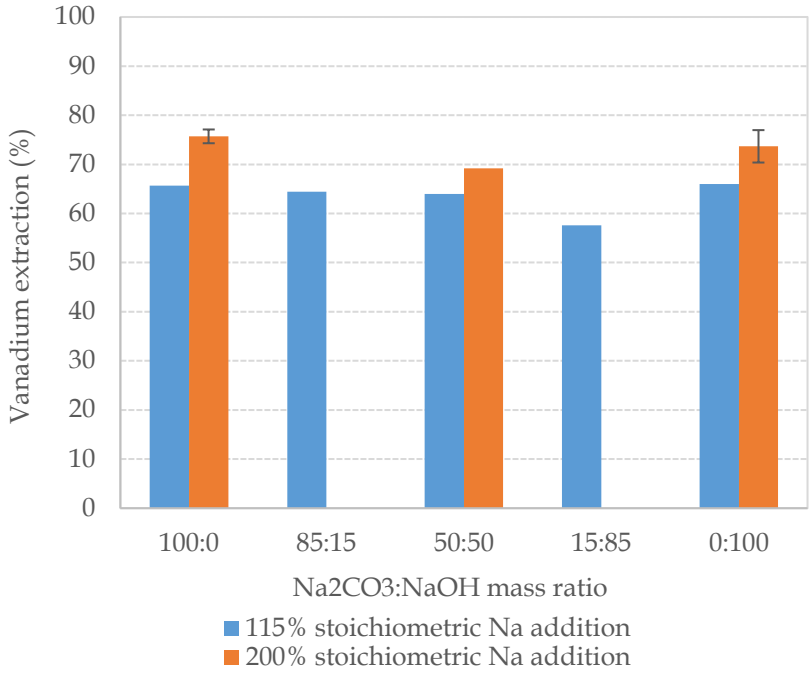


Figure 12 The effect of Na2CO3:NaOH mass ratio on V extraction efficiencies for titaniferous slags roasted in the presence of 115% stoichiometric Na addition

### 4.3.3 $TiO_2$ grades and recovery to the residues at different Na reagent composition and addition

The $TiO_2$ grades and recoveries to the residues attained after the removal of impurities during acid leaching are reported in Figure 13 and Figure 14. The acid leaching results showed a significant increase in $TiO_2$ concentrations at >40% for both 115% and 200% stoichiometric Na additions. The $TiO_2$ concentrations were generally higher at 115% stoichiometric Na additions as compared to the 200% stoichiometric Na additions. These high $TiO_2$ grades in the 115% stoichiometric Na additions may be attributed to higher degrees of impurity removal. The $TiO_2$ recoveries to the residues were generally at >86% for both 115% and 200% stoichiometric Na additions.

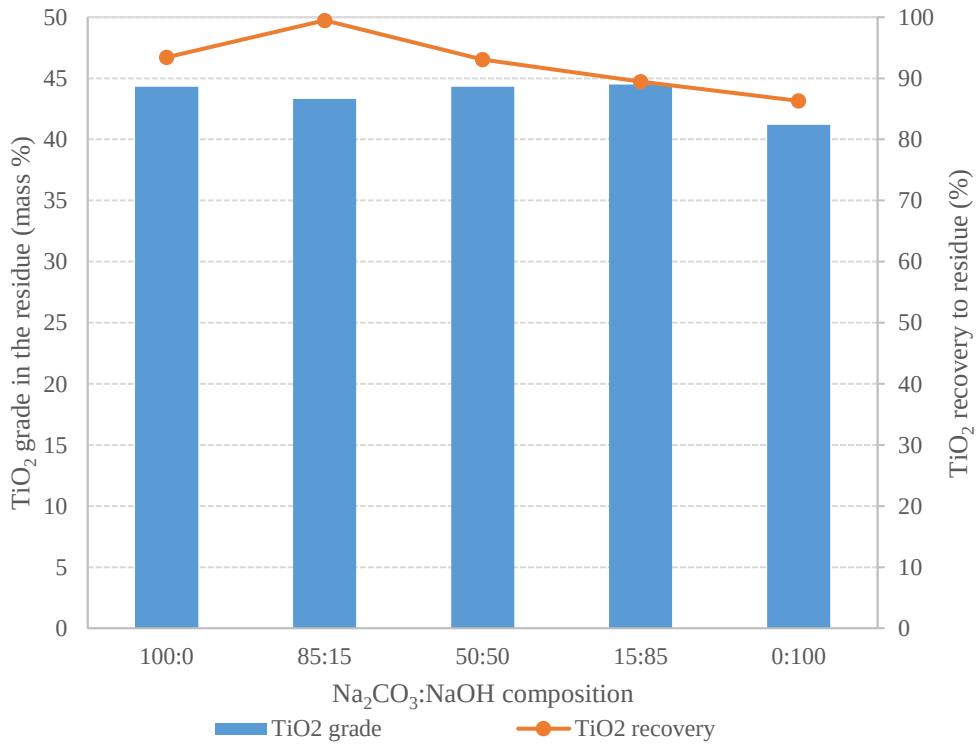


Figure 13 The titania grade and recovery to the residue for 115% Na addition after acid leaching

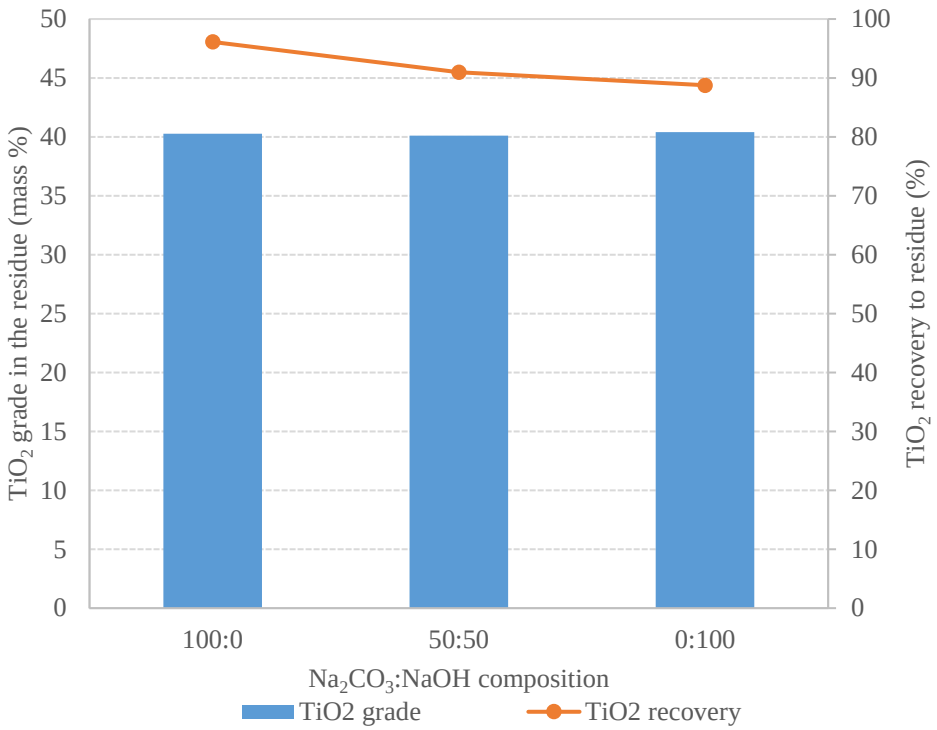


Figure 14 The titania grade and recovery to the residue for 200% Na addition after acid leaching

Figure 15 and Figure 16 show the $TiO_2$ grades and recoveries to the residue after the removal of Si impurity during the caustic leaching process. The $TiO_2$ grades were generally improved at both 115% and 200% stoichiometric Na additions with 200% additions being the highest. These high grades were attributed to the successful Si removal during the caustic leaching process. High $TiO_2$ grades were attained when salts were used individually as compared to the mixed salts. The $TiO_2$ recoveries to the residues were generally high for both stoichiometric Na additions investigated.

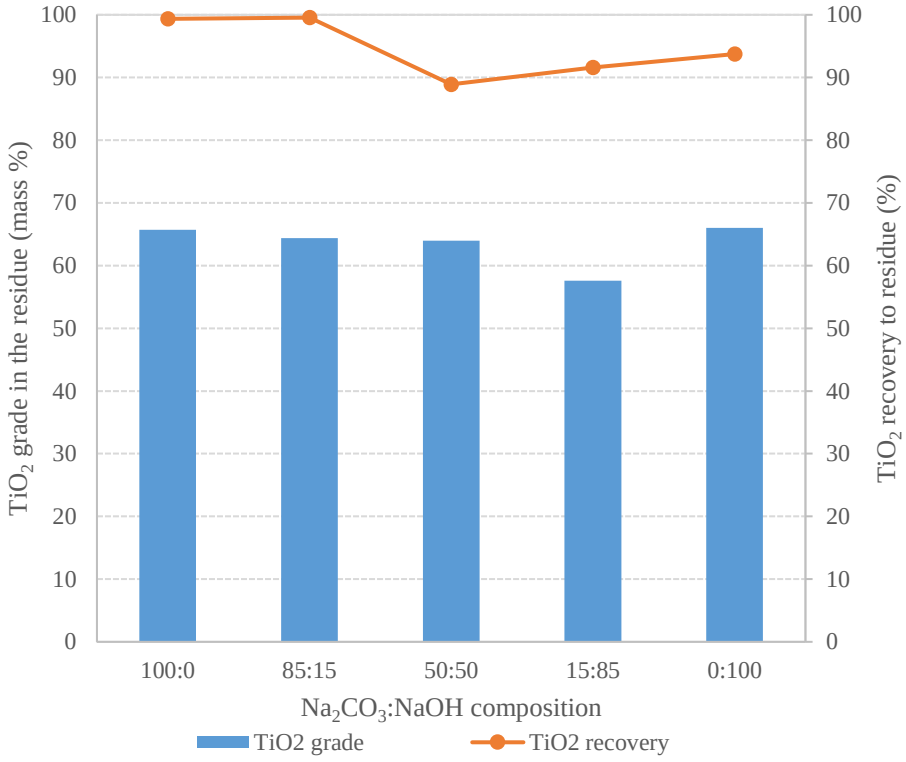


Figure 15 The titania grade and recovery to the residue for 115% Na addition after caustic leaching

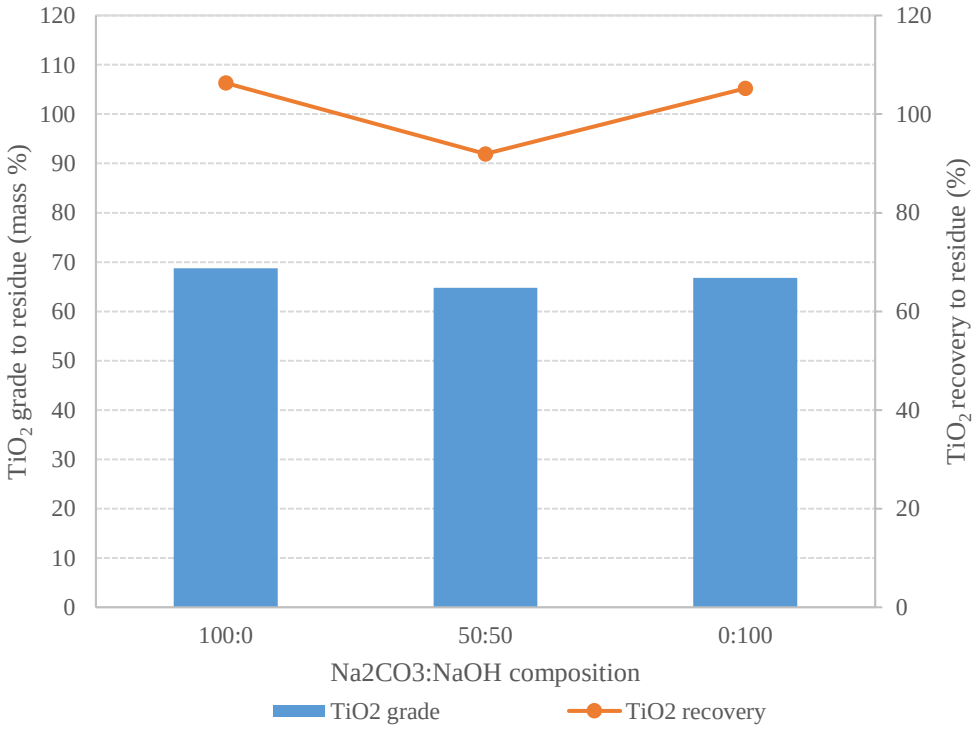


Figure 16 The titania grade and recovery to the residue for 200% Na addition after caustic leaching

The results showed that using individual salts resulted in high V extractions and $TiO_2$ grades as compared to the combination of salts for both 115% and 200% stoichiometric Na additions. Using either $Na_2CO_3$ or NaOH for further testing would be an acceptable choice since their results were almost similar. However, NaOH salt is quite expensive and is not used in the industrial V primary production process. It was therefore decided to adopt the use of $Na_2CO_3$ at 200% stoichiometric Na additions for further investigations.

## 4.4 Effect of temperature

The chemical composition results that were used to measure the effect of roasting temperature on V extraction efficiencies and the resulting $TiO_2$ grades produced after the removal of impurities are discussed in this section.

### 4.4.1 Chemical composition of the roasted slags and leached residues

The chemical compositions of the titaniferous slags roasted at different temperatures are presented in Table 18. The chemical compositions of the slags roasted at different temperatures were fairly comparable irrespective of the roasting temperature. As previously observed, the dilution of the roast material was also observed at different roasting temperatures. The concentrations of CaO, $Cr_2O_3$, FeO, MnO, $SiO_2$, $TiO_2$, and $V_2O_5$ were slightly decreased whilst concentrations of MgO and MnO remained the same in the feed and roast materials. A similar behaviour of a slightly increased $Al_2O_3$ concentration after roasting was also observed at different roasting temperatures, suggesting that the Al species stabilised in a new phase that formed during the roasting process.

Table 19 shows the chemical composition of the water leached residues after roasting at different temperatures. After water leaching, most of the compounds remained the same except for $V_2O_5$ and $TiO_2$ which showed a decrease and an increase in concentrations respectively. The leach residues showed an increase in $V_2O_5$ concentrations with a decrease in temperature suggesting higher oxidation degree of V at high temperatures. The concentrations of $Na_2O$ in the water leach residues increased with a decrease in temperature signifying that the reaction of Na with $V_2O_5$ to form a water soluble $NaVO_3$ was less favoured at lower temperatures. The water leach process aimed at leaching out V was more effective at higher temperatures.

Table 18 Chemical composition (mass %) of the slag roasted at different temperatures for 200% Na addition

| Test | Temperature (°C) | $Na_2O$ | $Al_2O_3$ | CaO | $Cr_2O_3$ | FeO | MgO | MnO | $SiO_2$ | $TiO_2$ | $V_2O_5$ |
|---|---|---|---|---|---|---|---|---|---|---|---|
| 6 | 1000 | 15.1 | 11.5 | 10.4 | 0.15 | 5.57 | 9.58 | 0.52 | 13.4 | 22.8 | 0.64 |
| 9 | 900 | 19.5 | 11.1 | 10.6 | 0.19 | 3.90 | 8.10 | 0.46 | 13.2 | 20.4 | 0.63 |
| 10 | 800 | 25.8 | 12.1 | 11.5 | 0.20 | 4.04 | 8.70 | 0.49 | 14.1 | 21.7 | 0.67 |

Table 19 Chemical composition (mass %) of the water leached residues at different temperatures for 200% Na addition

| Test | Temperature (°C) | $Na_2O$ | $Al_2O_3$ | CaO | $Cr_2O_3$ | FeO | MgO | MnO | $SiO_2$ | $TiO_2$ | $V_2O_5$ |
|---|---|---|---|---|---|---|---|---|---|---|---|
| 6 | 1000 | 14.1 | 10.4 | 12.4 | <0.05 | 5.50 | 10.4 | 0.63 | 14.8 | 24.1 | 0.17 |
| 9 | 900 | 16.0 | 10.2 | 11.8 | 0.10 | 3.99 | 8.83 | 0.51 | 15.5 | 25.1 | 0.23 |
| 10 | 800 | 14.4 | 12.5 | 12.1 | 0.20 | 3.91 | 9.13 | 0.55 | 15.6 | 25.4 | 0.35 |

Table 20 shows the chemical compositions of the acid-leached residues at different temperatures. The removal of impurities such as CaO, FeO, MgO, and MnO was observed at different temperatures since the concentrations significantly decreased. The concentrations of $V_2O_5$ and $Al_2O_3$ remained the same, while the concentration of $SiO_2$ increased. The removal of the impurities upgraded the $TiO_2$ in the acid-leach residue to concentrations above 34% $TiO_2$ for all the temperatures investigated. The acid-leaching process aimed at impurity removal was favoured for most of the compounds except for $Al_2O_3$. The impurity removal through acid-leaching was slightly higher at higher roasting temperatures.

Table 21 gives the chemical compositions of the residues that resulted after roasting the slag at different temperatures. A slight increase in $Al_2O_3$, MgO, and $V_2O_5$ concentrations was observed from the resulting chemical concentrations. The removal of $SiO_2$ was significant at higher temperatures of 1000°C. Temperatures of 900°C and below, resulted in $SiO_2$ concentrations of <9% suggesting that caustic leaching was favoured after roasting the slag at 1000°C. The concentrations of $TiO_2$ were upgraded after caustic leaching with the highest $TiO_2$ concentration of 68.7% attained at 1000°C. The caustic leaching results showed that it was possible to remove Si and upgrade $TiO_2$ for the titaniferous slag roasted at 1000°C. At lower roasting temperatures more Si species remained in the residue and the $TiO_2$ concentrations were at <57.4%.

Table 20 Chemical composition (mass %) of the acid-leached residues at different temperatures

| Test | Temperature (°C) | $Na_2O$ | $Al_2O_3$ | CaO | $Cr_2O_3$ | FeO | MgO | MnO | $SiO_2$ | $TiO_2$ | $V_2O_5$ |
|---|---|---|---|---|---|---|---|---|---|---|---|
| 6 | 1000 | 12.1 | 11.0 | 4.28 | <0.05 | 1.59 | 3.57 | 0.19 | 23.9 | 40.3 | 0.14 |
| 9 | 900 | 12.4 | 14.2 | 4.86 | 0.09 | 1.38 | 3.89 | 0.18 | 24.4 | 36.4 | 0.25 |
| 10 | 800 | 12.0 | 17.1 | 5.06 | 0.31 | 1.15 | 3.94 | 0.11 | 25.4 | 34.7 | 0.54 |

Table 21 Chemical composition (mass %) of the caustic leached residues at different temperatures for 200% Na addition

| Test | Temperature (°C) | $Na_2O$ | $Al_2O_3$ | CaO | $Cr_2O_3$ | FeO | MgO | MnO | $SiO_2$ | $TiO_2$ | $V_2O_5$ |
|---|---|---|---|---|---|---|---|---|---|---|---|
| 6 | 1000 | 3.04 | 13.0 | 4.19 | <0.05 | 1.54 | 5.05 | 0.28 | 2.95 | 68.7 | 0.51 |
| 9 | 900 | 3.63 | 16.2 | 4.86 | 0.09 | 1.38 | 5.19 | 0.18 | 9.39 | 57.4 | 0.55 |
| 10 | 800 | 3.50 | 18.1 | 4.56 | 0.31 | 1.15 | 5.34 | 0.11 | 10.4 | 54.7 | 0.54 |

### 4.4.2 Extraction efficiency of vanadium

Figure 17 presents a graph showing the effect of temperature on vanadium extractions. As it appears in the Figure, V extraction efficiencies decreased with a decrease in roasting temperature. The chemical composition results of the water-leach residues also showed higher $V_2O_5$ concentrations at lower roasting temperatures. These results suggest that V extraction is sensitive to the roasting temperature since these extractions depend on the reaction of Na with $V_2O_5$ to form a water-soluble $NaVO_3$. At higher temperatures, the formation of $NaVO_3$ is favoured when compared to lower temperatures. These results confirm those found by Gilligan & Nikoloski, 2020 who showed that high V extractions were mostly attained after roasting V-bearing materials at high temperatures.

The highest V extraction efficiency of 75.7% was achieved after roasting the titaniferous slag at a roasting temperature of 1000°C followed by 66.7% for 900°C. The lowest V extraction efficiency was reported to be 55.7% after roasting the slag at 800°C. These results agree with those found by Zhang, et al. (2019) and Deng, et al. (2020) who showed that the roasting temperature does affect the leaching efficiency of vanadium such that at higher roasting temperatures, higher V extractions would be attained.

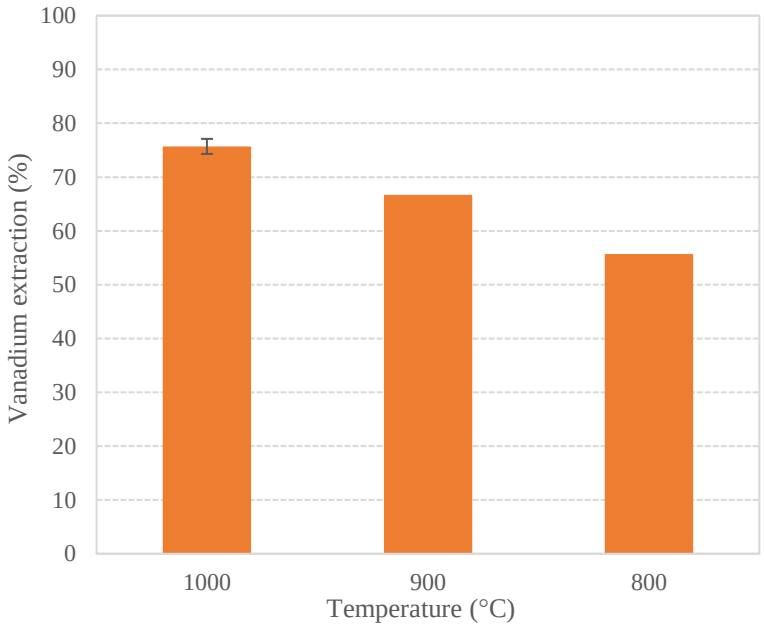


Figure 17 The effect of temperature on vanadium extraction efficiencies

### 4.4.3 $TiO_2$ grade and recovery to the residues

Figure 18 shows the effect of temperature on the upgraded $TiO_2$ and the $TiO_2$ recoveries to the acid-leach residue. The results showed a decrease in TiO2 grade with a decrease in temperature. This was due to the removal of impurities which was higher for the slag roasted at higher temperatures as shown in Table 20. The highest $TiO_2$ grade of 40.3% was attained after roasting the titaniferous slag at 1000°C. At lower temperatures, the resulting $TiO_2$ grade was 36.4% and 34.7% for 900°C and 800°C respectively. The $TiO_2$ recoveries to the residues was above 75% for all the temperatures investigated.

Figure 19 shows the $TiO_2$ grades and recoveries to the residues after caustic leaching of the titaniferous slag roasted at different temperatures. The results show higher $TiO_2$ grades of 68.7% for the slags roasted at 1000°C. The resulting $TiO_2$ grades for the slags roasted at lower temperatures were <56.4%. These results were confirmed by the chemical compositions of the caustic leach residues which showed low $SiO_2$ concentrations at higher temperatures of 1000°C, suggesting that the removal of $SiO_2$ through caustic leaching process was more effective for the slags roasted at higher temperature. The $TiO_2$ recoveries to the residues decreased with decreasing temperature.

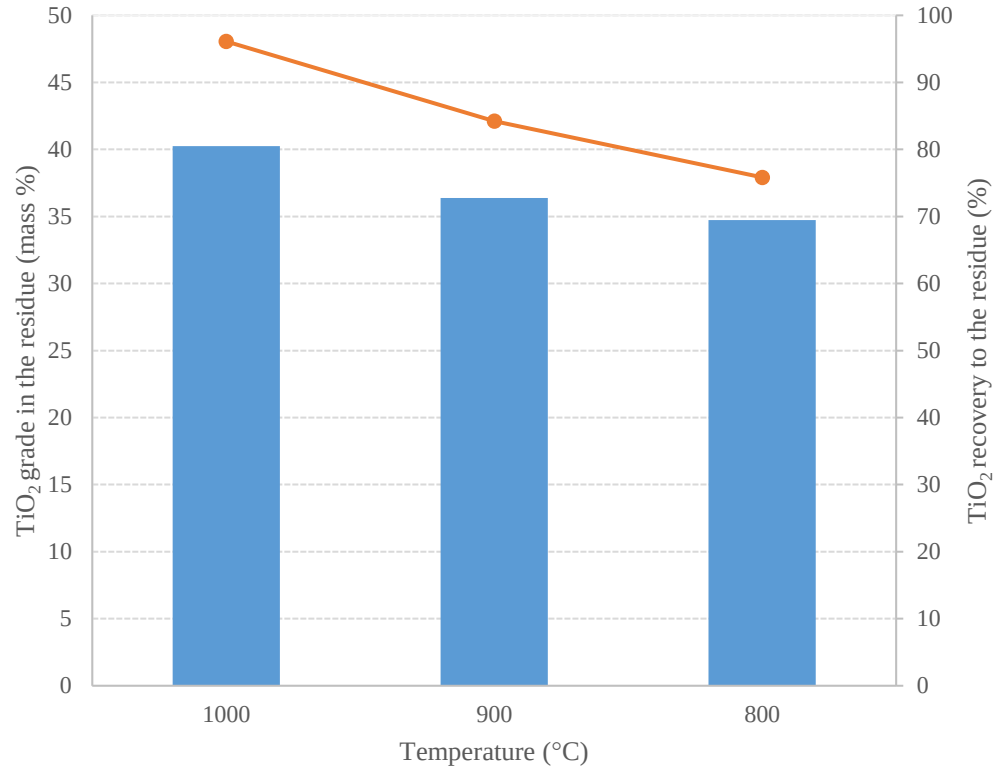


Figure 18 The $TiO_2$ grade and recovery to the residues after acid leaching

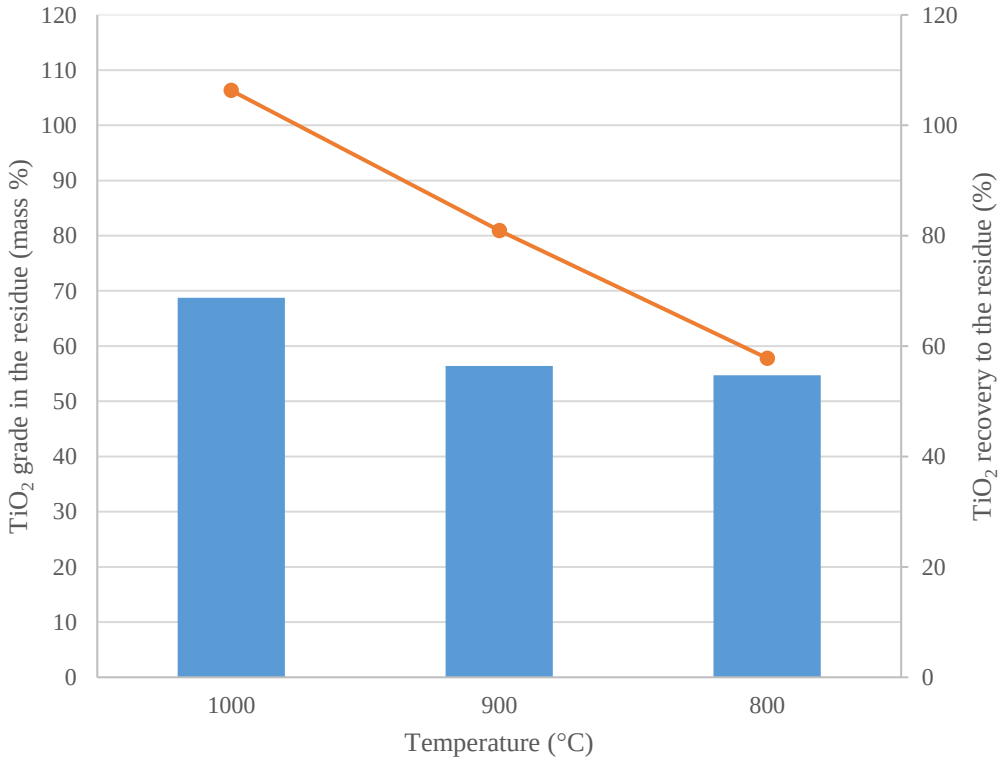


Figure 19 The $TiO_2$ grade and recovery to the residue after caustic leaching

The effect of temperature on V extractions and the $TiO_2$ grades that resulted after impurity removal has shown that 1000°C produced the best results. Therefore, the roasting temperature of 1000°C was selected for further investigations.

## 4.5 Effect of time

The results showing the effect of roasting time on V extraction efficiency and the resulting $TiO_2$ grade after the removal of impurities are reported in this section.

### 4.5.1 Chemical composition of the roasted slag and leached residues

The chemical compositions of the titaniferous slags roasted at different times are reported in Table 22. The dilution in concentrations due to high Na additions was visible for CaO, $Cr_2O_3$, FeO, $SiO_2$, $TiO_2$, and $V_2O_5$ whilst the concentrations of MgO and MnO remained the same. The same increase in $Al_2O_3$ concentrations was observed at different roasting times as previously observed for different stoichiometric Na additions and temperatures. This increase was attributed to the possible formation of the $NaAlO_2$ phase as shown in section 4.2.

Table 23 presents the chemical compositions of the water leached residues after roasting the titaniferous slag at different roasting times. The results showed a decrease in $V_2O_5$ concentration with increasing roasting time. These results recommend longer reaction periods for the reaction of $V_2O_5$ with the Na reagent.
Most of the other compounds generally remained the same after water leaching except for $SiO_2$ and $TiO_2$ concentrations which showed a slight increase.

The chemical compositions of the acid-leached residues roasted at different times are tabulated in Table 24. The results showed a decrease in CaO, FeO, MgO, and MnO concentrations suggesting the removal of these impurities, but not to completion. The removal of these impurities was the highest at higher roasting time of 180 minutes. An increase in $SiO_2$ concentration was visible at different roasting times whilst $Al_2O_3$ concentrations remained the same. These results suggest that the longer roasting periods results in lesser impurities in the residue. The highest $TiO_2$ grades of 40.7% were attained after roasting for a period of 180 minutes.

Table 25 presents the chemical compositions of the caustic leached residues at different roasting times. The results showed a slight increase in concentrations of $Al_2O_3$, CaO, FeO, MgO, MnO, and $V_2O_5$ whilst $TiO_2$ concentrations increased significantly. Caustic leaching aimed at removing $SiO_2$ showed a significant drop in $SiO_2$ concentrations. The caustic leaching process was successful since the highest $TiO_2$ grade of 68.7% and the lowest $SiO_2$ concentrations of about 3% were attained after roasting for a period of 120 minutes.

Table 22 Chemical composition (mass %) of the slags at different roasting time

| Test | Time (min) | $Na_2O$ | $Al_2O_3$ | CaO | $Cr_2O_3$ | FeO | MgO | MnO | $SiO_2$ | $TiO_2$ | $V_2O_5$ |
|---|---|---|---|---|---|---|---|---|---|---|---|
| 11 | 60 | 18.9 | 12.0 | 12.1 | 0.19 | 3.33 | 9.83 | 0.54 | 14.8 | 22.0 | 0.65 |
| 6 | 120 | 15.1 | 11.5 | 10.4 | 0.15 | 5.57 | 9.58 | 0.52 | 13.4 | 22.8 | 0.64 |
| 12 | 180 | 14.3 | 12.1 | 12.2 | 0.18 | 3.44 | 9.88 | 0.54 | 14.9 | 22.2 | 0.67 |

Table 23 Chemical composition (mass %) of the water leached residue different reaction periods

| Test | Time (min) | $Na_2O$ | $Al_2O_3$ | CaO | $Cr_2O_3$ | FeO | MgO | MnO | $SiO_2$ | $TiO_2$ | $V_2O_5$ |
|---|---|---|---|---|---|---|---|---|---|---|---|
| 11 | 60 | 14.8 | 11.2 | 13.1 | <0.05 | 3.61 | 10.8 | 0.58 | 16.1 | 24.0 | 0.39 |
| 6 | 120 | 15.1 | 10.4 | 12.4 | <0.05 | 5.50 | 10.4 | 0.63 | 14.8 | 24.1 | 0.17 |
| 12 | 180 | 14.8 | 10.9 | 13.1 | <0.05 | 3.60 | 10.7 | 0.58 | 16.2 | 24.4 | 0.13 |

Table 24 Chemical composition (mass %) of the acid leached residues at different reaction periods

| Test | Time(min) | $Na_2O$ | $Al_2O_3$ | CaO | $Cr_2O_3$ | FeO | MgO | MnO | $SiO_2$ | $TiO_2$ | $V_2O_5$ |
|---|---|---|---|---|---|---|---|---|---|---|---|
| 11 | 60 | 13.3 | 10.4 | 4.05 | <0.05 | 0.85 | 3.07 | 0.14 | 23.9 | 40.6 | 0.45 |
| 6 | 120 | 12.1 | 11.0 | 4.28 | <0.05 | 1.59 | 3.57 | 0.19 | 23.9 | 40.3 | 0.14 |
| 12 | 180 | 12.2 | 10.4 | 3.04 | <0.05 | 0.54 | 3.93 | 0.08 | 24.1 | 40.7 | 0.21 |

Table 25 Chemical composition (mass %) of the caustic leached residues at different reaction periods

| Test | Time(min) | $Na_2O$ | $Al_2O_3$ | CaO | $Cr_2O_3$ | FeO | MgO | MnO | $SiO_2$ | $TiO_2$ | $V_2O_5$ |
|---|---|---|---|---|---|---|---|---|---|---|---|
| 11 | 60 | 3.60 | 13.9 | 6.45 | 0.08 | 1.28 | 4.78 | 0.22 | 3.16 | 60.8 | 0.72 |
| 6 | 120 | 3.04 | 13.0 | 4.19 | <0.05 | 1.54 | 5.05 | 0.28 | 2.95 | 68.7 | 0.51 |
| 12 | 180 | 3.09 | 13.0 | 5.97 | 0.11 | 1.01 | 3.63 | 0.15 | 5.67 | 61.0 | 0.77 |

### 4.5.2 Extraction efficiencies and leaching rates of vanadium at different reaction times

Figure 20 shows the effect of roasting time on the V extraction efficiency after roasting the titaniferous slag at different roasting times. The results showed an increase in V extraction efficiencies when the roasting time was increased from 60 to 120 min and thereafter a slight decrease at longer roasting time of 180 minutes. V extraction efficiencies were reported to increase from 45.0% at 60 minutes to 75.7% at 120 minutes. Thereafter the V extractions decreased to 68.7% after roasting for a period of 180 minutes. Similar trends were reported by Li, et al., (2018) who showed that the leaching efficiency increased at lower roasting times and reached maximum, thereafter decreased at longer roasting times. Li, et al., (2018) results suggested that this was allegedly due to the sintering of the roast products.

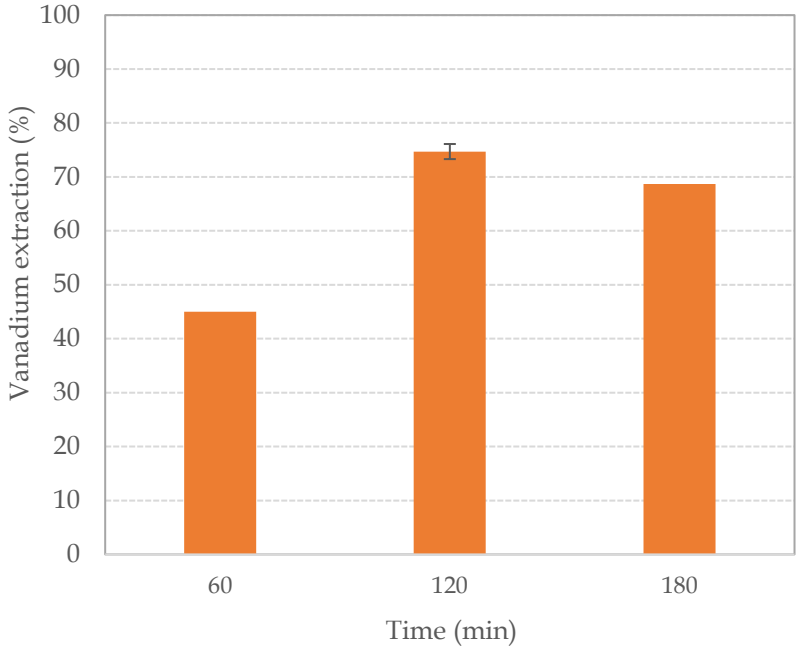


Figure 20 The effect of roasting time on the vanadium extraction efficiencies

### 4.5.3 Titania grades and recovery to the residue

Figure 21 shows the $TiO_2$ grades that resulted after roasting at different times. The results showed similar $TiO_2$ grades produced after roasting at different times. These grades ranged between 40.3 to 40.7% in $TiO_2$ concentrations. These results were expected since the removal of impurities at different roasting times was almost similar with 180 minutes which was slightly higher. The $TiO_2$ recoveries to the residues were fairly high at >82% for all roasting times investigated.

The effect of roasting time on $TiO_2$ grade and recoveries to the residues after caustic leaching are shown in Figure 22. The results showed an increase in $TiO_2$ grades with increasing roasting time up to 120 minutes, thereafter the grades decreased. The highest $TiO_2$ grade of 68.7 was attained at 120 minutes roasting times. These results agree with the chemical composition results which showed the highest $SiO_2$ removal at 120 minutes, suggesting that the more $SiO_2$ was removed the higher the resulting $TiO_2$ grade. The $TiO_2$ recoveries to the residues were generally high for all the tested roasting times.

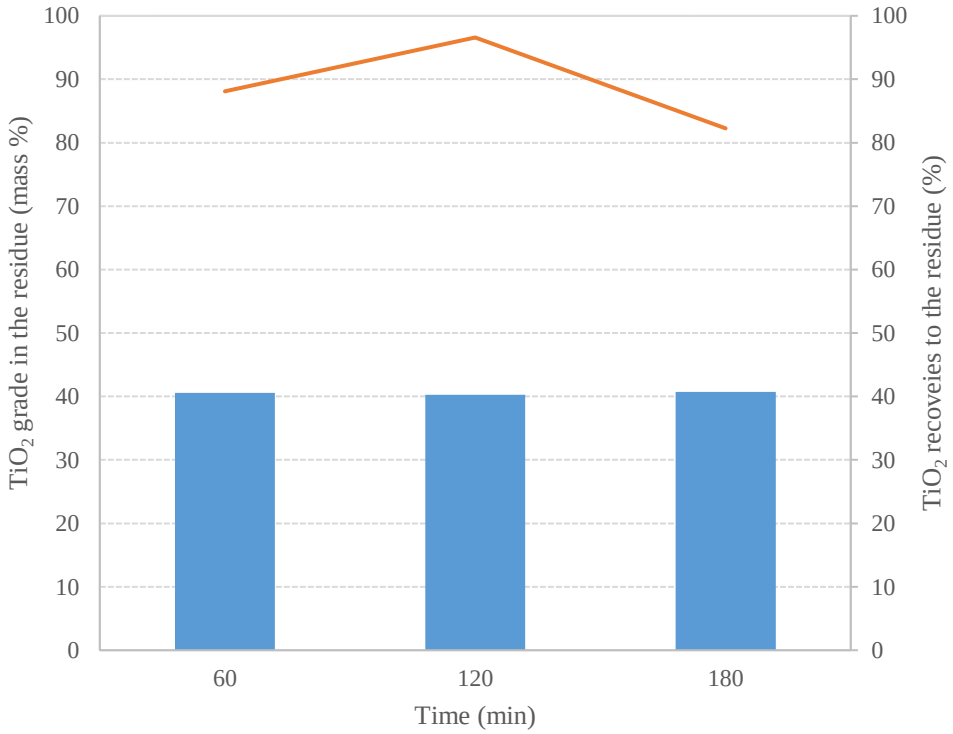


Figure 21 The $TiO_2$ grades and recovery to the residues after acid leaching

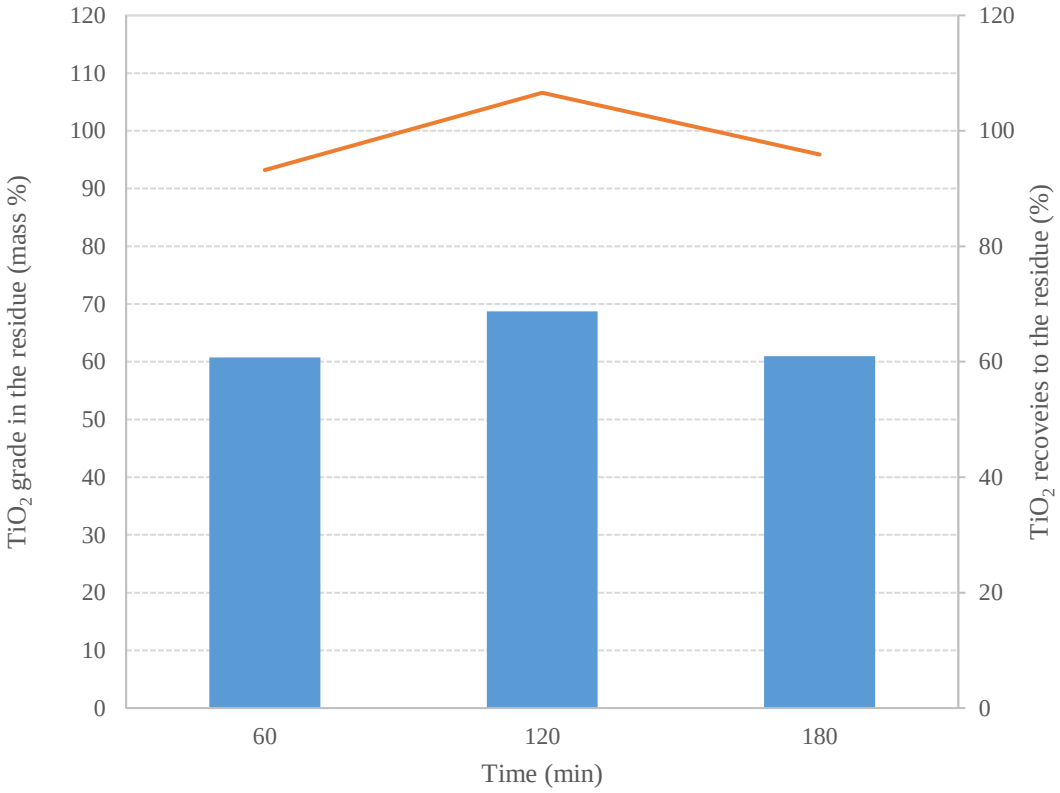


Figure 22 The $TiO_2$ grades and recovery to the residue after caustic leaching

The results showed high V extraction efficiencies and $TiO_2$ grades after roasting for a period of 120 minutes, thus 120 minutes was selected for further testwork.

## 4.6 Effect of PSD

### 4.6.1 Chemical compositions

The chemical compositions of the titaniferous slags roasted at different PSDs are summarised in Table 26. The results show the dilution of most compounds due to high Na additions as previously observed at different stoichiometric Na additions, roasting temperature, and roasting time. The same increase in $Al_2O_3$ concentrations was also observed at different PSDs with increased MgO for fine roast material of +106 – 300 µm.

Table 27 shows the chemical composition of the water leached residues after roasting the titaniferous slags at different PSDs. The results showed a decrease in $V_2O_5$ concentrations for both PSDs investigated, with the coarse material attaining lower $V_2O_5$ concentrations. These results contradict those of Li et.al 2017 who showed that finer particles resulted in higher V extractions.

Table 28 shows the chemical composition of the acid leach residues after roasting the titaniferous slags at different PSDs. The results showed that the concentrations of CaO, FeO, MgO, and MnO decreased significantly when the roast material was fine. The concentrations of $Al_2O_3$ and $SiO_2$ increased for roast materials at different PSDs. The removal of impurities, upgraded the $TiO_2$ concentration to >35%. The highest $TiO_2$ grade of 40.3% was attained when a coarse material was roasted. These results suggest that fine materials have the potential to remove more impurities when compared to coarse materials during the acid leach process.

The chemical composition of the caustic leached residues for the titaniferous slags roasted under at different PSDs are reported in Table 29. The chemical composition results showed an increase in $Al_2O_3$, MgO, and $V_2O_5$ concentrations. The concentrations of CaO, FeO, and MnO remained the same whilst the $SiO_2$ concentration significantly decreased. The decrease in $SiO_2$ concentration resulted in an upgrade of $TiO_2$ concentration with maximum of 68.7% attained for coarse material. These results suggest that the caustic leaching was successful as most of the $SiO_2$ was removed during the process.

Table 26 Chemical composition (mass %) of the roasted slags at different PSD

| Test | PSD (µm) | $Na_2O$ | $Al_2O_3$ | CaO | $Cr_2O_3$ | FeO | MgO | MnO | $SiO_2$ | $TiO_2$ | $V_2O_5$ |
|---|---|---|---|---|---|---|---|---|---|---|---|
| 6 | +106 – 850 | 15.1 | 11.5 | 10.4 | 0.15 | 5.57 | 9.58 | 0.52 | 13.4 | 22.8 | 0.64 |
| 13 | +106 - 300 | 17.3 | 10.4 | 13.2 | <0.05 | 3.32 | 11.0 | 0.55 | 15.6 | 23.4 | 0.65 |

Table 27 Chemical composition (mass %) of the water leach residue at different PSD

| Test | PSD (µm) | $Na_2O$ | $Al_2O_3$ | CaO | $Cr_2O_3$ | FeO | MgO | MnO | $SiO_2$ | $TiO_2$ | $V_2O_5$ |
|---|---|---|---|---|---|---|---|---|---|---|---|
| 6 | +106 – 850 | 14.1 | 10.4 | 12.4 | <0.05 | 5.50 | 10.4 | 0.63 | 14.8 | 24.1 | 0.17 |
| 13 | +106 - 300 | 13.2 | 11.5 | 11.8 | 0.25 | 3.17 | 10.0 | 0.52 | 14.2 | 34.4 | 0.25 |

Table 28 Chemical composition (mass %) of the acid leach residue at different PSD

| Test | PSD (µm) | $Na_2O$ | $Al_2O_3$ | CaO | $Cr_2O_3$ | FeO | MgO | MnO | $SiO_2$ | $TiO_2$ | $V_2O_5$ |
|---|---|---|---|---|---|---|---|---|---|---|---|
| 6 | +106 – 850 | 12.1 | 11.0 | 4.28 | <0.05 | 1.59 | 3.57 | 0.19 | 23.9 | 40.3 | 0.14 |
| 12 | +106 - 300 | 16.1 | 15.6 | 3.64 | 0.19 | 0.64 | 2.42 | 0.10 | 22.8 | 35.2 | 0.36 |

Table 29 Chemical composition (mass %) of the caustic leach residue at different PSD

| Test | PSD (µm) | $Na_2O$ | $Al_2O_3$ | CaO | $Cr_2O_3$ | FeO | MgO | MnO | $SiO_2$ | $TiO_2$ | $V_2O_5$ |
|---|---|---|---|---|---|---|---|---|---|---|---|
| 6 | +106 – 850 | 3.04 | 13.0 | 4.19 | <0.05 | 1.54 | 5.05 | 0.28 | 2.95 | 68.7 | 0.51 |
| 13 | +106 - 300 | 8.78 | 18.8 | 3.86 | 0.23 | 0.32 | 4.66 | 0.20 | 2.54 | 55.3 | 0.66 |

### 4.6.2 V extraction efficiencies at different PSDs

Figure 23 shows the effect of PSD on the V extraction efficiencies of the titaniferous slags roasted at different PSDs. The results showed lower V extraction efficiencies of 65.2% for fine titaniferous slag material of PSD +106 – 300 µm. The V extraction efficiencies for the coarse material with PSD of +106 – 850 µm were favoured at extractions of 75.7% suggesting that high PSDs resulted in high V extractions. These results agree with those reported by Goso, et al., (2016) who demonstrated high V extraction efficiencies when a coarser material was used as a feed material.

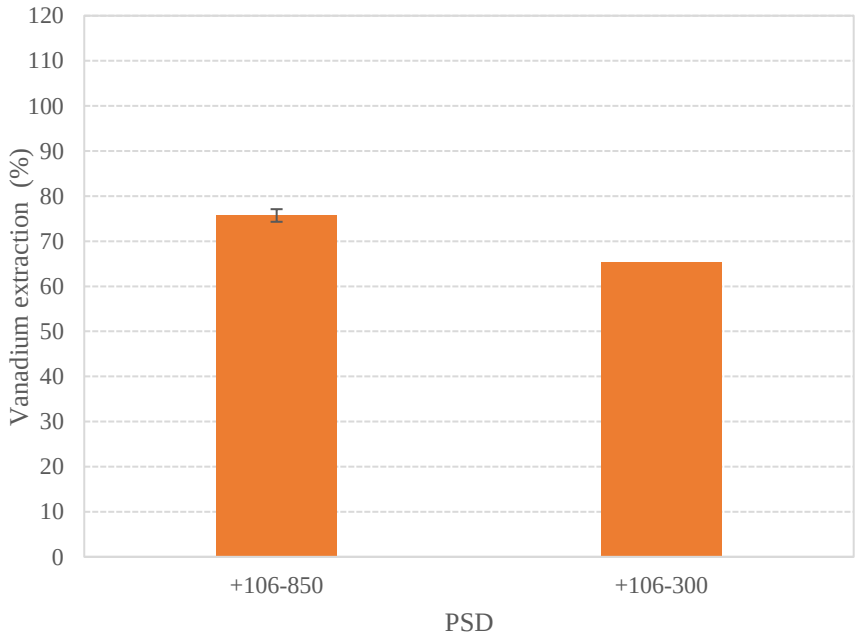


Figure 23 The effect of PSD on vanadium extraction efficiencies

### 4.6.3 $TiO_2$ grade and recovery to the residue

The effect of PSDs on $TiO_2$ grades that resulted after acid leaching are shown in Figure 24. The results showed that higher $TiO_2$ grades resulted when a coarse material was roasted. These results contradict the chemical composition results which showed higher removal of impurities which may result in higher $TiO_2$ grades. The lower $TiO_2$ grade after the removal of higher amounts of impurities requires further investigation. The $TiO_2$ recoveries to the residue decreased with a decrease in PSD.

The effect of PSDs on $TiO_2$ grades after caustic leaching are shown in Figure 25. The results showed an increase in $TiO_2$ grades with increasing PSD. The coarser material had the highest $TiO_2$ grade of 68.7% as compared to the finer material with a $TiO_2$ grade of 55.3%. The chemical composition results showed lower SiO2 concentrations for fine material suggesting that high TiO2 grades were expected for fine material. These results need further investigation to determine the cause of these lower $TiO_2$ grades with high impurity removal. The $TiO_2$ recoveries to the residues at different PSDs were generally high.

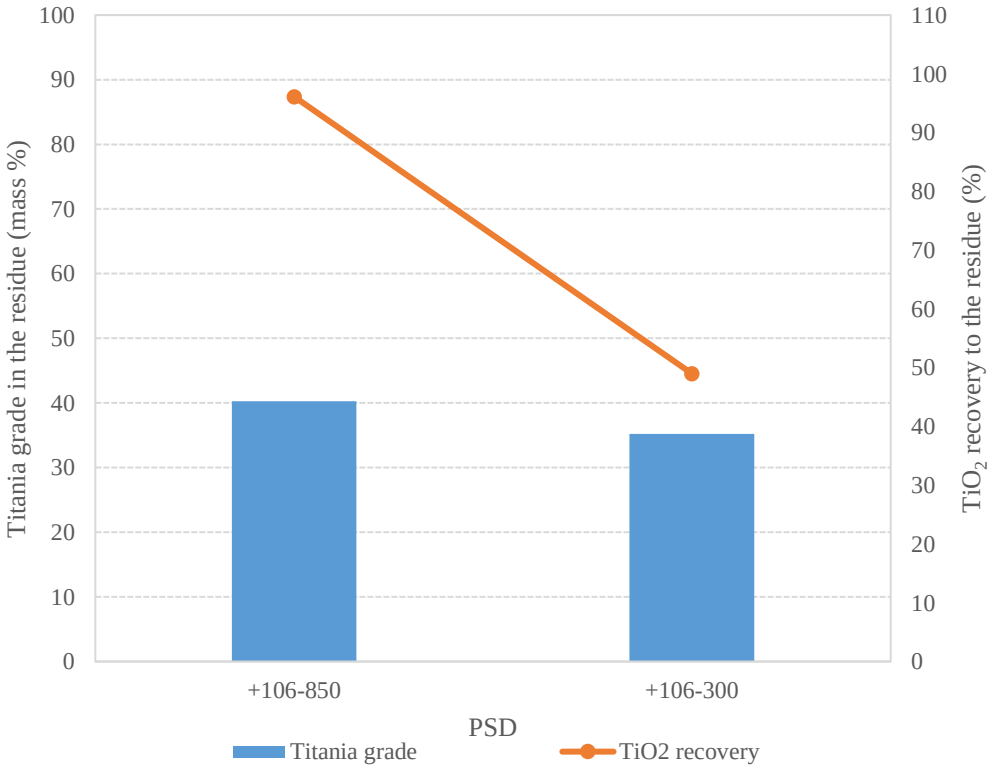


Figure 24 The effect of PSD on $TiO_2$ grade and recovery to the residue after acid leaching

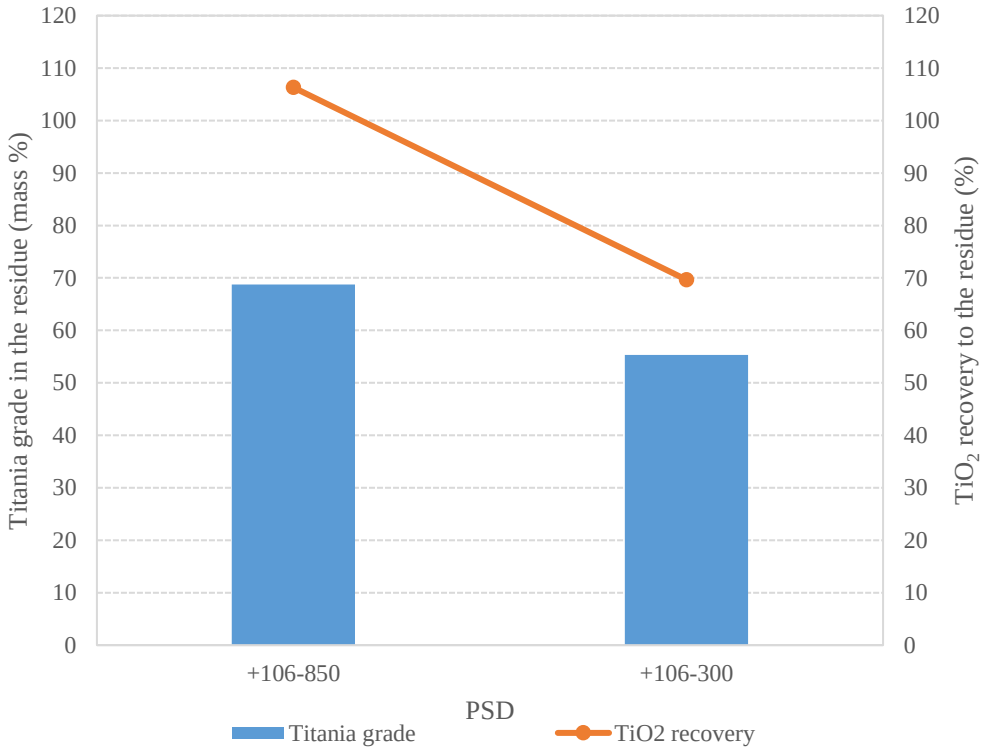


Figure 25 The effect of PSD on $TiO_2$ grade and recovery to the residue after caustic leaching

Although higher impurities were removed when the slag was roasted with fine material, the coarse material showed high V extractions and $TiO_2$ grades. Therefore, for further investigations, +106 – 850 µm material was used for further investigations.

## 4.7 Effect of Na reagents

### 4.7.1 Chemical compositions of the roasted slag and leached residues

The chemical compositions of the titaniferous slags roasted at different Na reagents are reported in Table 30. The roast material results showed the dilution of CaO, $Cr_2O_3$, FeO, MnO, $SiO_2$, $TiO_2$ and $V_2O_5$. The $Al_2O_3$ concentration increased in the roasted material whilst the MgO concentration remained fairly constant.

Table 31 shows the chemical compositions of water leach residues at different Na reagents. The results showed that the $Al_2O_3$ concentration remained fairly constant whilst the concentrations of CaO, FeO, MgO, MnO, $SiO_2$, and $TiO_2$ slightly increased. The overall $V_2O_5$ concentration decreased in the order of NaOH > $Na_2CO_3$ > $Na_2SO_4$.

The chemical compositions of the acid-leach residues roasted at different Na reagents are presented in Table 32. The results showed that the concentrations of CaO, FeO, MgO, and MnO significantly decreased whilst $Al_2O_3$ and $SiO_2$ increased. The $TiO_2$ grades that resulted after the impurity removal were >38% for all the Na reagents tested. The highest $TiO_2$ grades were seen for NaOH and $Na_2CO_3$ with $Na_2SO_4$ having the lowest $TiO_2$ grades.

The chemical compositions of the caustic leach residues roasted at different Na reagents are summarised in Table 33. The results showed no significant change in concentrations of CaO, FeO, and MnO of the caustic-leach residues whilst the $Al_2O_3$ and MgO concentrations increased. The $Na_2SO_4$ reagent resulted in the highest $Al_2O_3$ concentrations when compared to the NaOH and $Na_2CO_3$ reagents. A substantial decrease in $SiO_2$ concentrations was seen for all Na reagents with $Na_2CO_3$ having the lowest concentration. The $TiO_2$ grades for NaOH and $Na_2CO_3$ reagents were comparable whilst the $Na_2SO_4$ reagent had the lowest grade.

Table 30 Chemical composition (mass %) of the slag roasted for different Na reagents

| Test | Na reagent | $Na_2O$ | $Al_2O_3$ | CaO | $Cr_2O_3$ | FeO | MgO | MnO | $SiO_2$ | $TiO_2$ | $V_2O_5$ |
|---|---|---|---|---|---|---|---|---|---|---|---|
| 6 | $Na_2CO_3$ | 15.1 | 11.5 | 10.4 | 0.15 | 5.57 | 9.58 | 0.52 | 13.4 | 22.8 | 0.64 |
| 8 | NaOH | 14.2 | 11.8 | 9.86 | 0.13 | 5.39 | 9.20 | 0.50 | 13.1 | 22.5 | 0.64 |
| 14 | $Na_2SO_4$ | 20.3 | 11.9 | 10.4 | 0.16 | 5.28 | 10.3 | 0.49 | 14.0 | 22.6 | 0.65 |

Table 31 Chemical composition (mass %) of the water leached residues for different Na reagents

| Test | Na reagent | $Na_2O$ | $Al_2O_3$ | CaO | $Cr_2O_3$ | FeO | MgO | MnO | $SiO_2$ | $TiO_2$ | $V_2O_5$ |
|---|---|---|---|---|---|---|---|---|---|---|---|
| 6 | $Na_2CO_3$ | 14.1 | 10.4 | 12.4 | <0.05 | 5.50 | 10.4 | 0.63 | 14.8 | 24.1 | 0.17 |
| 8 | NaOH | 14.7 | 10.2 | 12.4 | <0.05 | 6.13 | 10.5 | 0.63 | 15.0 | 24.2 | 0.15 |
| 14 | $Na_2SO_4$ | 13.6 | 11.2 | 12.8 | <0.05 | 6.04 | 11.3 | 0.59 | 16.5 | 23.3 | 0.23 |

Table 32 Chemical composition (mass %) of the acid leached residues for different Na reagents

| Test | Na reagent | $Na_2O$ | $Al_2O_3$ | CaO | $Cr_2O_3$ | FeO | MgO | MnO | $SiO_2$ | $TiO_2$ | $V_2O_5$ |
|---|---|---|---|---|---|---|---|---|---|---|---|
| 6 | $Na_2CO_3$ | 12.1 | 11.0 | 4.28 | <0.05 | 1.59 | 3.57 | 0.19 | 23.9 | 40.3 | 0.14 |
| 8 | NaOH | 13.5 | 10.3 | 4.50 | <0.05 | 1.78 | 3.73 | 0.26 | 21.5 | 40.4 | 0.13 |
| 14 | $Na_2SO_4$ | 11.9 | 14.7 | 3.98 | <0.05 | 1.43 | 4.33 | 0.16 | 23.4 | 38.6 | 0.22 |

Table 33 Chemical composition (mass %) of the caustic leached residues at different Na reagents

| Test | Na reagent | $Na_2O$ | $Al_2O_3$ | CaO | $Cr_2O_3$ | FeO | MgO | MnO | $SiO_2$ | $TiO_2$ | $V_2O_5$ |
|---|---|---|---|---|---|---|---|---|---|---|---|
| 6 | $Na_2CO_3$ | 3.04 | 13.0 | 4.19 | <0.05 | 1.54 | 5.05 | 0.28 | 2.95 | 68.7 | 0.51 |
| 8 | NaOH | 2.93 | 13.1 | 4.56 | 0.37 | 1.81 | 6.31 | 0.31 | 4.86 | 66.8 | 0.53 |
| 14 | $Na_2SO_4$ | 5.60 | 15.8 | 5.33 | 0.31 | 1.77 | 5.69 | 0.35 | 3.8 | 59.7 | 0.47 |

### 4.7.2 Extraction efficiencies at different Na reagents

The effect of Na reagents on the V extraction efficiencies are shown in Figure 26. The results showed high V extraction efficiencies of 75.7% for $Na_2CO_3$ and 73.7% for NaOH, with the lowest V extraction efficiencies of 68.2% for $Na_2SO_4$. The $Na_2SO_4$ reagent required high reaction temperatures in order to maximise vanadium extractions. As reported by Nkosi, et al., (2017), the best V extraction efficiencies were attained at reaction temperatures of 1100°C and above when $Na_2SO_4$ reagent was used.

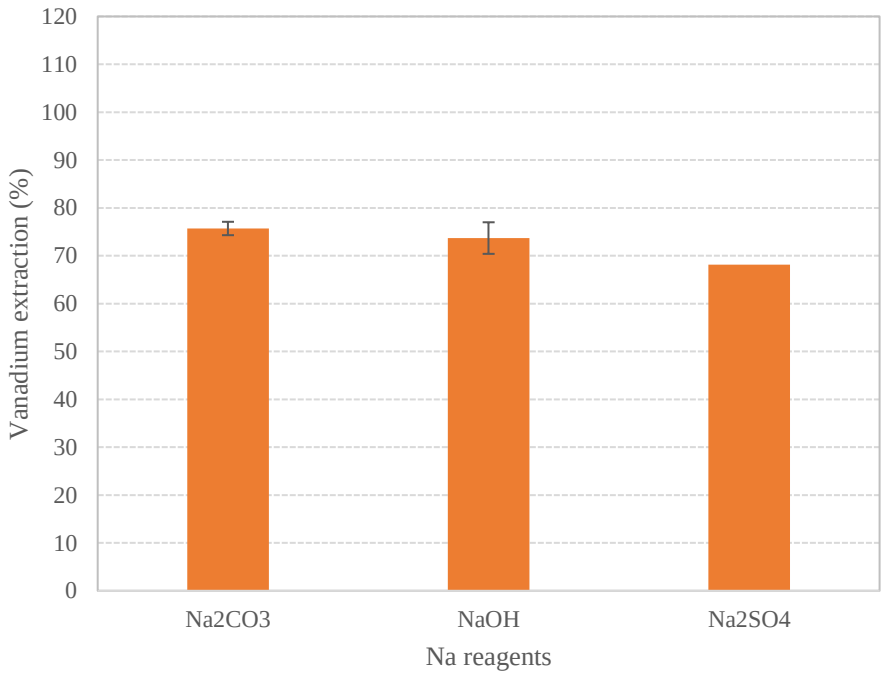


Figure 26 The effect of Na reagents on vanadium extraction efficiencies

### 4.7.3 $TiO_2$ grades and recovery to the residue at different Na reagents

The effect of different Na reagents on $TiO_2$ grades and recoveries to the residues after acid leaching are shown in Figure 27. The results showed similar high $TiO_2$ grades for NaOH and $Na_2CO_3$. The lowest $TiO_2$ grade of 38.6% was reported when $Na_2SO_4$ reagent was used. The $TiO_2$ recoveries to the residues were generally above 88% for all the different Na reagents investigated.

Figure 28 shows the effect of Na reagents on $TiO_2$ grades and recoveries to the residue after caustic leaching. The results showed increased $TiO_2$ grades For NaOH and $Na_2CO_3$ after the removal of Si impurities. The $TiO_2$ grades for the $Na_2SO_4$ reagents were 59.7% in the caustic leach residue. The $TiO_2$ grade followed the order of $Na_2CO_3$> NaOH. $Na_2SO_4$. The $TiO_2$ recoveries to the residues were generally high at above 95% for all the Na reagents examined.

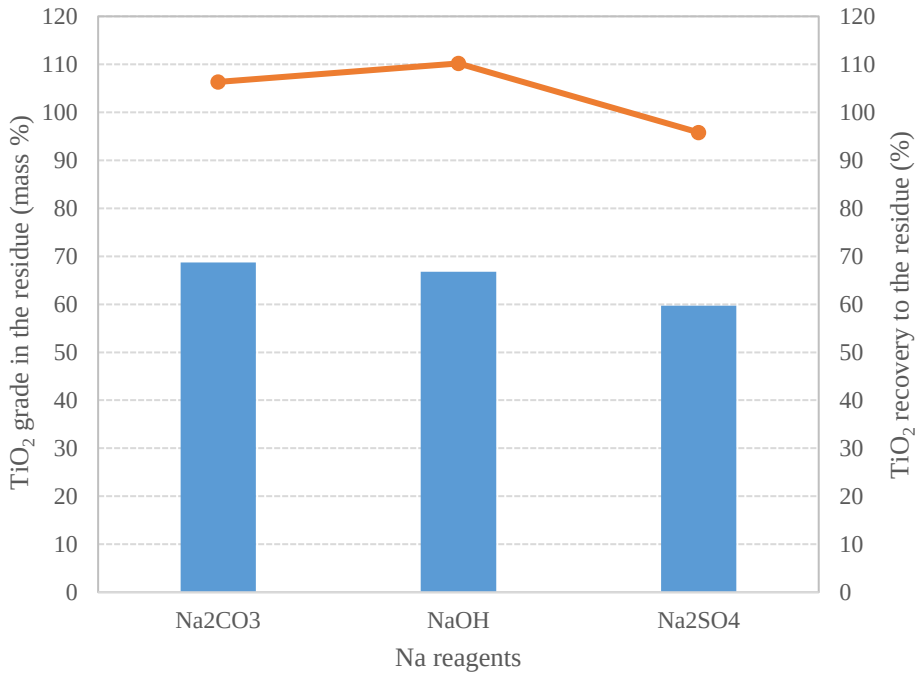


Figure 27 The effect of Na reagent on the $TiO_2$ grade and recovery to the residue after acid leaching

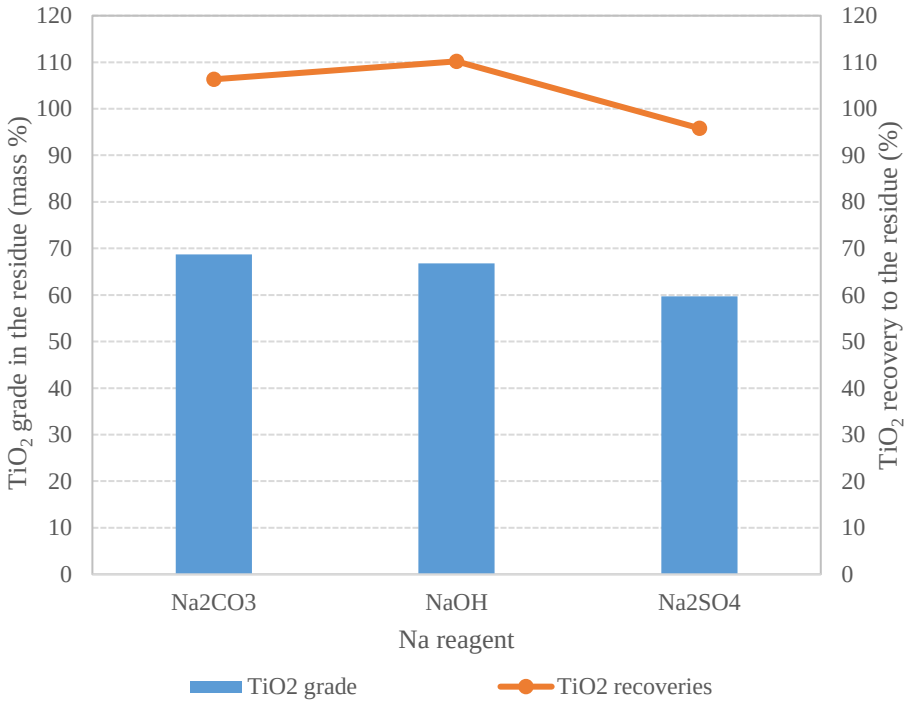


Figure 28 The effect of Na reagent on the $TiO_2$ grade and recovery to the residue after caustic leaching

The results showed that NaOH and $Na_2CO_3$ were comparable in terms of the resulting V extractions and $TiO_2$ grades. As previously explained NaOH is an expensive salt, therefore for leaching tests $Na_2CO_3$ was selected for further investigations.

## 4.8 Phase compositions of the roasted and residues

Figure 29, Figure 30, Table 34, Table 35, Table 36, and Table 37 show the backscattered SEM micrographs, EDS, and XRD results of the titaniferous slag roasted with the best roasting conditions and leached in water, acid, and caustic solutions. The results show that after roasting the titaniferous slag at the best roasting conditions, the vanadium-bearing phases i.e. the spinel and pseudobrookite ss, were decomposed during roasting with spinel levels of <5 mass % detected by the XRD. The phases that formed after roasting include titanaugite, perovskite, sodium magnesium aluminium silicate ($Na_3MgAlSi_2O_8$), and Fe-oxide. The EDS results show that V species were present in the $Na_3MgAlSi_2O_8$ and Titanaugite phases whilst Ti species were found in the Titanaugite, perovskite, and $Na_3MgAlSi_2O_8$ phases. The impurities in the different phases required the leaching of Mg, Ca, Al, Fe, and Si impurities. The Mg impurities were present in the Titanaugite and $Na_3MgAlSi_2O_8$ phases whilst Ca species were found to be present in Titanaugite and perovskite. The Al species were present in all the phases that formed after roasting whereas the Fe impurities were in the Titanaugite and $Na_3MgAlSi_2O_8$ phases. Si impurities were mainly found in the $Na_3MgAlSi_2O_8$ phase. The roasting stage was conducted to introduce a high Na reagent that would de-stabilise the phases containing V species such that V would be released into the solution in the leaching stage. The V-containing species included pseudobrookite ss and the spinel phase which were mostly decomposed after roasting.

The phase chemistry of the water-leached residue shows that the phases present after leaching include spinel, perovskite, sodium magnesium titanium oxide ($Na_2MgTi_2O_6$), and Fe-oxide. The spinel phase was present after leaching and the XRD confirmed the levels to be minimum at <5%. The Titanaugite and $Na_3MgAlSi_2O_8$ phases appeared to have decomposed, releasing the V incorporated in them through leaching into the solution. The V species that were not leached out assimilated into the spinel phase. These results confirm the chemical composition results which showed low concentrations of $V_2O_5$ in the residue suggesting that some of the V remained in the residue when most V was leached into the solution.

A new phase $Na_2MgTi_2O_6$ containing high Ti and Si species formed after water leaching. This phase contained several impurities, including Na, Mg, Al, Ca, and Fe. The Na impurities were leached out into the solution as the concentration levels significantly decreased. These results contradict with the chemical composition results which showed a slight decrease in the $Na_2O$ concentrations after leaching. Al species were dominant spinel and some in the $Na_2MgTi_2O_6$

phase. The slight decrease in $Al_2O_3$ concentration from roasting and residue chemical composition results might be associated with the removal of Fe species from the perovskite and Fe-oxide phases. Ca species appear to have increased in concentration levels of the perovskite and $Na_2MgTi_2O_6$ phases confirming an increase in CaO concentration of the roast material and the water leach residue. Fe species in the Fe-oxide phase remained high in the roast material and water leach residue confirming similar FeO concentrations from the chemical composition results of both stages.

The water leaching stage was conducted to extract most of the V into the solution. This was achieved since low concentrations of $V_2O_5$ were attained in the residue as shown from the chemical composition results and V species found in the spinel phase which was detected at trace levels of <5% in the phase chemistry of the water leach residue.

The SEM-EDS and XRD results show that the phases present after acid leaching include spinel, perovskite, Fe-oxide, rutile, Mg-Si-Fe oxide, and chromite. The acid leaching stage aimed to remove impurities such as Mg, Ca, Al, and Fe present after water leaching to upgrade the concentration of $TiO_2$ in the acid leach residue. The $Na_2MgTi_2O_6$ appeared to have decomposed after acid leaching. New phases formed after acid leaching which included the Mg-Si-Fe oxide and chromite phases. The Mg and Fe impurities seem to have combined with Si species to form a new Mg-Si-Fe oxide phase instead of being leached out into the solution. The Mg-Si-Fe oxide phase was detected at trace levels by the XRD confirming the decrease in MgO and FeO chemical compositions from the acid leach residues. Ca impurities dominated in the perovskite phase which was detected at minor levels between 5% and 20% by the XRD. These results confirm the decrease in CaO concentrations from the chemical composition results suggesting the removal of Ca species into the solution. The Al species seem to have been incorporated by all of the phases that formed after acid leaching suggesting that Al was barely leached out into the solution. These results were confirmed by a slight increase in $Al_2O_3$ concentration from the chemical composition results. The Ti species were mostly found in the rutile phase at high levels confirming the significant increase in $TiO_2$ concentrations as shown by the chemical composition of the acid leach residues.

The acid leaching stage aimed at the removal of impurities such as Mg, Ca, Al, and Fe and also upgrading the $TiO_2$ grade in the residue was successful as $TiO_2$ concentration increased and most of the impurities were minimised except for Al which slightly increased after acid leaching.

The caustic leaching phase chemistry revealed the presence of perovskite, spinel, rutile, Fe-oxide, chlorite, and aluminosilicates. The caustic leaching stage was aimed at the removal of Si impurities and to further upgrade the $TiO_2$ concentration in the residue. The decomposition of the Mg-Si-Fe oxide phase suggests that this process was successful since most of the Si species were incorporated in this phase. These results were confirmed by a decrease in $SiO_2$ concentration from the chemical composition results of the caustic leach residues. The remaining Si species were incorporated in the new chlorite and aluminosilicate phases that formed after caustic leaching. The chlorite phase resulted from the combination of Cl used in acid leaching and other impurities that remained after acid leaching. The high Al species that were not leached out in the acid-leaching stage merged with the remaining Si species to form the new aluminosilicate phase. The Ti species were found in the dominant rutile phase confirming the increase in $TiO_2$ concentrations as shown in the chemical composition of the caustic leach residues.

The caustic leaching stage was successful since most of the Si species were minimised and the $TiO_2$ concentration in the residue increased.

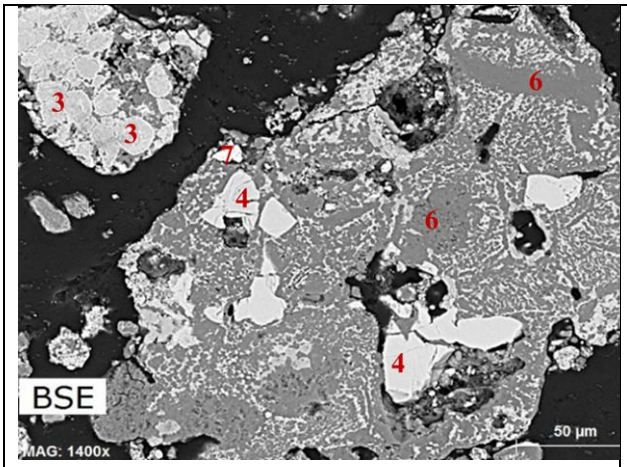


*a) Roasted titaniferous slag*

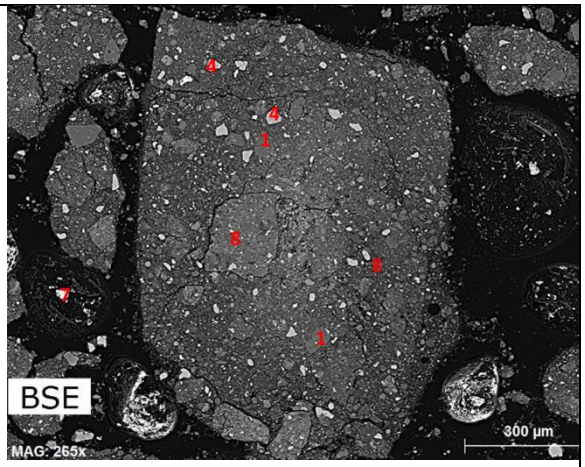


*b) Water leached residue*

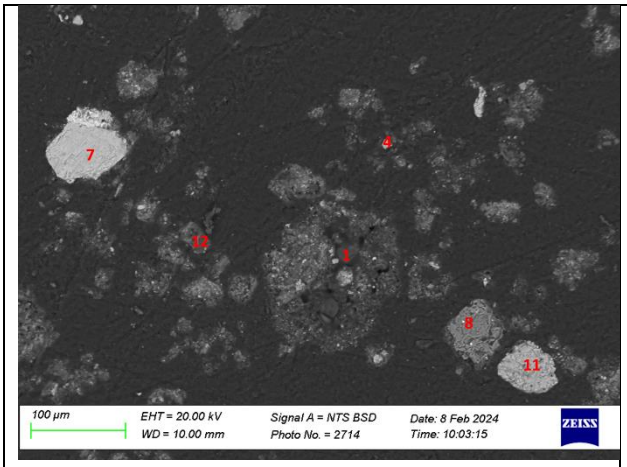


*c) Acid leach residue*

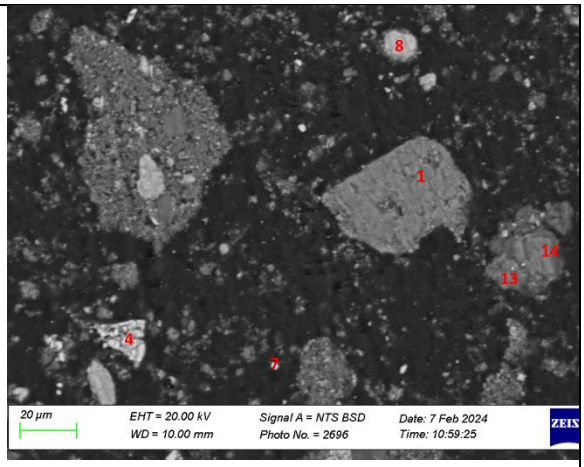


*d) Caustic leach residue*

Figure 29 Backscattered electron microstructure of the slag roasted, water, acid, and caustic leached with the best roasting conditions

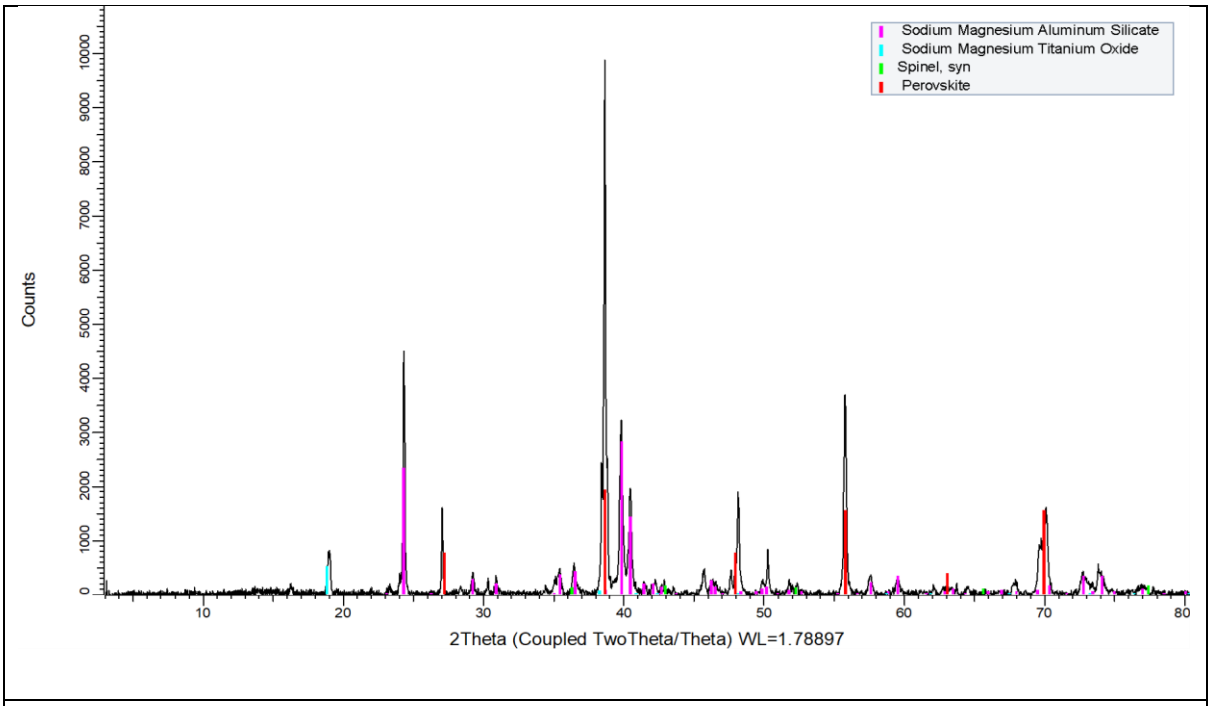


*a) Roast material*

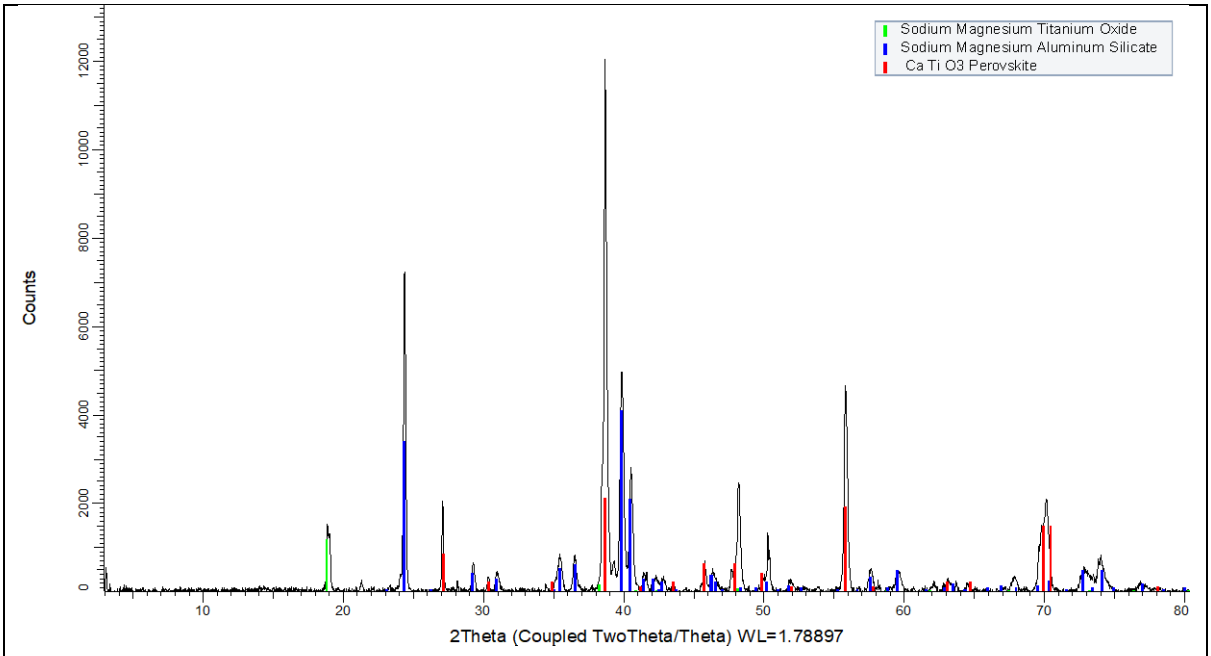


*b) Water-leach residue*

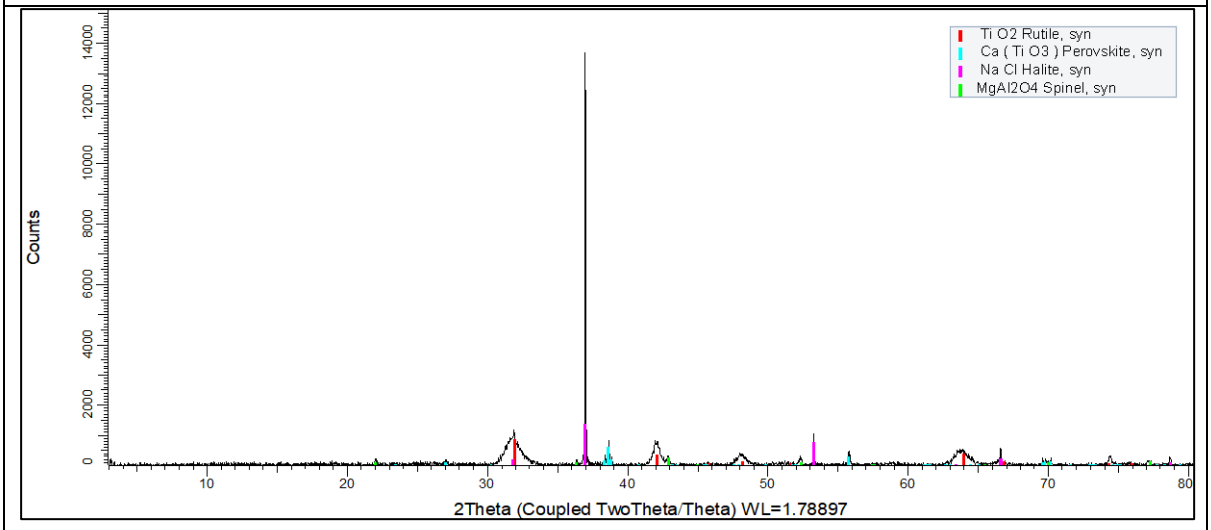


*c) Acid leach residue*

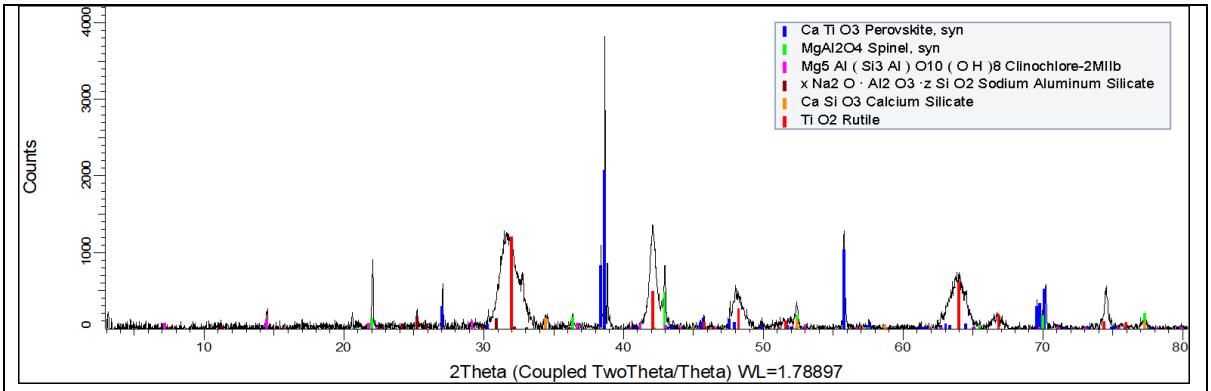


*d) Caustic leach residue*

Figure 30 XRD phase composition of a) roast material, b) water-leach residue, c) acid-leach residue, and d) caustic-leach residue

Table 34 Typical EDS analysis results of the BSE phases and XRD phase compositions of roasted material (mass %)

| Spot | O | Na | Mg | Al | Si | Ca | Ti | V | Mn | Fe | XRD results |
|---|---|---|---|---|---|---|---|---|---|---|---|
| 3 | 30.5 | 10.1 | 3.0 | 5.2 | | 1.8 | 13.8 | 0.5 | 0.9 | 34.0 | Titanaugite |
| 4 | 35.4 | | | 2.0 | | 30.4 | 32.1 | | | | Perovskite |
| 6 | 47.2 | 17.9 | 7.1 | 10.2 | 11.7 | | 3.5 | 0.2 | | 2.2 | $Na_3MgAlSi_2O_8$ |
| 7 | 24.4 | | | 4.6 | | | | | | 71.0 | Fe-oxide |

Table 35 Typical EDS analysis results of the BSE phases and XRD phase compositions of water leach residue (mass %)

| Spot | O | Na | Mg | Al | Si | Ca | Ti | V | Fe | XRD results |
|---|---|---|---|---|---|---|---|---|---|---|
| 1 | 46.1 | | 18.0 | 29.1 | | | 6.0 | 0.6 | 0.8 | Spinel |
| 4 | 35.0 | | | | | 31.3 | 33.7 | | | Perovskite |
| 7 | 22.5 | | | | | | 0.8 | | 76.8 | FeO |
| 8 | 42.7 | 2.9 | 6.7 | 4.1 | 14.2 | 2.5 | 23.0 | | 3.9 | $Na_2MgTi_2O_6$ |

Table 36 Typical EDS analysis results of the BSE phases and XRD phase compositions of acid leach residue (mass %)

| Spot | O | Na | Mg | Al | Si | P | Cl | Ca | Ti | V | Cr | Mn | Fe | XRD results |
|---|---|---|---|---|---|---|---|---|---|---|---|---|---|---|
| 1 | 40.3 | | 16.9 | 34.7 | | | | | 6.7 | 0.8 | 0.1 | 0.4 | 1.0 | Spinel |
| 4 | 27.4 | | | 0.4 | 0.3 | | | 32.0 | 40.4 | | | | | Perovskite |
| 7 | 34.9 | | | 4.2 | 1.4 | 1.3 | 0.3 | 0.8 | | | | | 57.1 | FeO |
| 9 | 40.0 | 0.5 | 0.6 | 1.1 | 3.1 | | 1.6 | 2.2 | 48.5 | | | | 2.6 | Rutile |
| 11 | 4.6 | | 21.9 | 1.7 | 59.5 | | | 0.9 | | | 0.3 | | 11.1 | Mg-Si-Fe oxide |
| 12 | 27.5 | | 5.1 | 9.1 | | | | | 0.7 | | 33.4 | | 24.2 | Chromite ss |

Table 37 Typical EDS analysis results of the BSE phases and XRD phase compositions of caustic leach residue (mass %)

| Spot | O | Na | Mg | Al | Si | Cl | Ca | Ti | V | Cr | Mn | Fe | XRD results |
|---|---|---|---|---|---|---|---|---|---|---|---|---|---|
| 1 | 38.7 | 0.9 | 16.5 | 34.5 | 0.2 | | 0.6 | 2.9 | 1.0 | 1.9 | 0.7 | 3.7 | Spinel |
| 4 | 39.9 | | | 0.4 | | | 27.1 | 32.8 | | | | | Perovskite |
| 7 | 34.9 | | | 0.7 | 0.4 | 0.3 | | 3.1 | | | | 61.0 | FeO |
| 9 | 43.2 | 2.1 | 1.7 | 0.8 | 2.2 | 1.0 | 1.2 | 49.7 | | | | 0.8 | Rutile |
| 13 | 39.4 | | 7.9 | 5.9 | 27.1 | 1.5 | 1.7 | 1.3 | | 0.7 | | 14.5 | Chlorite? |
| 14 | 50.2 | | | 33.9 | 15.6 | | | 0.3 | | | | | Aluminosilicate |

# CHAPTER 5

# LEACHING RESULTS

Leaching tests were conducted to remove the impurities through acid and caustic leaching, and therefore $TiO_2$ content in the residue was upgraded. The effect of leaching time and HCl concentration on the leaching of impurities and $TiO_2$ upgrade were discussed. The kinetics of the leaching of impurities were evaluated.

## 5.1 Leaching chemical reactions

The roasting of V-bearing materials with Na reagents typically forms $NaVO_3$ which dissolves in water. Leaching of NaVO3 in water dissolves according to the chemical reaction [6].

$$NaVO_3 + H_2O \rightarrow H_2VO_4^- + Na^+ \qquad H_2O \text{ leaching} \qquad [6]$$

Figure 31 shows the stability ranges of vanadium species at different pH and Eh values. From the graph it can be seen that $H_2VO_4^-$ is stable between the pH of 6 and 8 and oxidative Eh above 0 V. Since the pH of water is 7 and the roasting was conducted in an oxidising atmosphere, V was leached out as $H_2VO_4^-$ into the solution.

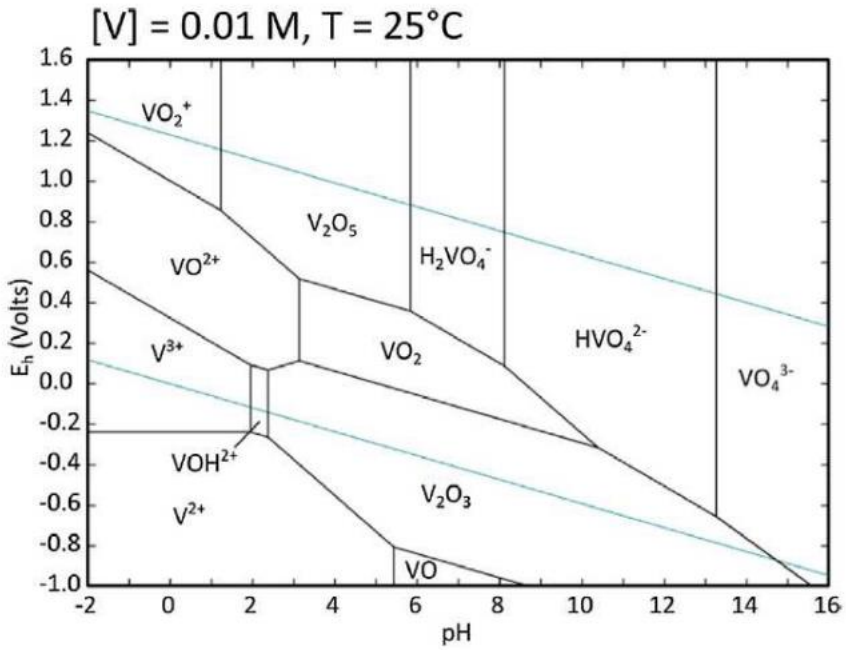


Figure 31 Pourbaix diagram showing the stable V species at different Eh and pH values (Gilligan & Nikoloski, 2020)

The water leach residue formed the $Na_2MgTi_2O_6$ phase which is a solid solution of $Na_2O$ and $MgTi_2O_6$. This phase has Al, Ca, Fe, and Si impurities. The possible chemical reaction involved in the upgrading of $TiO_2$ through the removal of impurities is shown by Equations [37] to [39].

$$MgTi_2O_5 + 6H+ \rightarrow Mg^{2+} + 2TiO^{2+} + 3H_2O \quad [37]$$

$$Fe2TiO_5 + 8H+ \rightarrow 2Fe^{3+} + TiO^{2+} + 4H_2O \quad [38]$$

$$AlTi_2O_5 + 8H+ \rightarrow 2Al^{3+} + TiO^{2+} + 4H_2O \quad [39]$$

The chemical reaction from caustic leaching is shown by Equation [26] which shows the removal of Si impurities.

$$SiO_{2(s)} + 2NaOH_{(aq)} \rightarrow Na_2SiO_3(aq) + H_2O(l) \quad [26]$$

## 5.2 Effect of leaching time

The effect of time on the leaching of impurities from the water-leach residue of the best vanadium extraction test was investigated. The chemical composition of this water-leach residue is presented in Table 38. As presented in CHAPTER 3 a set of standard acid leaching conditions were used, i.e. lixiviant of 20% HCl concentration, s:l mass ratio of 1:4, reflux-leaching temperature of 110°C, and slurry agitation speed of 350 rpm. The respective leaching times were 1, 4, 8, 16, and 24 hours.

Table 38 Chemical composition (mass %) of the feed material used for leaching optimization

| Test | $Na_2CO_3$:NaOH | $Na_2O$ | $Al_2O_3$ | CaO | $Cr_2O_3$ | FeO | MgO | MnO | $SiO_2$ | $TiO_2$ | $V_2O_5$ |
|---|---|---|---|---|---|---|---|---|---|---|---|
| 6 | 100:0 | 14.1 | 10.4 | 12.4 | <0.05 | 5.50 | 10.4 | 0.63 | 14.8 | 24.1 | 0.17 |

### 5.2.1 Chemical compositions of the acid leach residues at different leaching times

Table 39 presents the chemical compositions of the acid leach residues produced at different leaching times. The results show that the concentrations of CaO, FeO, and MgO impurities in the solids decreased after acid leaching, however, the CaO concentration only decreased slightly. As shown in Table 36, the residual CaO was contained in the sparingly soluble perovskite ($CaTiO_3$) phase, especially in HCl lixiviant. The leaching of Ca from $CaTiO_3$ is effectively achieved by an alkaline roasting and leaching process (Wang, et al., 2010).

The $Al_2O_3$ concentrations in the leach solids slightly decreased between 1 and 16 hours of leaching time, however higher $Al_2O_3$ concentrations were attained at a leaching time of 24 hours. High $Al_2O_3$ concentrations that resulted after leaching for longer times were attributed to the formation and stabilisation of the sparingly-soluble chromite solid solution, which contained high contents of $Al_2O_3$ as shown in Table 36. $SiO_2$ concentrations were generally high in the acid leach residues. This was attributed to the stabilisation of silicate phase(s), which are generally insoluble in the HCl lixiviant.

These results suggest that it was feasible to remove most of the impurities over a shorter leaching time, however, the $TiO_2$ concentration in the solids was still low owing to the further dissolution of sodium-bearing phase(s).

Table 39 Chemical composition (mass %) of the acid leach residue leached at different times

| Test | Leach time (hrs) | *$Na_2O$ | $Al_2O_3$ | CaO | FeO | MgO | MnO | $SiO_2$ | $TiO_2$ | $V_2O_5$ |
|---|---|---|---|---|---|---|---|---|---|---|
| 15 | 1 | 31.9 | 2.82 | 7.49 | 0.97 | 3.03 | 0.13 | 26.3 | **27.2** | 0.20 |
| 16 | 4 | 34.2 | 2.63 | 6.90 | 1.07 | 2.75 | 0.12 | 22.9 | **29.2** | 0.23 |
| 17 | 8 | 39.1 | 2.55 | 5.01 | 1.10 | 2.54 | 0.12 | 20.3 | **29.0** | 0.25 |
| 18 | 16 | 41.3 | 2.49 | 4.52 | 1.12 | 2.17 | 0.12 | 19.2 | **28.9** | 0.25 |
| 6 | 24 | 12.1 | 11.0 | 4.28 | 1.59 | 3.57 | 0.19 | 23.9 | **40.3** | 0.14 |

*- determined by difference

### 5.2.2 Effect of leaching time on $TiO_2$ grade

Figure 32 shows the results of the effect of acid leaching time on the $TiO_2$ grade and recovery to the residues. The results show that the $TiO_2$ grade in the residues increased with leaching time. The highest $TiO_2$ grade of 40.3% was achieved after leaching for a period of 24 hours. These results suggest that leaching for a longer period of time results in high $TiO_2$ grade in the solids. Therefore, the best leaching time of 24 hours was recommended for investigating other parameters. $TiO_2$ recoveries to the residues were generally high at more than 90%.

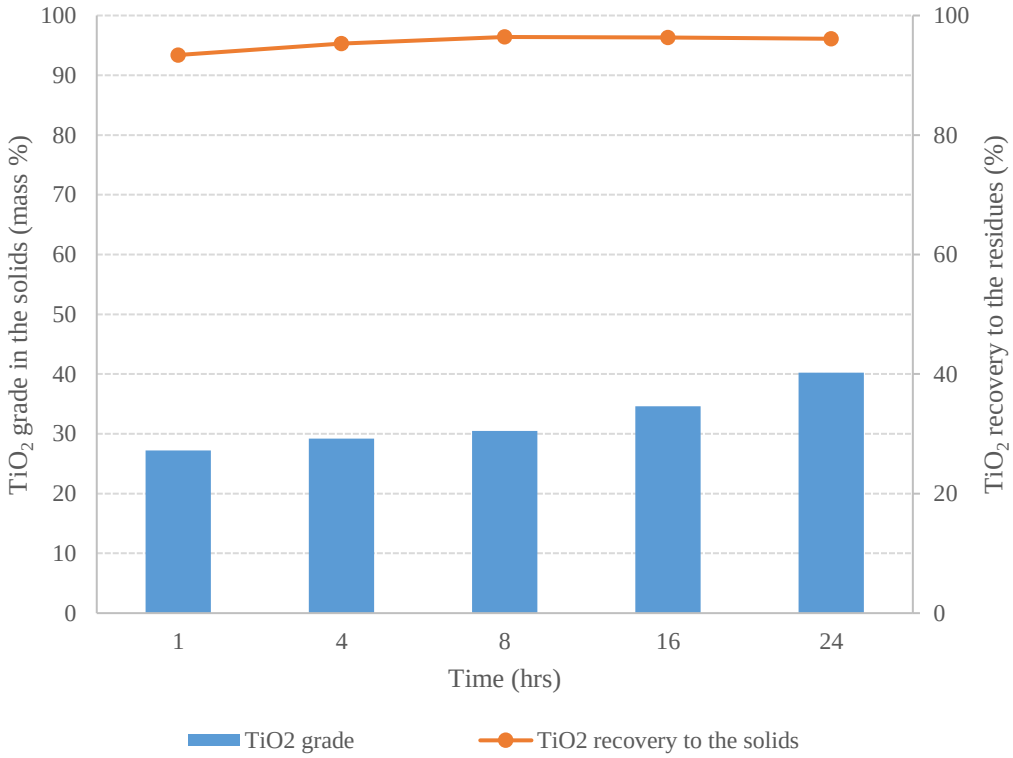


Figure 32 Effect of HCl leaching time on $TiO_2$ upgrading and recovery to the solids

## 5.3 Effect of acid concentration

The effect of acid concentration on impurity removal was investigated using the standard leaching conditions of s:l mass ratio of 1:4, leaching temperature of 110°C, slurry agitation speed of 350 rpm, and leaching time of 24 hours. The acid concentrations used for leaching tests were 15%, 20%, and 25%.

A 'blank' test was conducted. This test refers to an experiment that involved direct leaching of unroasted or as-is titaniferous slag using 20% HCl as lixiviant. This test was conducted as a baseline.

### 5.3.1 Chemical compositions of the residues at different HCl concentrations

Table 40 shows the chemical compositions of the acid leach residues that were obtained at different HCl concentrations. The results show that the increase in acid concentration from 20% to 25% HCl resulted in a further removal of impurities such as Ca, Fe, and Mg. Higher HCl concentration of 25% in the lixiviant appears to have leached some Ca in $CaTiO_3$. The concentrations of CaO and MgO impurities were significantly minimised at high HCl

concentration of 25%. The removal of these impurities resulted in the concentration of $SiO_2$ in the solids – $SiO_2$ likely stabilised as a sodium silicate phase as shown by the high estimated $Na_2O$ concentration in the residue, which was determined by difference. The removal of impurities at high acid concentrations resulted in a slight upgrade of $TiO_2$ concentration to 42.0%. These results suggest that higher acid concentrations have the potential to remove Ca, Fe, and Mg impurities.

Blank test results show higher concentrations of Al, Mg, and Si impurities in the residues compared to the residue produced from leaching the slag that was roasted using the best conditions. The $TiO_2$ grade in the 'blank' test was comparable with that attained when leaching the roasted slag using the best roasting conditions (Test 6). Besides the presence of $Na_2O$ in the roasted leach residue, the other notable difference between the blank and the roasted slags was the high $V_2O_5$ concentration in the "blank" sample since the titaniferous slag was directly leached with HCl without involving the initial preliminary roast-leach process for V extraction.

Table 40 Chemical composition (mass %) at different HCl concentrations

| **Test** | **HCl conc (%)** | ***$Na_2O$** | **$Al_2O_3$** | **CaO** | **FeO** | **MgO** | **MnO** | **$SiO_2$** | **$TiO_2$** | **$V_2O_5$** |
|---|---|---|---|---|---|---|---|---|---|---|
| 19 | "Blank " - 20 | 15.1 | 6.56 | 3.60 | 0.90 | 5.60 | 0.21 | 27.6 | **39.4** | 0.91 |
| 20 | 15 | 29.2 | 2.91 | 9.50 | 4.13 | 1.97 | 0.22 | 20.8 | **30.9** | 0.29 |
| 6 | 20 | 12.1 | 11.0 | 4.28 | 1.59 | 3.57 | 0.19 | 23.9 | **40.3** | 0.14 |
| 21 | 25 | 24.0 | 2.31 | 1.04 | 0.34 | 1.36 | <0.05 | 28.7 | **42.0** | 0.29 |

*-determined by difference

### 5.3.2 Effect of HCl concentration on $TiO_2$ grade in the residues

Figure 33 shows the effect of HCl concentration on the $TiO_2$ grade and recovery to the residue after acid leaching. The results show that the $TiO_2$ grade in the residues increased with increasing HCl concentration. The $TiO_2$ grades in the residues leached at 20% and 25% HCl concentration were not significantly different at about 40% and 42%, respectively. $TiO_2$ recoveries were generally high at more than 95% at 20% and 25% HCl concentrations, however, the recovery at lower HCl concentration of 15% was low. The reason for lower recoveries at the lower HCl acid strength is not clear at this stage.

The blank test results show a $TiO_2$ grade of 39.4%. This $TiO_2$ grade in the blank leach residue was comparable to the $TiO_2$ grades in the residues produced at 20% and 25% HCl concentrations. The $TiO_2$ recovery to the residue in the blank test was very low.

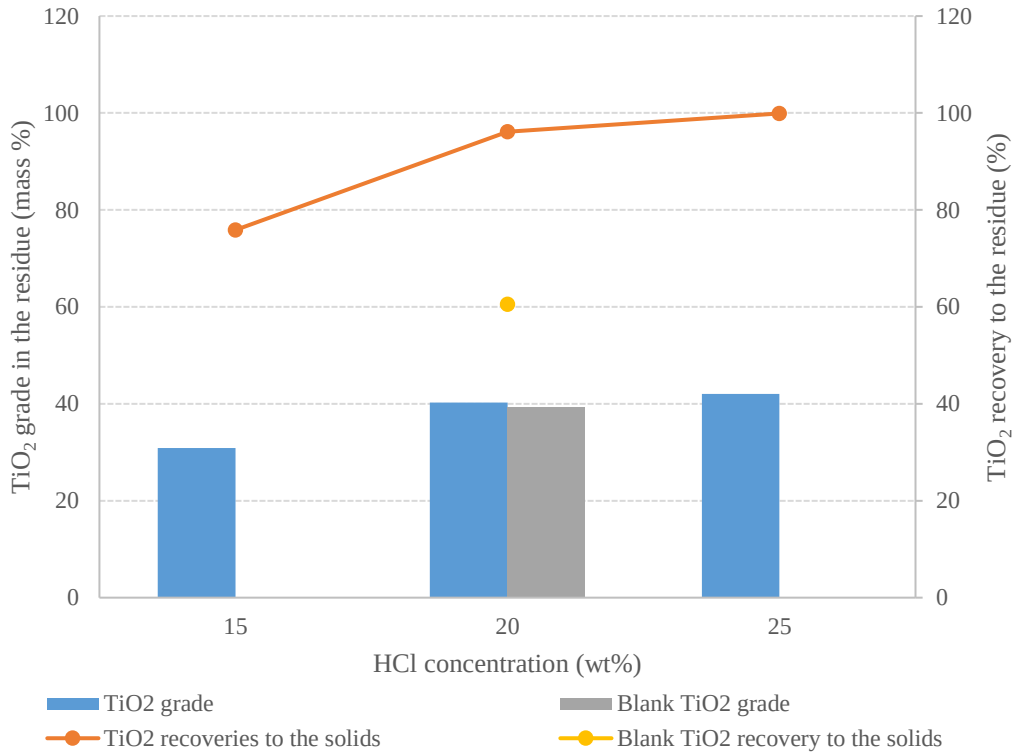


Figure 33 $TiO_2$ upgrading and recovery to the residue after acid leaching at different HCl concentrations

### 5.3.3 Chemical compositions of the residues of caustic leaching

Table 41 presents the chemical compositions of the residues produced after caustic leaching. The results show that the $SiO_2$ concentrations in the HCl leach residues reported in Table 40, significantly decreased after caustic leaching. $SiO_2$ removal from the 25% HCl leach residue was accompanied by $TiO_2$ upgrading to 71.0%. Further optimisation of the HCl and NaOH leaching stages have a potential to remove impurities and upgrade $TiO_2$ even further, through the decompositions of the impurity phases presented in Table 37 and leaching of detrimental species. These results concur with the results reported by Goso et al. (2016), where it was reported that caustic leaching of HCl residue result in silica removal and significant upgrading of $TiO_2$ in the residue. In this work, a residue with as high as 75% TiO2 concentration was produced from a titaniferous slag through a similar processing involving HCl and NaOH leaching stages (Goso, et al., 2016).

Table 41 Chemical composition (mass %) of the residue produced after caustic leaching

| Test | HCl conc. (%) | *$Na_2O$ | $Al_2O_3$ | CaO | FeO | MgO | MnO | $SiO_2$ | $TiO_2$ | $V_2O_5$ |
|---|---|---|---|---|---|---|---|---|---|---|
| 20 | 15 | 11.3 | 4.20 | 15.5 | 6.44 | 3.27 | 0.35 | 7.66 | **50.7** | 0.46 |
| 6 | 20 | 3.04 | 13.0 | 4.19 | 1.54 | 5.05 | 0.28 | 2.95 | **68.7** | 0.51 |
| 21 | 25 | 10.9 | 3.83 | 2.63 | 0.73 | 2.93 | 0.07 | 7.43 | **71.0** | 0.46 |

*-determined by difference

### 5.3.4 Effect of HCl concentration on $TiO_2$ grade after caustic leaching

Figure 34 presents the resulting $TiO_2$ grades and recoveries to the residues after further upgrading of the HCl leach solids through caustic leaching. The results show that the $TiO_2$ grades in the caustic leach residues increased with the concentration of the acid lixiviant concentration – the residues produced using higher acid concentrations already had higher $TiO_2$ concentrations. The highest $TiO_2$ grades of 71.0% and recovery of 99.1% were achieved when the HCl concentration was 25%.

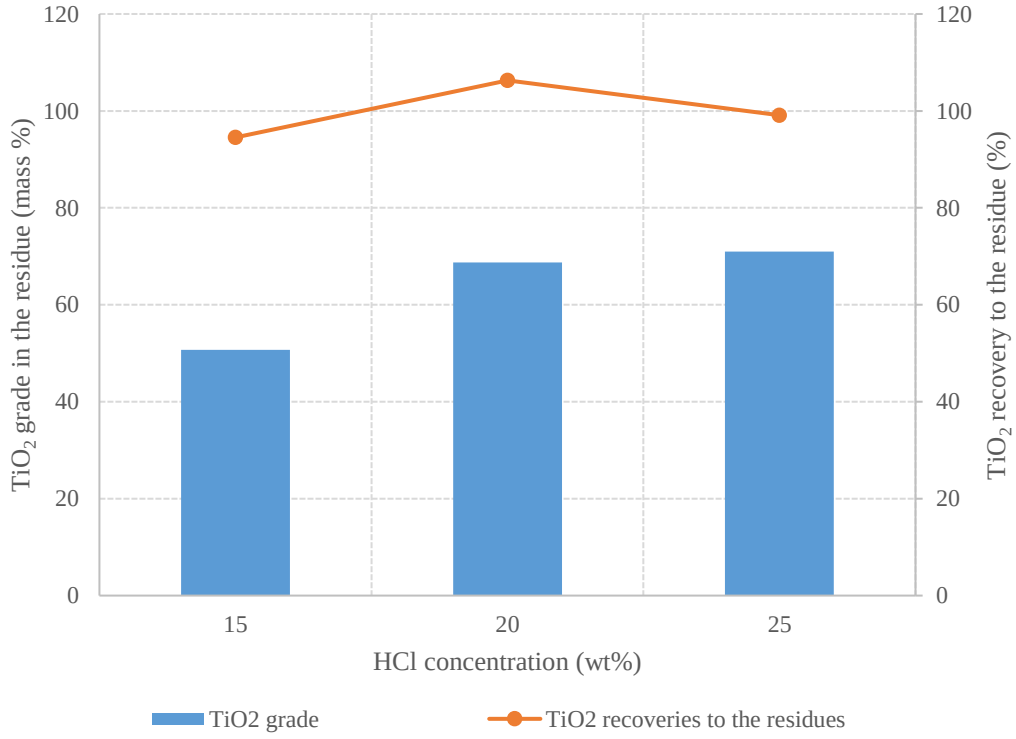


Figure 34 The $TiO_2$ upgrading and recovery to the residue after caustic leaching at different HCl concentrations

### 5.3.5 Washing of the caustic residues for Na removal

The caustic leach residue that contained the highest $TiO_2$ grade of 71% was washed to remove the Na species that were present on the residue after caustic leaching. The washing was conducted using hot water at a s:l mass ratio of 1:4 and stirring at 350 rpm for a period of 2 hours whilst keeping the water temperature above at 50°C. This process was carried out on the caustic leach residue that resulted in highest and lowest $TiO_2$ grade.

Table 42 presents the chemical composition of the washed caustic leach residue. From the results, it can be seen that the $TiO_2$ grade increased from 71.0% to 79.6%. A decrease in the $Na_2O$ and $SiO_2$ concentrations was observed in the residues. These results suggest that the washing of the residues resulted in the removal of $Na_2O$ and $SiO_2$, which likely occurred as the water-soluble sodium silicate ($Na_2SiO_3$) though this phase was not observed in the phase compositions presented in Table 42. Further washing of the caustic leach residue had the potential to remove the residual $Na_2O$ and $SiO_2$ species, especially if they existed as $Na_2SiO_3$.

Table 42 Chemical composition (mass %) of the washed caustic leach residues

| Test | HCl concentration (%) | *$Na_2O$ | $Al_2O_3$ | CaO | FeO | MgO | MnO | $SiO_2$ | $TiO_2$ | $V_2O_5$ |
|---|---|---|---|---|---|---|---|---|---|---|
| 20 | 25 | 6.26 | 3.53 | 1.43 | 0.59 | 2.78 | 0.06 | 5.43 | **79.6** | 0.32 |

*- determined by difference

#### *5.3.5.1 Phase composition of the washed residue*

Figure 35 shows the backscattered electron image of the washed caustic leach residue. The micrographs shows that the phases present in the final washed caustic leach residue were spinel, perovskite, rutile, quartz, and chromite. The EDS chemical composition results show that Na, Mg, Al, Si, Cl, and Ca existed as impurities in the rutile phase. The presence of Na in the rutile phase indicates that the washing of the caustic leach residue could be improved. Longer washing times are required to remove the impurities to minimal concentrations thus increasing the $TiO_2$ grade.

Mg, Al and Fe impurities in the upgraded residue mainly occurred as spinel and chromite. These species could be effectively removed by optimising the roasting and flux stages. Ca impurity mainly occurred in perovskite. As shown earlier in section 5.3.1, leaching of Ca from perovskite can be achieved by higher HCl acid concentrations. Wang et al. (2010) showed that

perovskite can be processed through alkaline roasting and leaching process to produce a high-purity $TiO_2$ product after successful removal of Ca impurity.

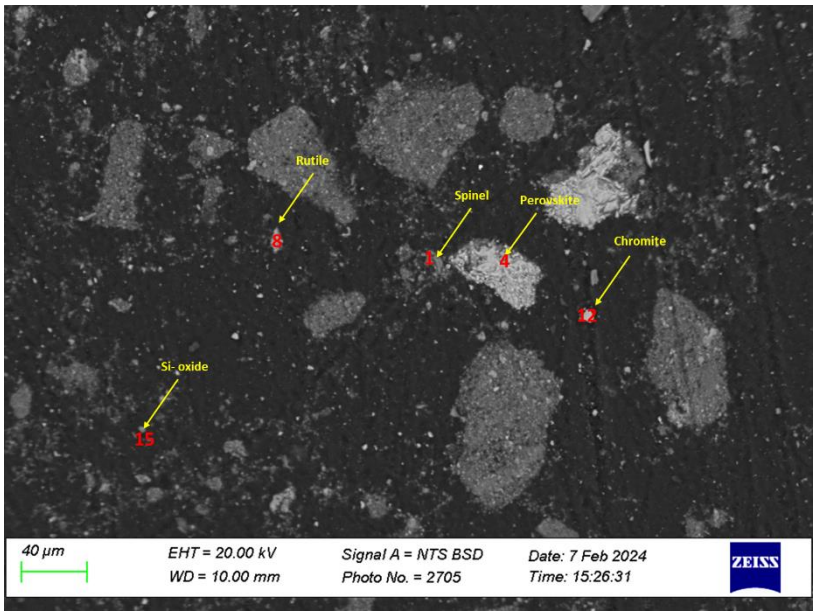


Figure 35 Backscattered electron image of the washed caustic residue

Table 43 Typical EDS analysis results of the BSE phases and XRD phase compositions of the washed residue (mass %)

| Spot | O | Na | Mg | Al | Si | Cl | Ca | Ti | V | Cr | Fe | XRD results |
|---|---|---|---|---|---|---|---|---|---|---|---|---|
| 1 | 40.9 | | 15.8 | 33.3 | 0.3 | | | 6.4 | 1.1 | 0.7 | 1.5 | Spinel |
| 4 | 35.9 | | | | | | 28.7 | 35.4 | | | | Perovskite |
| 8 | 44.4 | 1.8 | 0.4 | 0.3 | 1.8 | 0.4 | 0.6 | 50.3 | | | 0.7 | Rutile |
| 12 | 36.7 | | 4.2 | 7.6 | | | | 1.4 | | 31.4 | 18.7 | Chromite ss |
| 15 | 14.3 | | | | 85.7 | | | | | | | Quartz |

## 5.4 Kinetic analysis of leaching of impurities

Leaching is a solid-liquid reaction. It is important to understand the mechanism and mathematical models involved in leaching kinetics. There are four models commonly used to describe the solid-liquid reactions. These reactions include the shrinking core, homogeneous, grain and pore models (Georgiou & Papangelakis, 1998). In the shrinking core model, the reaction takes place on the particle surface where the particle dissolves in the liquid and the particle size shrinks. Also, the shrinking core model is applied on the particles that are non-porous. Other models are commonly applied to particles that are porous for the solid-liquid

systems. Therefore, the shrinking core model was selected for describing the leaching of impurities from the titaniferous slag. This selection of this model was based on that the slags are considered to have compact particles and are also regarded as non-porous (Nie, et al., 2020; Zheng, et al., 2016).

The shrinking core model can be determined by surface chemical reaction, film diffusion control, diffusion through the ash/product layer, and sometimes diffusion across the product layer and interface transfer as described in Equations [37] to [40], respectively (Nie, et al., 2020).

$1-(1-X)^{\frac{1}{3}} = k_r t$ [40] Surface chemical reaction

$1-(1-X)^{1/F_p} = k_r t$ [41] Film diffusion control

$1-\left(\frac{2}{3}\right)X-(1-X)^{\frac{2}{3}} = k_r t$ [42] Diffusion through ash/product layer

$\left(\frac{1}{3}\right) ln(1-X)-(1-(1-X)^{1/3}) = k_r t$ [43] Diffusion across product layer and interface transfer

where X represents the leaching rate of impurities, t is the leaching time, $k_r$ is the reaction rate constant, and $F_p$ is the shape coefficient of the titaniferous slag particles. In this study it was assumed that the solid particles from the water-leach stage of vanadium extraction were spherical such that $F_p$ was equal to 3, therefore Equations [37] and [38] became the same. Thus, the film diffusion control reaction was eliminated from the kinetics calculations (Nie, et al., 2020).

### 5.4.1 Effect of leaching time on removal of impurities

The impurity removal generally followed the order: Mg > Fe > Al > Ca, as shown in Figure 36. The leaching efficiency of impurities increased with leaching time. After 4 hours, Mg, Fe, and Al reached a plateau. Ca reached a plateau after leaching for 8 hours.

Figure 37 shows the effect of acid concentration on the leaching of impurities. At lower HCl concentrations of 15%, the order of leaching of impurities followed: Mg > Al > Fe > Ca. Thereafter, Al leaching efficiency decreased from 20% to 25% acid concentration. Mg removal was highest at 20% HCl concentration and above, followed by Fe and lastly Ca.

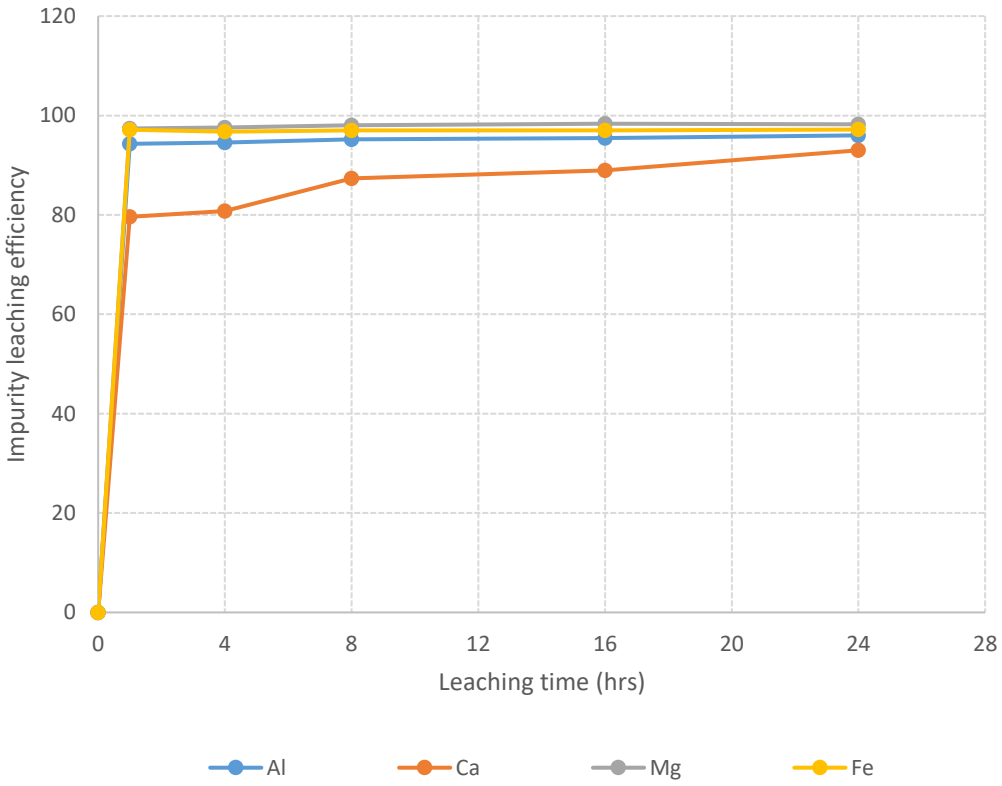


Figure 36 Effect of leaching time on impurity removal

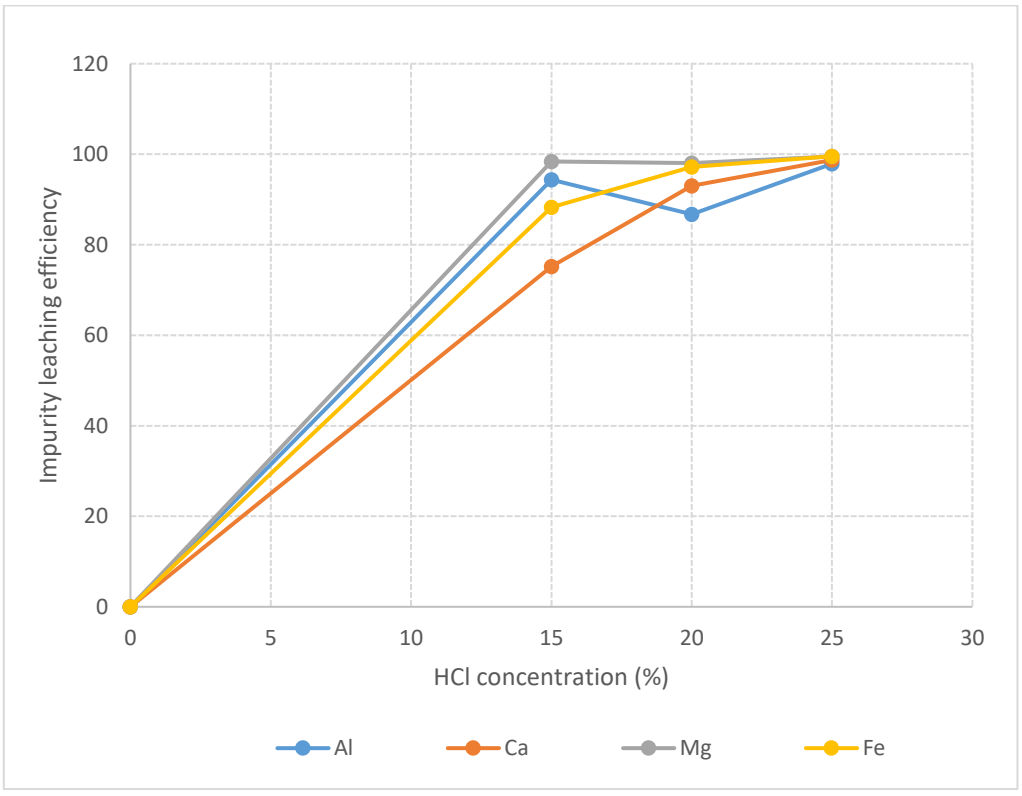


Figure 37 The effect of HCl concentration on impurity removal

### 5.4.2 Determination of rate controlling step for the leaching of impurities

Different models and mechanisms can control the leaching rate of the solid-liquid reaction. Since the controlling mechanism is unknown, it is important to test all the different mechanism in order to determine the rate controlling model. The best mechanism would be to compare different plots of $1 – (1 – X)^{1/3}$, $1 – (2/3)X – (1 – X)^{1/3}$, and $(1/3) \ln (1 – X) – [1 – (1 – X)^{1/3}]$ versus the leaching time and HCl concentration. The best mechanism will be determined by the plot that displays a good linear relationship with time and has the highest correlation coefficient (Faraji, et al., 2020).

The rate controlling model for impurities at different leaching times, differ from one impurity to the next as shown by the $R^2$ values shown in Table 44. Al and Ca had the highest $R^2$ values of 0.9548 and 0.9497 respectively, and were controlled by diffusion across product layer and interface transfer. The highest $R^2$ value of Mg is 0.9844 and for Fe is 0.9461, and these were controlled by the surface chemical reaction.

Table 44 $R^2$ values for impurities leached at different times

| Impurity | 1-(1-X)^1/3 | 1-2/3X-(1-X)^2/3 | (ln(1-X))/3-(1-(1-X)^(1/3)) |
|---|---|---|---|
| Al | 0.9514 | 0.9493 | **0.9548** |
| Ca | 0.9430 | 0.9431 | **0.9497** |
| Mg | **0.9844** | 0.9469 | 0.8888 |
| Fe | **0.9461** | 0.9245 | 0.9432 |

# CHAPTER 6

# CONCLUSION AND RECOMMENDATIONS

This study aimed at developing a method that would maximise the extraction of V and remove the impurities, improving the $TiO_2$ grade in the final residue.

## 6.1 Roasting results

The best roasting conditions attained during this investigation were from roasting the titaniferous slag with 200% stoichiometric Na addition for both $Na_2CO_3$:NaOH mass ratios of 100:0 and 0:100. The best roasting temperature and time were attained at 1000°C and 2 hours respectively. The particle size distribution that produced the best V extractions and $TiO_2$ grades was of +106 – 850 µm. The results from these conditions gave the best V extraction efficiency of 75.7% and 73.7% for $Na_2CO_3$ and NaOH respectively. Downstream processing of the water-leach residue was conducted with $Na_2CO_3$ since it is less expensive and used in industrial operations. The removal of impurities from the water-leach residue was conducted through the acid and caustic leaching process and resulted in $TiO_2$ grade of 68.7%. This $TiO_2$ grade of the caustic leach residue does not meet the minimum requirements mentioned in Table 5 for qualifying as a competitive $TiO_2$ feedstock. This residue still contained high concentrations of MgO and CaO impurities.

The phase composition results showed that the decomposition of the spinel phase with high Na additions was possible. The nepheline phase, previously reported by Lekobotja et.al (2016), did not form from these experiment. These tests showed the formation of a sodium magnesium aluminium silicate ($Na_3MgAlSi_2O_8$) after roasting. High V extractions were high since the pseudobrookite ss and spinel phases, which incorporated high concentrations of V, were decomposed with excess Na additions. The $Na_3MgAlSi_2O_8$ phase was decomposed after water-leaching. A new phase $Na_2MgTi_2O_6$ was seen in the water-leach residue. This phase contained high Ti and Si concentrations and a number of impurities. The spinel phase in the water-leach residue was detected at trace levels by XRD.

Acid leaching tests which were aimed at removing impurities such as Mg, Ca, Al, and Fe was a success for Mg, Ca, and Fe species. The Al impurities still remained high in the acid-leach residue.

The removal of Si impurities during caustic leaching was successful but not to completion since some of the Si species remained in the caustic-leach residue. The remaining Si impurities in the caustic leach residue were found in the rutile phase and dominant in the aluminosilicate and chlorite phases. The removal of Si did upgrade the $TiO_2$ concentration in the caustic-leach residue. Also, the Na species were present in the rutile and spinel phases of the caustic-leach residue.

## 6.2 Leaching results

The best acid-leach conditions that resulted in high $TiO_2$ grades on the residue were attained at 24 hours leaching time and 25% acid concentration. The highest $TiO_2$ grade of 71% produced after the removal of Si impurities through caustic leaching was attained when the best acid-leaching conditions were used. The results from the best acid-leaching conditions also showed high Ca, Mg, and Fe impurity removal through acid leaching and high Si impurity removal through caustic leaching. Washing of the produced caustic leach residue further upgraded the $TiO_2$ grade to 79.6% as Na and Si impurities were minimised. Although the $TiO_2$ grade has been greatly improved to a higher $TiO_2$ concentration, the resulting product still did not meet the minimum requirements for material to be considered a feedstock for the $TiO_2$ pigment production.

The phase composition results of the washed residue showed that several impurities were still present in the rutile phase. These impurities were Na, Mg, Al, Si, Cl, and Ca species. The presence of Na in the rutile phase could be decreased by washing the residue for longer periods of time whilst Mg, Al, and Fe could be removed by improving the optimisation of roasting and fluxing stages. Ca impurities could be minimised by using high HCl lixiviant concentrations during the acid-leaching stage.

Leaching of impurities was studied through the shrinking core model leaching mechanism. The result showed that the effect of leaching time affect the leaching efficiency of the impurities. The change in leaching time followed the order of Mg > Fe> Al > Ca impurity leaching efficiency. The leaching efficiency of Mg, Fe, and Al increased significantly at lower temperature to up to 4 hours leaching time. Thereafter the impurities reached equilibrium and remained constant irrespective of the change in leaching time. The $R^2$ values for Mg and Fe show that the rate controlling mechanism for leaching these impurities was controlled by the

surface chemical reaction whilst Al and Ca were controlled by the interface transfer and diffusion across the product layer.

## 6.3 Recommendations

- Further optimization of the roasting conditions is required to maximize the spinel decomposition which will release V for maximum extractions. This may include additional stoichiometric Na additions above 200%, as this study proved the possibility of decomposing pseudobrookite ss and spinel phases at high Na additions. The main focus would be the removal of Na and Si species that were present in the rutile phase. Also, the study on the removal of $Al_2O_3$ impurities is crucial as Al is one of the species that is not required in $TiO_2$ feedstock.
- Additional optimization of the leaching conditions is required to help with the removal of impurities up to completion for both acid and caustic-leached residues. The current study proved the possibility of impurity removal but not to completion. Most of the impurities that were removed include Ca, Fe, and Mg whilst Al remained persistent throughout the leaching stages. Perhaps increasing the HCl concentration to above 25% might assist in decreasing the impurities. Also, different techniques of Na from the residue must be investigated as this will minimise the amount of Na in the products. Optimization of the caustic leach conditions is also required as relative amounts of Si were visible in the residue.
- Upon achieving the $TiO_2$ feedstock from this process, a corresponding techno-economic study is required in order to evaluate the viability of the proposed flowsheet.

# REFERENCES


Hosseinzadeh, M., Alizadeh, M. & Raouf Hosseini, S. M., 2017. Mineralogical and physical beneficiation studies for iron extraction from Bardaskan titanomagnetite placer deposit. . *Journal of Mining and Environment,* 8(2), pp. 191-201.

Africa, Mining Review, 2017. *Mining Review Africa.* [Online] Available at: https://www.miningreview.com/news/nyanza-light-metals-plant-to-provide-titanium-dioxide-pigment-to-africa/

[Accessed 04 December 2023].

Barnes, S.-J., Maier, W. D. & Ashwal, L. D., 2004. Platinum-group element distribution in the main zone and upper zone of the Bushveld Complex, South Africa. *Chemical Geology,* Volume 208, pp. 293-317.

Becker, J. H. & Dutton, D. F., 2002. *Recovery of titanium from titanium bearing materials.* United states, South Africa, Patent No. United States Patent 7258847.

Blue Project, 2022. *Largo Physical Vanadium.* [Online] Available at: https://www.lpvanadium.com/dist/assets/docs/Project-Blue-2023-Vanadium-Report.pdf

[Accessed 12 2023].

Boni, M. et al., 2023. Vanadium ore resources of the African continent: State of the Art. *Ore Geology Reviews,* 157(105423), pp. 1-31.

Borowiec, K., Grau, A. E., Gueguin, M. & Turgeon, J. F., 1998. *Method to upgrade titania slag and resulting product.* US Patent, Patent No. 5830420.

Boyd, M. D., Schoukens, A. K. & Denton, G. M., 1993. *The recovery of titanium from titanomagnetite.* South Africa, Patent No. P11756.

Bushveld Minerals, 2014. *Bushveld Minerals.* [Online] Available at: https://www.bushveldminerals.com/wp-content/uploads/2022/07/201411280104480.pdf

[Accessed 18 12 2023].

Cawthorn, R. G., 2015. The Bushveld Complex, South Africa. In: *Layered Intrusions.* s.l.:s.n., pp. 517-587.

Faraji, F., Alizadeh, A., Rashchi, F. & Mostouf, N., 2020. Kinetics of leaching: a review. *Reviews in Chemical Engineering,* pp. 1-36.

Fischer, R. P., 1975. Vanadium Resources in Titaniferous Magnetite Deposits. In: U. S. G. P. Office, ed. *Geological Survey Professional 926-B.* Washington: s.n.

Fouad, O. A., 2005. Upgrading of a low-grade titanium slag by sulphation roasting technique to produce synthetic rutile. *Acta Metallurgical Slovaca,* 11(1), pp. 14-24.

Gambogi, J., 2022. *USGS, Mineral Commodity Summaries.* [Online] [Accessed January 2024].
Gázquez, M. J., Bolívar, J. P., Tenorio, R. G. & Vaca, F., 2014. A review of the production cycle of titanoim dioxide pigment. *Materials science and applications,* Volume 5, pp. 441-458.
Georgiou, D. & Papangelakis, V. G., 1998. Sulphuric acid pressure leaching of a limonitic laterite: chemistry and kinetics. *Hydrometallurgy,* Volume 49, pp. 23-46.
Gilligan, R. & Nikoloski, A. N., 2020. The extraction of vanadium from titanomagnetites and other sources. *Minerals Engineering,* Volume 146, pp. 1-18.
Goso, X. C., Lagendijk, H., Erwee, M. W. & Khosa, G., 2016. *Indicative Vanadium Deportment in the Processing of Titaniferous Magnetite by Roast-Leach and Electric Furnace Smelting Processes.* Cape Town, s.n.
Goso, X. C., Petersen, J., Nell, J. & Bisaka, K., 2016. *Scoping study of the upgrading of fluxed and fluxless titaniferous magnetite slag using the upgraded slag process.* Cape Town, Hydrometallurgy Conference 2016: Sustainable Hydrometallurgical Extraction of Metals.
Goso, X. C., Petersen, J., Nell, J. & Bisaka, K., 2016. *Scoping study of the upgrading of fluxed and fluxless titaniferous magnetite slags using the upgraded slag process.* Cape Town, Hydrometallurgy Conference 2016: Sustainable Hydrometallurgical Extraction of Metals - Southern African Institute of Mining and Metallurgy.
Goso, X. C., Petersen, J., Tangstad, M. & Safarian, J., 2021. Beneficiation of fluxed titaniferous slag to a marketable titania product using the modified upgraded slag process. *Mineral Processign and Extractive Metallurgy,* 131(3), pp. 1-10.
Hassell, D. J. et al., 2016. *Extraction of products from titanium-bearing minerals.* s.l. Patent No. WO 2016/007021 A1.
Hassell, D. J. et al., 2016. *Extraction of products from titanium-bearing minerals.* New Zealand, Patent No. WO 2016/007021 A1.
Kinnaird, J. A., 2005. *The Bushveld Large Igneous Province* , Johannesburg: School of Geosciences, University of the Witwatersrand .
Kitsara, I. et al., 2023. *Production of titanium and titanium dioxide from ilmenite and related applications,* Switzerland: World Interllectual Property Organization.
Lee, J. et al., 2021. A review on the metallurgical recycling of vanadium from slags: towards a sustainable vanadium production. *Journal of Materials Research and Technology,* Volume 12, pp. 343-364.
Lee, J. et al., 2021. A review on the metallurgical recycling of vanadium from slags: towards a sustainable vanadium production. *Journal of Materials Research and Technology,* Volume 12, pp. 343-364.

Lekobotja, M., Mojapelo, M., Goso, X. C. & Lagendijk, H., 2017. *Recovery of vanadium from discard titaniferous magnetite slag using soda ash roast-leach process.* Pretoria, South Africa, Proceeding of 3rd Young Professionals Conference (YPC 2017).

Li, H. et al., 2003. Effects of Al2O3, B2O3, Na2O, and SiO2 on nepheline formation in borosilicate glasses: Chemical and physical correlations. *Journal of Non-Crystalline Solids*, pp. 202-216.

Lin, W. & Guo, P., 2017. Research on the titaniferous slag smelting process and furnace. *IOP Conference Series: Materials Science and Engineering,* Volume 275, pp. 1-4.

Li, X. & Xie, B., 2012. Extraction of vanadium from high calcium vanadium slag using direct roasting and soda leaching. *International Journal of Minerals, Metallurgy and Materials,* 19(7), pp. 595-601.

Lv, C. & Bai, S., 2019. Upgrading of raw vanadium. *The Journal of the Southern African Institute of Mining and Metallurgy,* Volume 119, pp. 957-961.

Lv, H. et al., 2022. Effective Extraction of the Al Element from Secondary Aluminum Dross Using a Combined Dry Prossing and Alkaline Roasting Process. *Materials,* 16(5686), pp. 1-16.

Maphango, L., 2013. *Overview of South Africa's titanium industry and global market review, 2012,* Pretoria: Department: Minerals Resources.

Maphutha, M. P., Ramaili, M., Sitefane, M. B. & Goso, X. C., 2017. The effect of magnesia and alumina crucible wear on the smelting characteristics of titaniferous magnetite. *The Journal of the Southern African Institute of Mining and Metallurgy,* 117(7), pp. 649-655.

McRae, L. B., Pothas, E., Jochens, P. R. & Howat, D. D., 1969. Physico - chemicaI properties of titaniferous slags. *Journal of the South African Iinstitute of Mining and Metallurgy,* pp. 45-49.

Mefos, G. Y., 2006. *Recovery of vanadium from LD slag. A state of art report, Part 1 - Facts and metallurgy of vanadium.* [Art] (Jernkontorets Forskning, Swedish Steel Producers Association Stalkretsloppet).

Mefos, G. Y., 2006. *Recovery of vanadium from LD slag. A state of the art report, Part 1 - Facts and metallurgy of vanadium ,* Stalkretsloppet: Jernkontorets Forskning.

Moitse, R., 2008. *An overview of South Africa's titanium mineral concentrate industry,* Pretoria: Department of Mineral Resources.

Murty, C., Upadhyay, R. & Asokan, S., 2007. *Electro smelting of ilmenite for production of TiO2 slag - potential of india as a global player.* New Delhi, INFACON XI.

Nasimifar, A. & Mehrabani, J. V., 2022. A review on the extraction of vanadium pentoxide from primary, secondary, and co-product sources. *International Journal of Mining and Geo-Engineering*, 56(4), pp. 361-382.

Ngugen, T. H. & Lee, M. S., 2019. A review on the recovery of titanium dioxide from ilmenite ores by direct leaching technologies. *Extractive Metallurgy Review,* Volume 40, pp. 231-247.

Nie, W. et al., 2020. Leaching behaviors of impurities in titanium-bearing electric furnace slag in sulfuric acid. *Processes,* 8(56), pp. 1-18.

Nkosi, S., Dire, P., Nyambeni, N. & Goso, X. C., 2017. *A comparative study of vanadium recovery from titaniferous magnetite using salt, sulphate, and soda ash roast-leach process.* Pretoria, 3rd Young Professionals Conference.

Parirenyatwa, S. et al., 2016. Comparative study of alkali roasting and leaching of chromite ores and titaniferous minerals. *Hydrometallurgy,* Volume 165, pp. 213-226.

Pistorius, P. C., 2008. Ilmenite smelting: The basics. *Journal of the Southern African institue of Mining and Metallurgy,* Volume 108, pp. 35-43.

Pistorius, P. C., 2011. Titania slag smelting and calcination of crude zinc oxide: examples of processing under thermodynamic and kinetic constraints". *Proceedings of the second international slag valorization symposium, Leuven Belgium,* pp. 263-270.

Polyak, D. E., 2022. *Vanadium. Mineral Commodity Summaries*, United States: United States Geology Survey.

Polyak, D. E., 2023. *USGS, Mineral commodity summaries.* [Online] Available at: https://pubs.usgs.gov/periodicals/mcs2023/mcs2023.pdf[Accessed 21 November 2023].

Sadykhov, G. B. & Karyazin, I. A., 2007. Titanium - Vanadium slags produced upon the direct reduction of iron from titanomagnetite concentrates. *Russian Metallurgy (Metally),* 2007(6), pp. 447-454.

Sitefane, M., Masipa, M., Maphutha, P. & Goso, X., 2017. *The effect of CaO and MgO ratio on the smelting characteristics of vanadium bearing titaniferous magnetite.* Pretoria, South Africa, Proceedings of the 3rd Young Professionals Conference, The Southern African Institute of Mining and Metallurgy, pp. 467-480.

Stanaway, K. J., 1994. Overview of titanium dioxide feedstock. *Mining Engineering,* pp. 1367-1370.

Statista , 2023. *Distribution of titanium dioxide minerals production worldwide in 2021, by country*. [Online] Available at: https://www.statista.com/statistics/480822/titanium-dioxide-global-production-by-country-share/ [Accessed 02 February 2024].

Steinberg, W. S., 2008. *https://repository.up.ac.za/bitstream/handle/2263/26090/dissertation.pdf.* [Online] [Accessed 06 June 2022].

Steinberg, W. S., Geyser, W. & Nell, J., 2011. The history and development of the pyrometallurgical processes at Evraz Highveld Steel & Vanadium. *The Journal of the Southern African Institute of Mining and Metallurgy,* p. 705.

Subasinghe, H. C. & Ratnayake, A. S., 2022. General review of titanium ores in exploitation: present atatus and forecast. *Comunicações Geológicas,* 109(1), pp. 21-31.

Sui, Z. et al., 2004. *Feasibility of recovering metals from associated slags.* Cape Town, The South African Institute of Mining and Metallurgy.

Sutradhar, M., Da Silva, J. A. & Pombeiro, A. J., 2020. Introduction: Vanadium, its compounds and applications. In: *Vanadium Catalysis.* s.l.:s.n.

Taylor, P. R., Shuey, S. A., Vidal, E. E. & Gomez, J. C., 2006. Extractive metallurgy of vanadium-containing titaniferous magnetite ores: a review. *Minerals & Metallurgical Processing,* 23(2), pp. 80-86.

Technology, M., 2022. *Maracás Menchen Mine, Bahia, Brazil.* [Online] Available at: https://www.mining-technology.com/projects/maracas-menchen-mine-bahia-brazil/?cf-view&cf-closed [Accessed 21 11 2023].

Tole, M. P., Lasaga, A. C., Pantano, C. & White, W. B., 1986. The kinetics of dissolution of nepheline (NaAlSiO4). *Geochimica et Cosmochimica Acta,* 50(3), pp. 379-392.

USAID, 2021. *General energy mineral: Key Facts Vanadium.* [Online] Available at: https://www.land-links.org/wp-content/uploads/2021/11/USAID_GM_Vanadium.pdf

Van Vuuren, D. S. & Tshilombo, G. T., 2011. Nitriding of ilmenite and high-grade slag fines. *Journal of the South African Institute of Mining and Metallurgy, South Africa,* Volume 111, pp. 173-181.

Vanitec, 2022. *Making vanadium.* [Online] Available at: https://vanitec.org/vanadium/making-vanadium/

Wang, Y., Qi, T., Chu, J. & Zhao, W., 2010. Production of TiO2 from CaTiO3 by alkaline roasting method. *Rare metals,* 29(2), pp. 162-167.

Wu, X., 2021. Applications of titanium dioxide materials. In: *Titanium dioxide - Advances and applications.* s.l.:s.n.

Xiao-hua, L. et al., 2008. Kinetics of the leaching of TiO2 from Ti-bearing blast furnace slag. *J China Univ Mining & Technol,* 18(2), pp. 275-278.

Yang, B., He, J., Zhang, G. & Guo, J., 2020. Extraction of Vanadium from Titanoferrous Magnetite: Mineral Processing and Enrichment Methods. In: *Vanadium: Extraction, Manufacturing and Applications.* s.l.:Elsevier, pp. 59-88.

Zhang, L. et al., 2007. Recovery of titanium compounds from molten Ti-bearing blast furnace slag under the dynamic oxidation condition. *Minerals Engineering*, Volume 20, p. 684–693.

Zheng, F. et al., 2016. Kinetics of hydrochloric acid leaching of titanium from titanium-bearing electric furnace slag. *The Minerals, Metals & Materials Society*, 68(5), pp. 1476-1484.

# APPENDIX

**Roasted material at $Na_2CO_3$: NaOH ratio of 50:50**

Figure 38 shows the backscattered SEM micrograph, EDS, and XRD of the titaniferous slag roasted in the presence of $Na_2CO_3$: NaOH ratio of 50:50 and 200% stoichiometric Na addition. The phases that were present in this slag include nepheline, perovskite, Titanaugite, and spinel. The EDS results showed the presence of high vanadium concentrations in the spinel phase. The addition of NaOH on the $Na_2CO_3$ reagent did not seem to fully break the spinel phase since it was visible from the SEM microstructure, unlike the previous slag roasted in the presence of $Na_2CO_3$: NaOH ratio of 100:0. Although the spinel phase was still present as seen from the SEM micrograph, the nepheline phase did form. This implies that the formation of the nepheline phase is possible with high Na additions irrespective of the $Na_2CO_3$: NaOH ratio investigated. XRD results showed the presence of the spinel as the predominant phase. This suggests that the $Na_2CO_3$: NaOH ratio does affect the decomposition of the spinel phase.

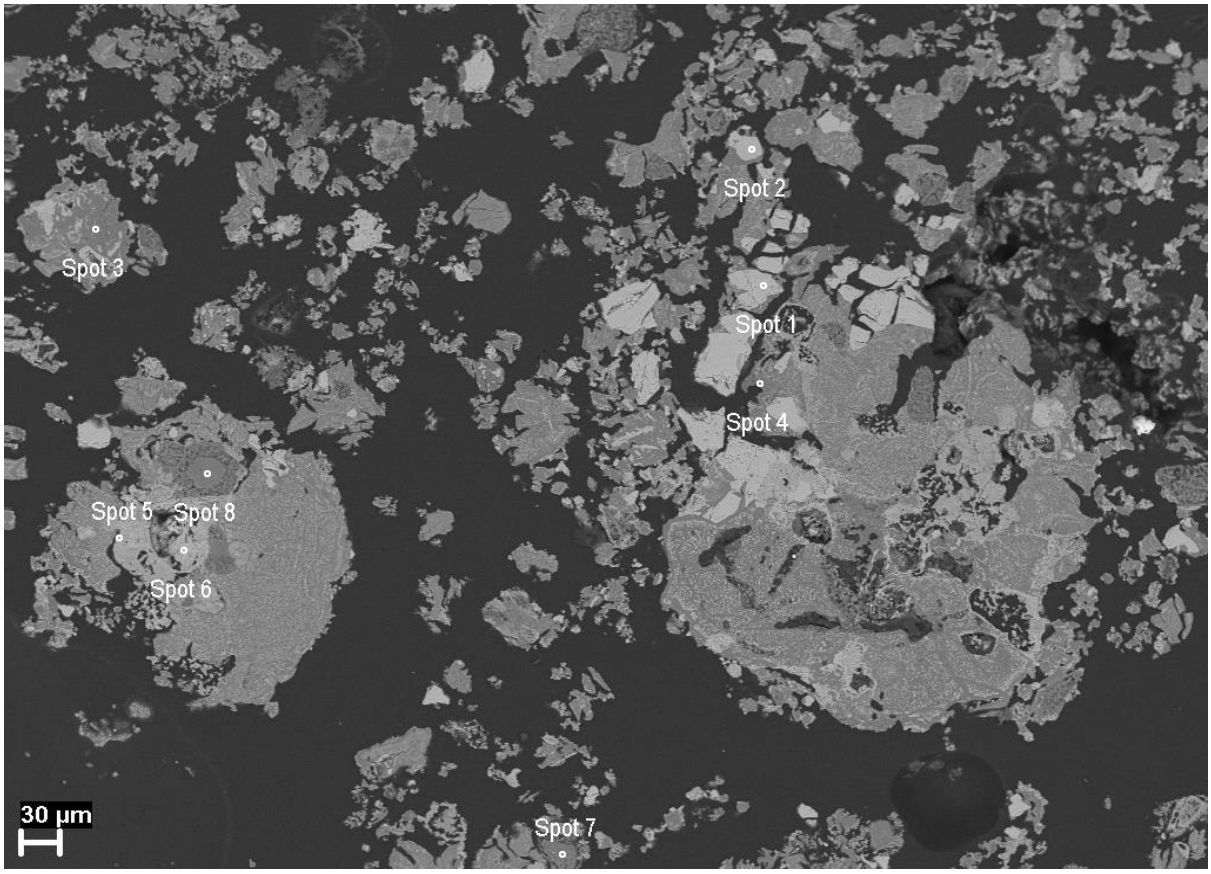


Figure 38 Backscattered electron microstructure of roast material produced from a slag roasted with 200% stoichiometric $Na_2CO_3$:NaOH mass ratio of 50:50

Table 45 EDS analysis results of the BSE phases of roast material produced from a slag roasted with 200% stoichiometric $Na_2CO_3$:NaOH mass ratio of 50:50

| Spot | O | Na | Mg | Al | Si | Ca | Ti | V | Mn | Fe | Total | Phase |
|---|---|---|---|---|---|---|---|---|---|---|---|---|
| 1 | 35.0 | | | | | 31.5 | 33.5 | | | | 100.0 | Perovskite |
| 2 | 34.9 | | | | | 31.7 | 33.4 | | | | 100.0 | |
| 3 | 40.1 | 22.7 | 9.3 | 6.8 | 15.1 | 0.6 | 2.6 | | | 2.9 | 100.0 | $Na_3MgAlSi_2O_8$ |
| 4 | 46.5 | 16.5 | 7.8 | 5.2 | 14.4 | 1.4 | 6.7 | | | 1.5 | 100.0 | |
| 5 | 29.2 | 17.2 | 4.6 | | | | 15.9 | | 1.3 | 31.7 | 100.0 | $Na_2MgTi_2O_6$ |
| 6 | 32.0 | 17.4 | 6.1 | | | | 24.1 | | 1.1 | 19.3 | 100.0 | |
| 7 | 44.1 | | 18.8 | 31.1 | | | 5.0 | 0.9 | | | 100.0 | Spinel |
| 8 | 50.8 | | 12.5 | 21.7 | | | 9.4 | 3.0 | | 2.6 | 100.0 | |

**Water leached residue at $Na_2CO_3$: NaOH ratio of 50:50**

The backscattered electron microstructure, EDS, and XRD results of the water leached residue at $Na_2CO_3$: NaOH ratio of 50:50 are shown in Figure 39. Similar phases as those that resulted from the water leach residue at $Na_2CO_3$: NaOH ratio of 100:0 were found. The only difference was the rutile phase that was present in the water leach residue. The XRD results showed that spinel phase was the dominant phase after water leaching. Perovskite and nepheline were also dominant as suggested by the XRD results. These results suggest that the $Na_2CO_3$: NaOH ratio of 50:50 was not successful as the spinel phase was the predominant phase in the water leach residue.

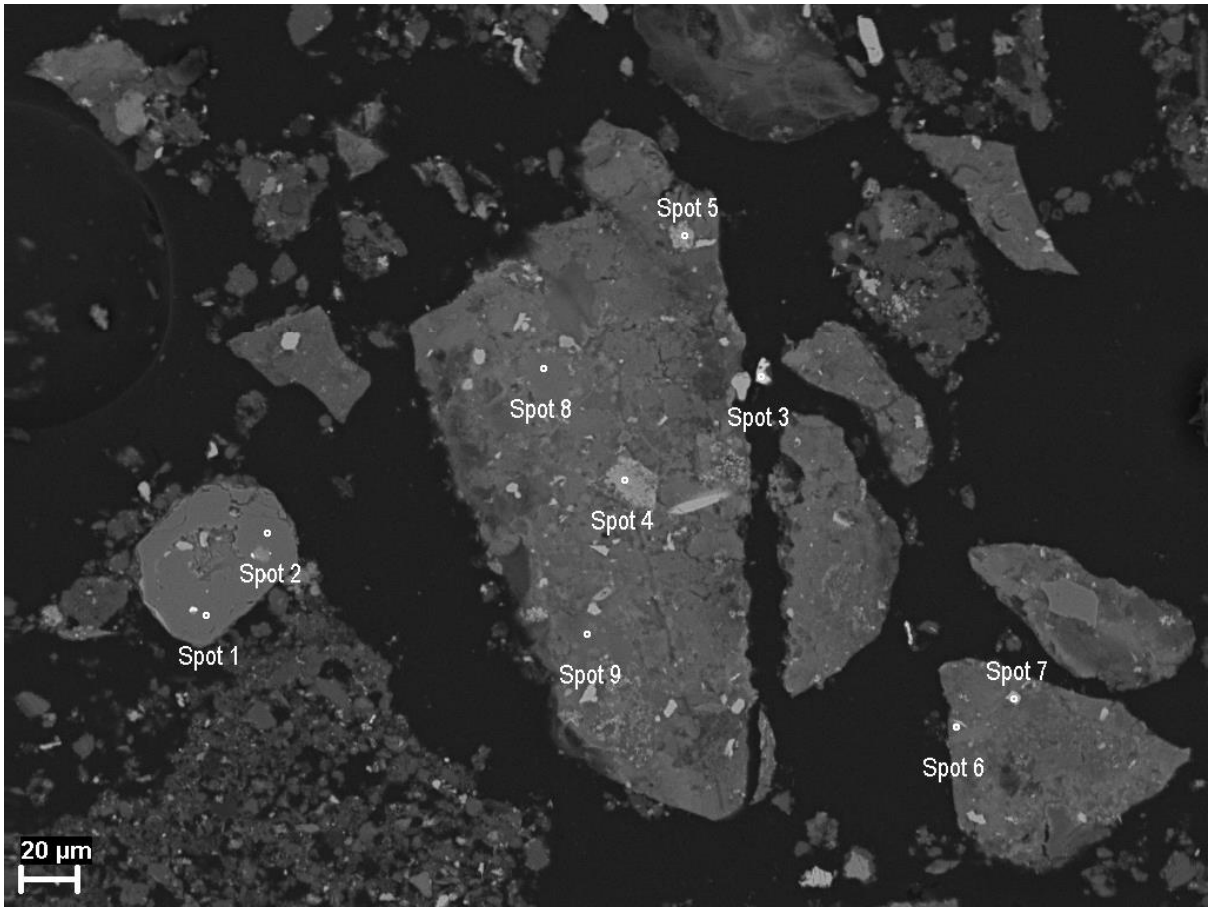


Figure 39 Backscattered electron microstructure of water-leach residue produced from a slag roasted with 200% stoichiometric $Na_2CO_3$:NaOH mass ratio of 50:50

Table 46 EDS analysis results of the BSE phases of water-leach residue produced from a slag roasted with 200% stoichiometric $Na_2CO_3$:NaOH mass ratio of 50:50

| Spot | O | Na | Mg | Al | Si | Ca | Ti | V | Fe | Total | Phase |
|---|---|---|---|---|---|---|---|---|---|---|---|
| 1 | 44.1 | | 19.7 | 31.6 | | | 3.7 | 0.5 | 0.4 | 100.0 | Spinel |
| 2 | 44.2 | | 19.5 | 32.5 | | | 2.6 | 0.8 | 0.3 | 100.0 | |
| 3 | 22.9 | | | | | | 2.2 | | 74.9 | 100.0 | Iron-Oxide |
| 4 | 38.8 | 4.3 | 2.7 | 2.6 | 2.5 | 2.9 | 42.0 | | 4.3 | 100.0 | Rutile |
| 5 | 36.7 | 1.1 | 0.2 | 0.8 | 1.2 | 19.3 | 38.6 | | 2.1 | 100.0 | |
| 6 | 35.0 | | | | | 31.5 | 33.5 | | | 100.0 | Perovskite |
| 7 | 35.0 | | | | | 31.2 | 33.8 | | | 100.0 | |
| 8 | 41.9 | 3.0 | 3.8 | 8.4 | 14.2 | 4.8 | 15.6 | | 8.3 | 100.0 | Ti-Si-Fe oxide |
| 9 | 39.9 | 2.3 | 3.6 | 7.1 | 12.3 | 12.8 | 13.2 | | 8.7 | 100.0 | |

**Roasted material at $Na_2CO_3$: NaOH ratio of 0:100**

Figure 40 presents the backscattered SEM micrograph, EDS and XRD results of the titaniferous slag roasted in the presence of $Na_2CO_3$: NaOH ratio of 0:100 at 200% stoichiometric Na addition. The SEM microstructure shows that perovskite, nepheline, and Titanaugite are the only phases present after roasting the slag. The spinel phase was not visible from the SEM microstructure. XRD results show the presence of the spinel as the predominant phase. This phase is in co-existence with the perovskite and nepheline phase at major levels. These results suggests that the NaOH reagent was not enough to completely decompose the spinel phase for maximum V extractions.

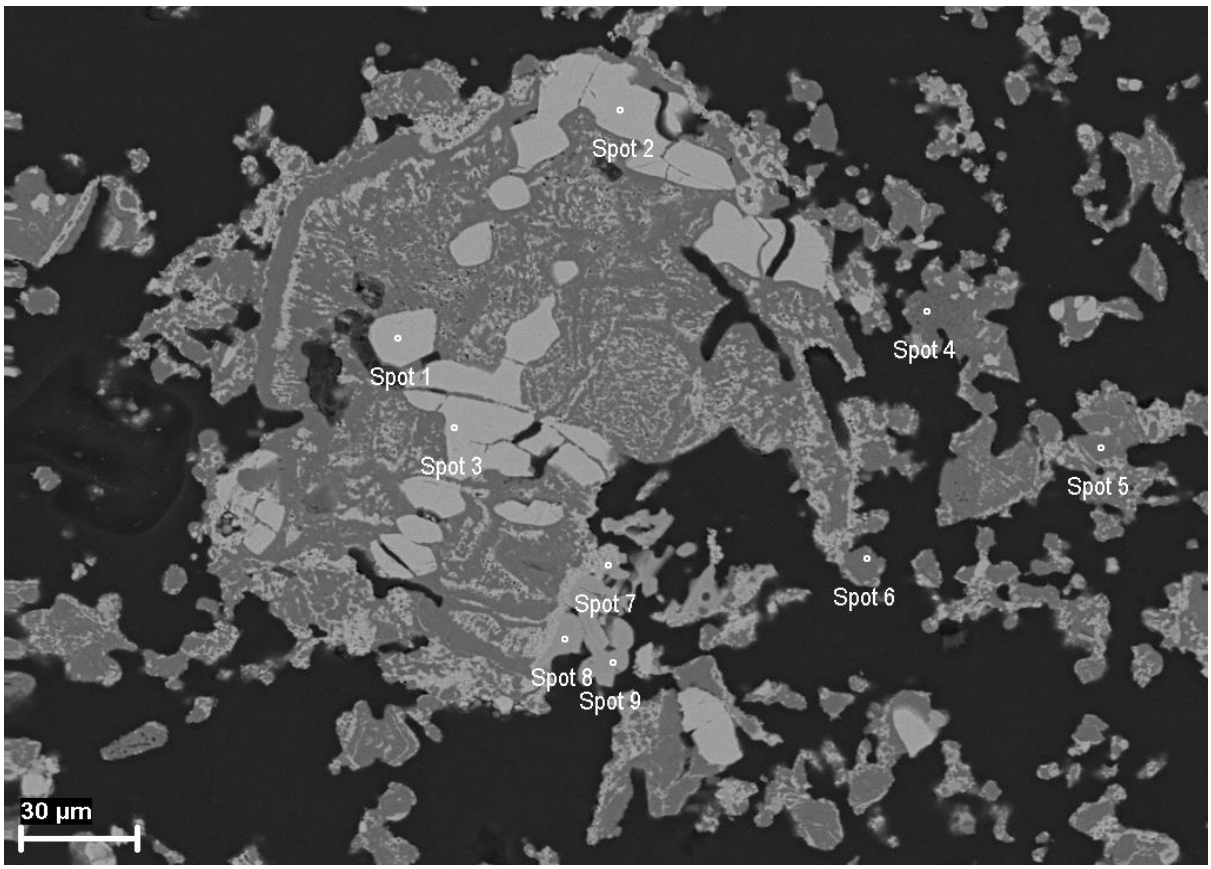


Figure 40 Backscattered electron microstructure of roast material produced from a slag roasted with 200% stoichiometric $Na_2CO_3$:NaOH mass ratio of 0:100

Table 47 EDS analysis results of the BSE phases of roast material produced from a slag roasted with 200% stoichiometric $Na_2CO_3$:NaOH mass ratio of 0:100

| Spot | O | Na | Mg | Al | Si | Ca | Ti | Mn | Fe | Total | Phase |
|---|---|---|---|---|---|---|---|---|---|---|---|
| 1 | 35.0 | | | | | 31.2 | 33.8 | | | 100.0 | Perovskite |
| 2 | 35.0 | | | | | 31.7 | 33.4 | | | 100.0 | |
| 3 | 35.0 | | | | | 31.3 | 33.7 | | | 100.0 | |
| 4 | 47.0 | 15.2 | 14.4 | 4.6 | 13.9 | | 3.0 | | 1.9 | 100.0 | $Na_3MgAlSi_2O_8$ |
| 5 | 46.6 | 16.7 | 6.6 | 7.4 | 13.9 | 0.7 | 4.4 | | 3.7 | 100.0 | |
| 6 | 47.5 | 17.1 | 4.4 | 13.3 | 10.2 | 0.1 | 3.9 | | 3.4 | 100.0 | |
| 7 | 35.5 | 10.8 | 5.3 | | | | 29.0 | 8.5 | 10.9 | 100.0 | $Na_2MgTi_2O_6$ |
| 8 | 35.6 | 9.6 | 4.9 | | | | 30.5 | 8.4 | 11.1 | 100.0 | |
| 9 | 35.4 | 11.0 | 5.2 | | | | 28.4 | 8.1 | 12.0 | 100.0 | |

**Water leached residue at $Na_2CO_3$: NaOH ratio of 0:100**

Backscattered SEM micrograph, EDS, and XRD analysis results of the water leached residue of the slag roasted at $Na_2CO_3$: NaOH ratio of 0:100 and 200% stoichiometric Na addition is shown in Figure 41. Similar phases as those found on the water leach residue of $Na_2CO_3$: NaOH ratio of 0:100 were seen for this residue. The XRD showed the predominant phase as perovskite, with major phases presented as quartz, rutile, and spinel phases. Also, XRD results showed new phases namely; anatase and silicon oxide, present in minor levels. These results suggest that the addition of NaOH on the titaniferous results in the formation of different phases.

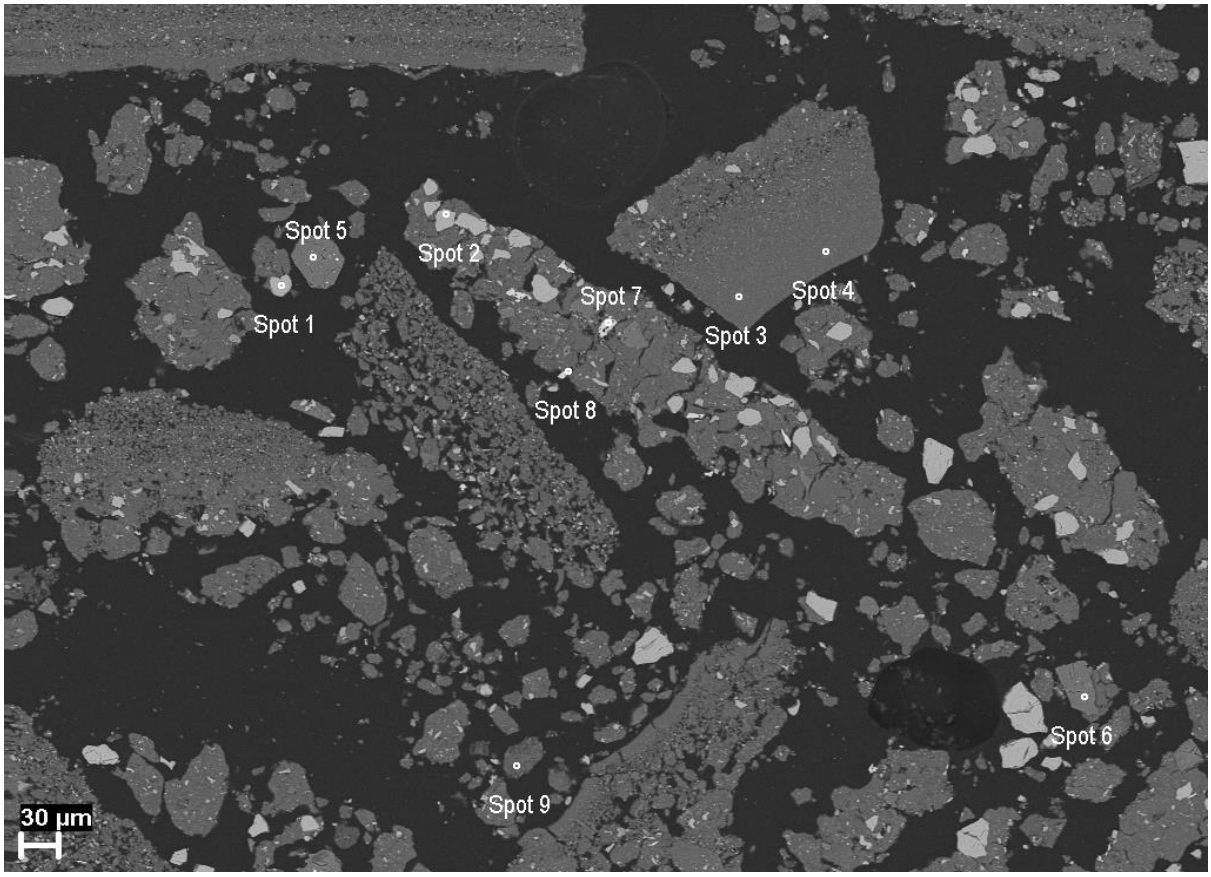


Figure 41 Backscattered electron microstructure water-leach residue produced from a slag roasted with 200% stoichiometric $Na_2CO_3$:NaOH mass ratio of 0:100

Table 48 EDS analysis results of the BSE phases of water-leach residue produced from a slag roasted with 200% stoichiometric $Na_2CO_3$:NaOH mass ratio of 0:100

| Spot | O | Na | Mg | Al | Si | Ca | Ti | V | Cr | Fe | Total | Phase |
|---|---|---|---|---|---|---|---|---|---|---|---|---|
| 1 | 35.0 | | | | | 31.5 | 33.5 | | | | 100.0 | Perovskite |
| 2 | 35.1 | | | | | 31.0 | 33.9 | | | | 100.0 | |
| 3 | 38.9 | 1.4 | 0.7 | 0.5 | 3.0 | 2.1 | 47.1 | | | 6.2 | 100.0 | Rutile |
| 4 | 38.9 | 1.7 | 0.8 | 0.9 | 3.2 | 2.6 | 45.6 | | | 6.3 | 100.0 | |
| 5 | 44.1 | | 19.0 | 31.1 | | | 5.9 | | | | 100.0 | Spinel |
| 6 | 44.3 | | 19.8 | 32.1 | | | 2.9 | 0.9 | | | 100.0 | |
| 7 | 23.8 | 0.4 | | | 0.6 | | 3.4 | | 1.1 | 70.7 | 100.0 | Iron-Oxide |
| 8 | 42.2 | 4.0 | 1.4 | 6.9 | 14.1 | 4.7 | 21.4 | | | 5.3 | 100.0 | $Na_3MgAlSi_2O_8$ |

**Roasted material at 900°C**

Figure 42 shows the backscattered electron microstructure, EDS, and XRD of the titaniferous slag roasted at 900°C. The resulting phases after roasting include perovskite, nepheline, and spinel. The XRD results showed spinel as the predominant phase, followed by the perovskite phase. The nepheline phase was on minor levels, suggesting that roasting the titaniferous slag at 900°C was not sufficient for maximum decomposition of the spinel phase. The formation of the nepheline phase was possible at lower roasting temperatures of 900°C even though the spinel remained after roasting. These results suggest that the roasting temperature have an effect on the decomposition of the spinel.

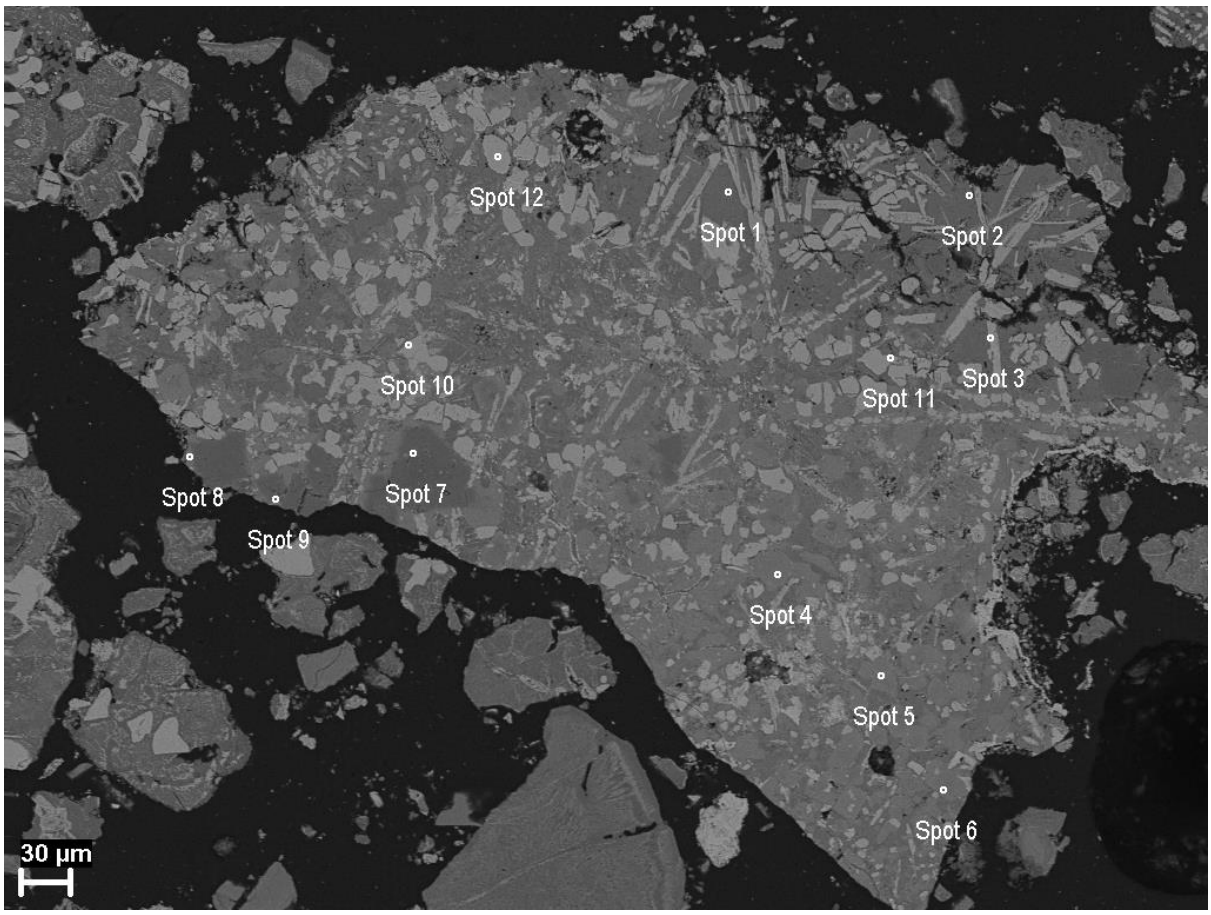


Figure 42 Backscattered electron microstructure of the slag roasted at 900°C

Table 49 EDS analysis of the slag roasted at 900°C

| Spot | O | Na | Mg | Al | Si | Ca | Ti | V | Fe | Total | Phase |
|---|---|---|---|---|---|---|---|---|---|---|---|
| 1 | 39.4 | 15.2 | 6.4 | 6.5 | 12.7 | 8.1 | 7.8 | 0.1 | 3.7 | 100.0 | |
| 2 | 37.8 | 24.8 | 9.2 | 6.5 | 9.8 | 4.5 | 5.4 | 0.3 | 1.6 | 100.0 | |
| 3 | 39.9 | 17.1 | 7.0 | 6.9 | 13.3 | 6.1 | 7.1 | 0.2 | 2.5 | 100.0 | $Na_3MgAlSi_2O_8$ |
| 4 | 37.5 | 12.1 | 5.4 | 7.5 | 8.5 | 8.5 | 10.6 | 0.1 | 9.9 | 100.0 | |
| 5 | 37.5 | 12.3 | 2.3 | 10.1 | 7.2 | 10.7 | 11.9 | 0.1 | 7.9 | 100.0 | |
| 6 | 38.3 | 13.5 | 2.3 | 11.7 | 7.7 | 10.8 | 10.7 | 0.3 | 4.8 | 100.0 | |
| 7 | 43.5 | | 19.2 | 30.2 | | | 3.7 | 1.2 | 2.2 | 100.0 | |
| 8 | 43.9 | | 18.7 | 31.5 | | | 2.4 | 2.1 | 1.4 | 100.0 | Spinel |
| 9 | 43.7 | | 18.6 | 30.4 | | | 3.1 | 2.2 | 1.9 | 100.0 | |
| 10 | 34.9 | | | | | 32.0 | 33.1 | | | 100.0 | |
| 11 | 34.8 | | | | | 32.4 | 32.7 | | | 100.0 | Perovskite |
| 12 | 35.1 | | | | | 30.9 | 34.0 | | | 100.0 | |

**Water leached resides at 900°C**

The backscattered SEM micrograph, EDS and XRD results of the water leach residue for the titaniferous slag roasted at 900°C are shown in Figure 43. The results showed the presence of spinel, pseudobrookite ss, perovskite, and Titanaugite phases. These results suggest that lower temperatures of 900°C were not adequate for decompose the spinel and pseudobrookite ss inert phases. XRD showed the pseudobrookite ss, spinel, and perovskite as the major phases in the water leach residue. These results confirm the difficulty of completely decomposing the chemically inert pseudobrookite ss and spinel phases.

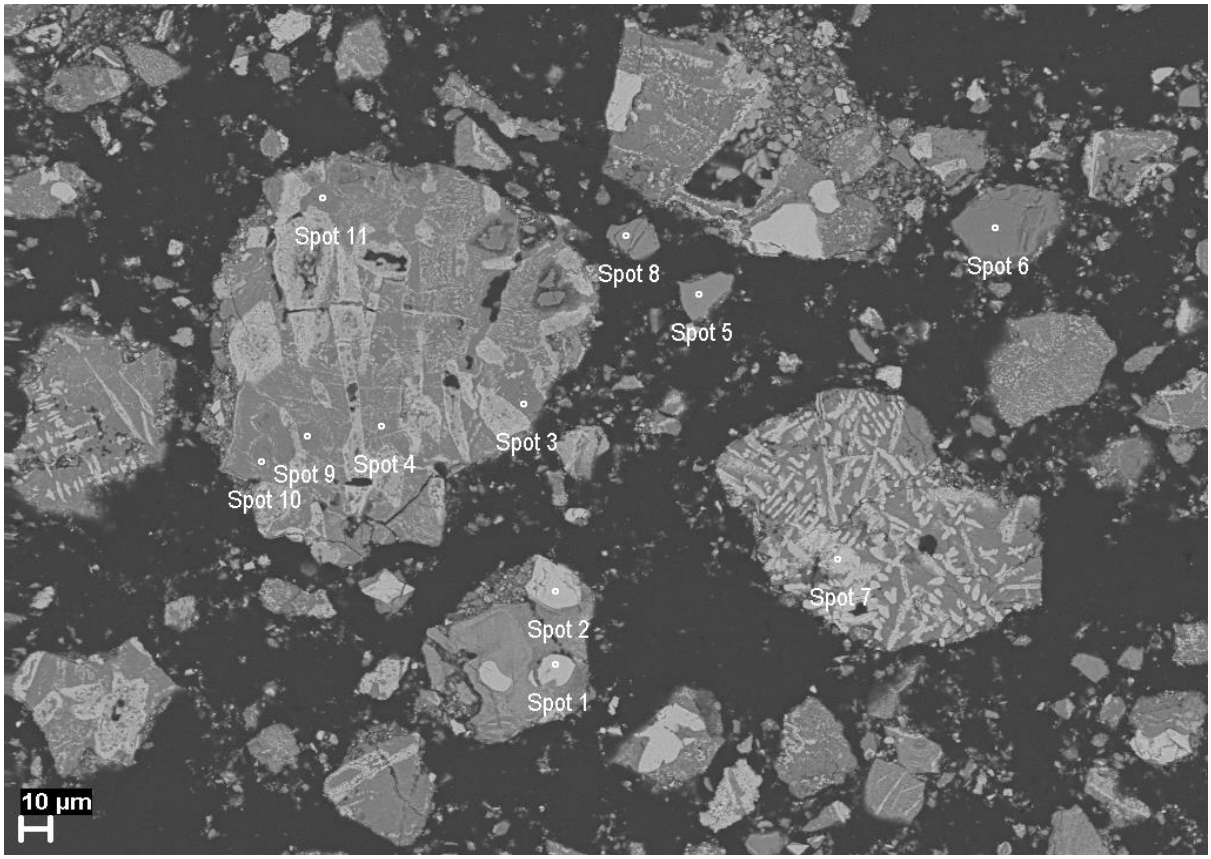


Figure 43 Backscattered electron microstructure of a water-leach residue produced from a slag roasted at 900°C

Table 50 EDS analysis of the water leach residues produced from a slag roasted at 900°C

| Spot | O | Na | Mg | Al | Si | Ca | Ti | V | Mn | Fe | Total | Phase |
|---|---|---|---|---|---|---|---|---|---|---|---|---|
| 1 | 34.9 | | | | | 31.7 | 33.4 | 0.0 | | | 100.0 | Perovskite |
| 2 | 34.9 | | | | | 31.7 | 33.3 | 0.0 | | | 100.0 | |
| 3 | 48.4 | 15.8 | 6.3 | 9.1 | 15.6 | | 3.4 | 0.0 | | 1.4 | 100.0 | $Na_3MgAlSi_2O_8$ |
| 4 | 46.9 | 12.9 | 5.2 | 7.8 | 12.3 | 3.5 | 9.6 | 0.4 | | 1.4 | 100.0 | |
| 5 | 46.0 | 7.9 | 8.3 | 7.8 | 6.9 | 7.5 | 15.1 | 0.5 | | | 100.0 | |
| 6 | 44.2 | | 19.2 | 31.7 | | | 4.4 | 0.6 | | | 100.0 | Spinel |
| 7 | 27.8 | 3.0 | 5.0 | | | 0.7 | 12.8 | | 3.4 | 47.2 | 100.0 | $Na_2MgTi_2O_6$ |
| 8 | 43.8 | | 17.3 | 29.7 | | | 3.2 | 4.3 | | 1.7 | 100.0 | Spinel |
| 9 | 50.4 | 12.6 | 0.9 | 23.4 | 6.5 | | 3.7 | 0.1 | | 2.5 | 100.0 | $Na_3MgAlSi_2O_8$ |
| 10 | 48.8 | 16.9 | 1.7 | 19.0 | 7.8 | | 3.6 | | | 2.2 | 100.0 | |
| 11 | 48.8 | 14.1 | 3.5 | 14.4 | 11.6 | 0.5 | 4.9 | | | 2.0 | 100.0 | |

**Roast material at 800°C**

Figure 44 presents the backscattered SEM micrograph, EDS, and XRD results of the titaniferous slag roasted at 800°C. The spinel, perovskite, nepheline, quartz, iron oxide, and Titanaugite phases were visible from the SEM microstructure. XRD confirmed the major phases as the pseudobrookite ss, spinel, and perovskite similar as those produced after roasting at 900°C. Natrite ($Na_2CO_3$) phase was also present at minor levels suggesting that roasting at 800°C was not sufficient to react $Na_2CO_3$ and $V_2O_5$ for the production of $NaVO_3$. The other phases that are present at trace levels include quartz and nepheline phase.

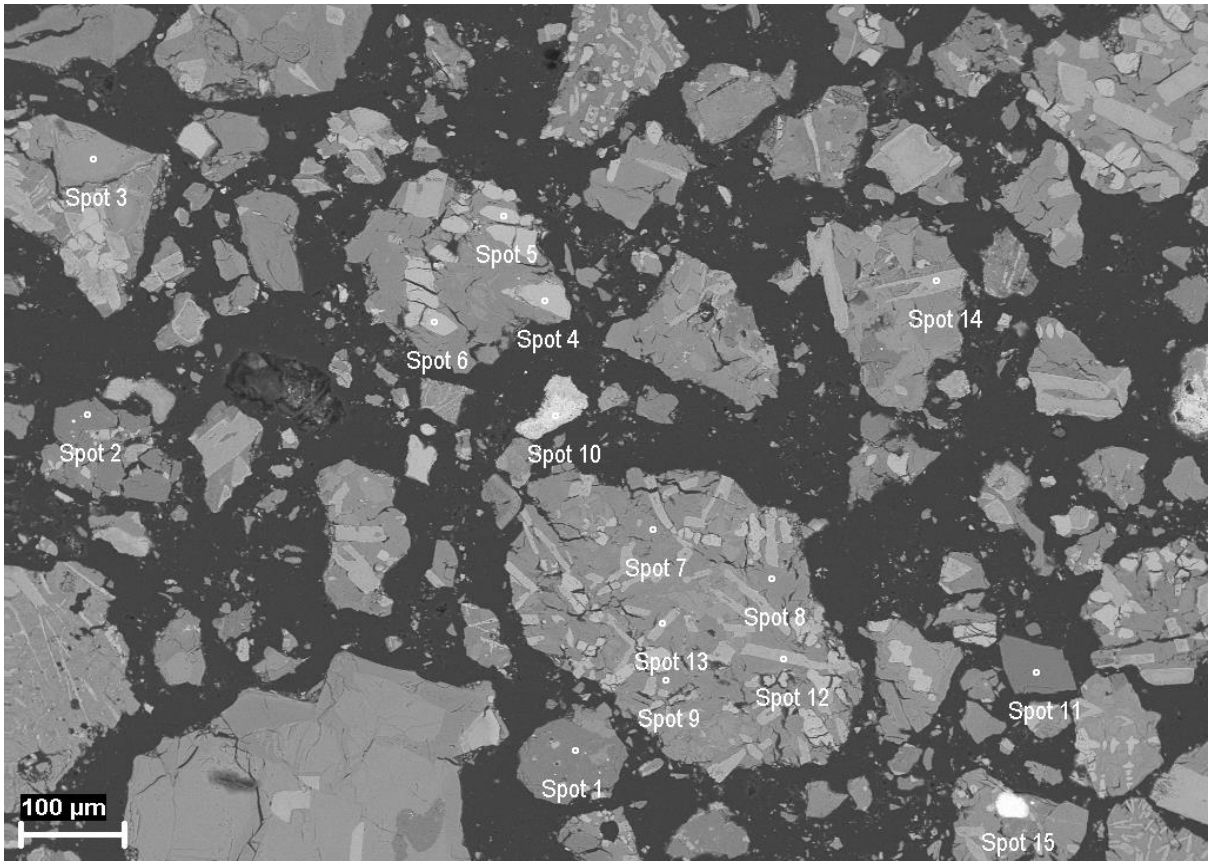


Figure 44 Backscattered electron microstructure of the slag roasted at 800°C

Table 51 EDS analysis of the slag roasted at 800°C

| Spot | O | Na | Mg | Al | Si | Ca | Ti | V | Cr | Mn | Fe | Total | Phase |
|---|---|---|---|---|---|---|---|---|---|---|---|---|---|
| 1 | 44.1 | | 19.9 | 31.0 | | | 3.8 | 1.1 | | | | 100.0 | |
| 2 | 44.4 | | 18.1 | 32.5 | | | 3.7 | 1.4 | | | | 100.0 | Spinel |
| 3 | 42.0 | | 15.3 | 20.3 | | | 8.6 | 7.4 | 2.4 | | 4.0 | 100.0 | |
| 4 | 35.1 | | | | | 30.7 | 34.2 | | | | | 100.0 | |
| 5 | 35.0 | | | | | 31.4 | 33.6 | | | | | 100.0 | Perovskite |
| 6 | 35.1 | | | | | 30.8 | 34.1 | | | | | 100.0 | |
| 7 | 39.1 | 13.1 | 6.2 | 5.5 | 13.0 | 11.8 | 7.5 | | | | 3.9 | 100.0 | |
| 8 | 46.7 | 12.1 | 3.9 | 5.2 | 15.7 | 6.9 | 8.3 | | | | 1.3 | 100.0 | Na3MgAlSi2O8 |
| 9 | 39.9 | 15.6 | 5.5 | 5.3 | 15.0 | 9.0 | 6.9 | | | | 2.8 | 100.0 | |
| 10 | 22.3 | | | | | | | | | | 77.7 | 100.0 | Iron-Oxide |
| 11 | 53.3 | | | | 46.7 | | | | | | | 100.0 | Quartz |
| 12 | 38.1 | 6.7 | 2.4 | 1.6 | | 0.8 | 47.0 | 0.0 | | | 3.5 | 100.0 | |
| 13 | 37.0 | 13.6 | 9.9 | 1.4 | | 0.3 | 35.4 | 0.0 | | | 2.5 | 100.0 | Na2MgTi2O6 |
| 14 | 38.1 | 10.6 | 4.5 | 1.1 | | 0.6 | 45.2 | 0.0 | | | 0.0 | 100.0 | |
| 15 | 22.9 | | | | | | | 1.5 | 0.5 | | 75.1 | 100.0 | Iron-Oxide |

**Water leached residue at 800°C**

Figure 45 shows the backscattered SEM micrograph, EDS, and XRD results of the titaniferous slag roasted at 800°C. The phases that were visible from the microstructure include perovskite, Titanaugite, nepheline, spinel, iron oxide, and Ca-Fe oxide. The XRD results showed pseudobrookite ss, spinel and perovskite as the major phases on the water leach residue. Quartz and nepheline phases are present in minor levels, whilst the periclase (MgO) phase is present in trace levels. These results show that roasting at 800°C was inadequate for the decomposition of the pseudobrookite ss and spinel phases.

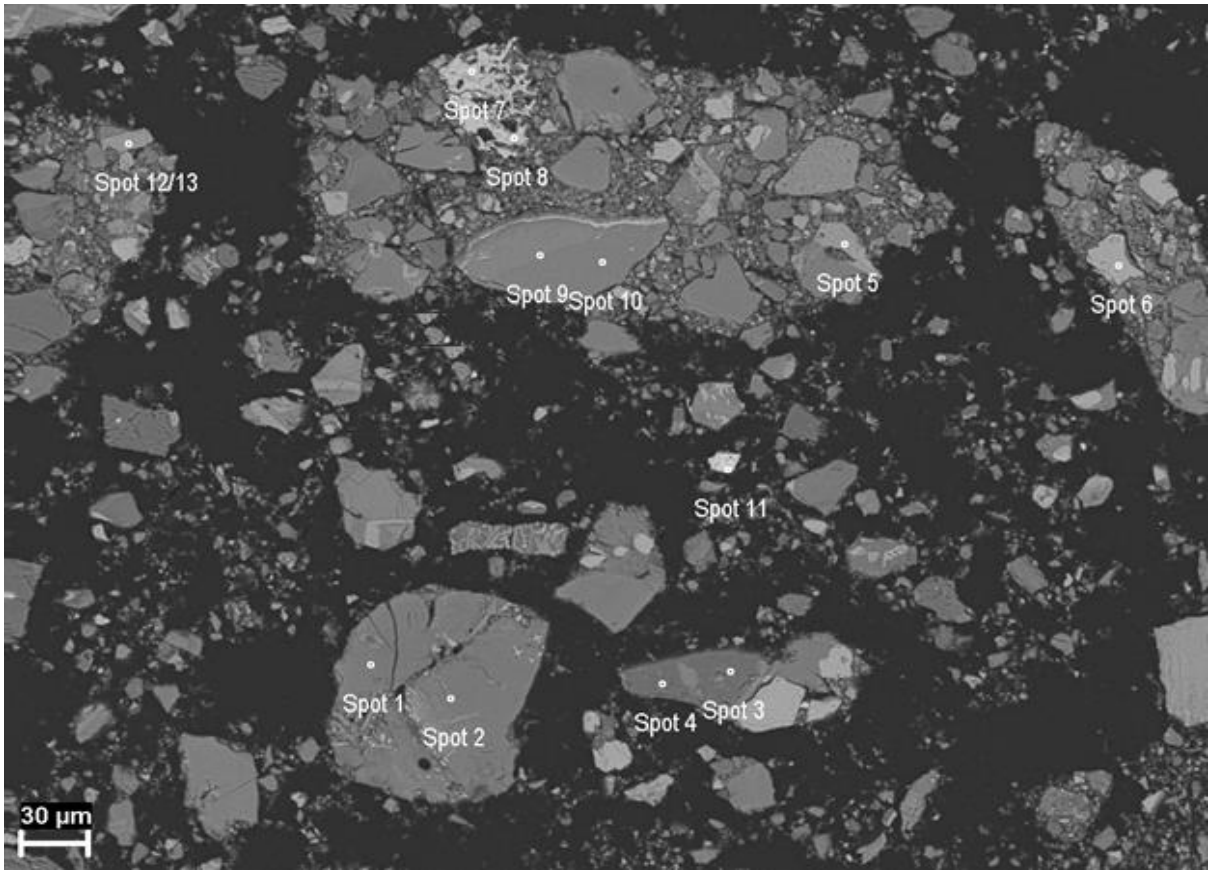


Figure 45 Backscattered electron microstructure of a water-leach residue produced from a slag roasted at 800°C

Table 52 EDS analysis of a water leach residue produced from a slag roasted at 800°C

| Spot | O | Na | Mg | Al | Si | Ca | Ti | V | Mn | Fe | Total | Phase |
|---|---|---|---|---|---|---|---|---|---|---|---|---|
| 1 | 38.4 | 23.2 | 6.8 | 7.4 | 10.5 | 7.0 | 6.7 | | | | 100.0 | $Na_3MgAlSi_2O_8$ |
| 2 | 40.1 | 14.8 | 5.1 | 7.2 | 13.0 | 10.3 | 9.4 | | | | 100.0 | |
| 3 | 44.2 | | 18.4 | 31.7 | | | 5.1 | 0.7 | | | 100.0 | Spinel |
| 4 | 44.2 | | 18.7 | 31.7 | | | 4.6 | 0.7 | | | 100.0 | |
| 5 | 35.1 | | | | | 31.0 | 33.9 | | | | 100.0 | |
| 6 | 35.1 | | | | | 31.0 | 33.9 | | | | 100.0 | Perovskite |
| 7 | 35.0 | | | | | 31.5 | 33.5 | | | | 100.0 | |
| 8 | 26.8 | 0.8 | | 1.6 | 1.3 | 27.1 | | 1.3 | 1.2 | 39.9 | 100.0 | |
| 9 | 36.6 | 16.2 | 6.6 | 0.6 | 17.1 | | 0.1 | 0.1 | | 22.7 | 100.0 | Ca-Fe-O |
| 10 | 36.4 | 16.1 | 6.5 | 0.5 | 16.9 | | | | | 23.5 | 100.0 | |
| 11 | 22.9 | | | | | | 0.9 | 0.9 | | 75.3 | 100.0 | Iron-Oxide |
| 12 | 38.2 | 9.4 | 3.8 | 1.6 | | | 45.9 | | | 1.2 | 100.0 | $Na_2MgTi_2O_6$ |
| 13 | 38.2 | 10.7 | 5.1 | 1.6 | | | 44.4 | | | | 100.0 | |
| 14 | 24.8 | 1.1 | 3.6 | | | 13.5 | 0.6 | 0.1 | 10.7 | 45.5 | 100.0 | Ca-Fe-Mn-O |
| 15 | 24.6 | 2.5 | 1.9 | | | 15.2 | 0.7 | 0.2 | 7.8 | 47.2 | 100.0 | |